


5-2010

## CIP4 and Src in Promoting the Migration and Invasion of Breast Cancers

Christina S. Pichot

Follow this and additional works at: [https://digitalcommons.library.tmc.edu/utgsbs\\_dissertations](https://digitalcommons.library.tmc.edu/utgsbs_dissertations)

 Part of the [Cancer Biology Commons](#), [Cell Biology Commons](#), [Medical Cell Biology Commons](#), [Medical Pharmacology Commons](#), and the [Other Chemicals and Drugs Commons](#)

---

### Recommended Citation

Pichot, Christina S., "CIP4 and Src in Promoting the Migration and Invasion of Breast Cancers" (2010). *The University of Texas MD Anderson Cancer Center UTHealth Graduate School of Biomedical Sciences Dissertations and Theses (Open Access)*. 40.  
[https://digitalcommons.library.tmc.edu/utgsbs\\_dissertations/40](https://digitalcommons.library.tmc.edu/utgsbs_dissertations/40)

This Dissertation (PhD) is brought to you for free and open access by the The University of Texas MD Anderson Cancer Center UTHealth Graduate School of Biomedical Sciences at DigitalCommons@TMC. It has been accepted for inclusion in The University of Texas MD Anderson Cancer Center UTHealth Graduate School of Biomedical Sciences Dissertations and Theses (Open Access) by an authorized administrator of DigitalCommons@TMC. For more information, please contact [digitalcommons@library.tmc.edu](mailto:digitalcommons@library.tmc.edu).

CIP4 AND SRC IN PROMOTING THE MIGRATION AND INVASION OF BREAST CANCERS

by

CHRISTINA STEWART PICHOT

APPROVED:

---

Seth J. Corey, M.D., Supervisory Professor

---

Jeffrey A. Frost, Ph.D.

---

Janet Price, D. Phil.

---

Joseph McCarty, Ph.D.

---

Fernando Cabral, Ph.D.

---

APPROVED:

---

Dean George Stancel, The University of Texas  
Health Science Center at Houston  
Graduate School of Biomedical Sciences at Houston

CIP4 AND SRC IN PROMOTING THE MIGRATION AND INVASION OF BREAST CANCERS

A DISSERTATION

Presented to the Faculty of

The University of Texas

Health Science Center at Houston

and

The University of Texas

M. D. Anderson Cancer Center

Graduate School of Biomedical Sciences

in Partial Fulfillment

of the Requirements

for the Degree of

DOCTOR OF PHILOSOPHY

by

Christina Stewart Pichot

Houston, Texas

May 2010

## **DEDICATION**

To my Pack



## **ACKNOWLEDGEMENTS**

First and foremost, I have to extend my thanks to my mentor, Seth Corey, for his guidance, support, and determination to see my project to its end. His drive and endless creativity have kept me inspired to always strive for knowledge and understanding of the world around me.

Also, I thank my committee members: Jeff Frost, Janet Price, Joe McCarty, Fernando Cabral, Maria Georgescu, Mike Gilcrease, and Jill Schumacher. Your direction and advice have been invaluable. My special thanks go to Jeff Frost for extending me space, support, and guidance to keep my project alive.

To all of my lab mates over the last many years- especially Elisabeth Blanchard, Sean Hartig, and Bella G: you've kept me honest, sane, and running in the right direction. Your advice and friendships will follow me wherever I go. Thank you!

My fellow students, faculty, and staff of both the Cancer Biology Program and the Cell and Regulatory Program have been such important sources of advice- academically, scientifically, and beyond. Many thanks! Thanks also to the staff of the GSBS- for more than I probably even know!

Of course, none of my research or education would be possible without my sources of support: Seth Corey, the Department of Defense Pre-Doctoral Fellowship in Breast Cancer Research, and the UT Graduate School of Biomedical Sciences.

And last, but in no way the least, I thank my family. From the bottom of my heart, I say thank you for every push, kick, and shove it took to keep me going, the reminders of why I do this, and for enduring all my complaints and late nights. I would never be here without your love and support. Thank you.

# **CIP4 AND SRC IN PROMOTING THE MIGRATION AND INVASION OF BREAST CANCER**

Publication No. \_\_\_\_\_

Christina Stewart Pichot

Supervisory Professor: Seth J. Corey, M.D.

Cellular invasion represents a critical early step in the metastatic cascade, and many proteins have been identified as part of an “invasive signature.” The non-receptor tyrosine kinase Src is commonly upregulated in breast cancers, often in conjunction with overexpression of EGFR. Signaling from this pathway stimulates cell proliferation, migration, and invasion and frequently involves proteins that regulate the cytoskeleton. My data demonstrates that inhibition of Src, using the small-molecule inhibitor dasatinib, impairs cellular migration and invasion. Furthermore, Src inhibition sensitizes the cells to the effects of the chemotherapeutic doxorubicin resulting in dramatic, synergistic inhibition of proliferation with combination treatments. The Src-targeted protein CIP4 (Cdc42-interacting protein 4) associates with curved plasma membranes to scaffold complexes of Cdc42 and N-WASp. In these experiments, I show that CIP4 overexpression correlates with triple-negative biomarker status, cellular migration, and invasion of (breast cancer cells. Inhibition of CIP4 expression significantly decreases migration and invasion. Furthermore, I demonstrate the novel finding that CIP4 localizes to invadopodia, which are finger-like projections of the actin cytoskeleton that are associated with matrix degradation and cellular invasion. Depletion of CIP4 in invasive cells impairs the formation of invadopodia and the degradation of gelatin. Therefore, CIP4 is a critical component of the invasive phenotype acquired by human breast cancer cells. In this body of work, I propose a model in which CIP4 promotes actin polymerization by stabilizing the active conformation of N-WASp. CIP4 and N-WASp are both phosphorylated by Src, implicating this pathway in Src-dependent cytoskeletal rearrangement. This represents a novel role for F-BAR proteins in migration and invasion.

| <b>TABLE OF CONTENTS</b>                                    | <b>Page</b> |
|---|-------------|
| <b>APPROVAL PAGE</b>  | <b>i</b>    |
| <b>TITLE PAGE</b>   | <b>ii</b>   |
| <b>DEDICATION</b>   | <b>iii</b>  |
| <b>ACKNOWLEDGEMENTS</b>                                     | <b>iv</b>   |
| <b>ABSTRACT</b>   | <b>v</b>    |
| <b>TABLE OF CONTENTS</b>                                    | <b>vi</b>   |
| <b>LIST OF FIGURES</b>                                      | <b>ix</b>   |
| <b>LIST OF TABLES</b>                                       | <b>xi</b>   |
| <b>ABBREVIATIONS</b>  | <b>xii</b>  |
| <b>CHAPTER 1: INTRODUCTION</b>                              | <b>16</b>   |
| <b>1.1 BIOLOGY OF BREAST CANCER</b>                         |             |
| 1.1.1 <i>Etiology</i>                                       |             |
| 1.1.2 <i>Clinical impact of metastatic disease</i>          |             |
| 1.1.3 <i>EGFR and HER2 oncogenesis in breast cancer</i>     |             |
| 1.1.4 <i>Src in breast cancer</i>                           |             |
| <b>1.2 THE ACTIN CYTOSKELETON</b>                           | <b>19</b>   |
| 1.2.1 <i>Actin filament structure &amp; dynamics</i>        |             |
| 1.2.2 <i>Actin-based structures of motility</i>             |             |
| 1.2.3 <i>Structure and signaling of invadopodia</i>         |             |
| <b>1.3 SRC</b>  | <b>31</b>   |
| 1.3.1 <i>History of Src research</i>                        |             |
| 1.3.2 <i>Structure and regulation of Src</i>                |             |
| 1.3.2 <i>Src and cytoskeletal reorganization/regulation</i> |             |
| <b>1.4 CELLULAR REGULATION OF CDC42 AND N-WASP ACTIVITY</b> | <b>35</b>   |
| 1.4.1 <i>Rho GTPases</i>                                    |             |
| 1.4.2 <i>Cdc42 Functions and Effector Proteins</i>          |             |
| 1.4.3 <i>N-WASP Family and Regulation</i>                   |             |
| <b>1.5 CIP4 AND THE F-BAR FAMILY</b>                        | <b>41</b>   |
| 1.5.1 <i>Characterization of CIP4</i>                       |             |

|                            |   |           |
|----------------------------|---|-----------|
| 1.5.2                      | <i>BAR Domains and membrane curvature</i>   |           |
| 1.5.3                      | <i>TOCA-1 and Actin Polymerization</i>  |           |
| <b>1.6</b>                 | <b>HYPOTHESIS AND MODEL</b>   | <b>45</b> |
| <b>CHAPTER 2:</b>          | <b>SRC PROMOTES MIGRATION AND INVASION OF BREAST</b>  |           |
| <b>CANCERS</b>             |   | <b>48</b> |
| <b>2.1</b>                 | <b>INTRODUCTION</b>   |           |
| <b>2.2</b>                 | <b>MATERIALS AND METHODS</b>  | <b>49</b> |
| 2.2.1                      | <i>Cell Culture</i>   |           |
| 2.2.2                      | <i>Viability and Proliferation Assays</i>   |           |
| 2.2.3                      | <i>Statistics and Combination Index</i>   |           |
| 2.2.4                      | <i>Immunoblotting</i>   |           |
| 2.2.5                      | <i>Cell Cycle and Cell Death Assays</i>   |           |
| 2.2.6                      | <i>Immunofluorescence and Invadopodia Imaging</i>   |           |
| 2.2.7                      | <i>Migration and Invasion Assays</i>  |           |
| <b>2.3</b>                 | <b>RESULTS</b>  | <b>53</b> |
| 2.3.1                      | <i>Dasatinib inhibits proliferation and metabolism of MDA-MB-231 cells</i>                    |           |
| 2.3.2                      | <i>Src inhibition does not correlate with proliferative inhibition by dasatinib</i>           |           |
| 2.3.3                      | <i>Dasatinib treatment induces G<sub>1</sub> arrest in MDA-MB-231 cells</i>                   |           |
| 2.3.4                      | <i>Combination treatment of dasatinib and doxorubicin synergistically inhibits metabolism</i> |           |
| 2.3.5                      | <i>Dasatinib-sensitive cells undergo cytoskeletal contraction</i>                             |           |
| 2.3.6                      | <i>Migration and invasion are inhibited by dasatinib treatment</i>                            |           |
| <b>2.4</b>                 | <b>DISCUSSION</b>   | <b>72</b> |
| <b>CHAPTER 3:</b>          | <b>CIP4 IS REQUIRED FOR MIGRATION AND INVASION OF</b>   | <b>76</b> |
| <b>BREAST CANCER CELLS</b> |   |           |
| <b>3.1</b>                 | <b>INTRODUCTION</b>   |           |
| <b>3.2</b>                 | <b>MATERIALS AND METHODS</b>  | <b>77</b> |
| 3.2.1                      | <i>siRNA-mediated knockdown of CIP4 and N-WASp expression</i>                                 |           |

|                   |   |            |
|-------------------|---|------------|
| 3.2.2             | <i>Immunofluorescence and Invadopodia imaging</i>                             |            |
| 3.2.3             | <i>Migration and Invasion Assays</i>  |            |
| 3.2.4             | <i>Acceptor-photobleaching FRET</i>   |            |
| <b>3.3</b>        | <b>RESULTS</b>  | <b>80</b>  |
| 3.3.1             | <i>Invasive breast cancer cell lines express high levels of CIP4</i>          |            |
| 3.3.2             | <i>CIP4 promotes cellular migration in MDA-MB-231 cells</i>                   |            |
| 3.3.3             | <i>CIP4 controls N-WASp activation in response to EGF</i>                     |            |
| 3.3.4             | <i>CIP4 promotes invasion of MDA-MB-231 cells in vitro</i>                    |            |
| 3.3.5             | <i>CIP4 localizes to invadopodia, but is not essential to their formation</i> |            |
| <b>3.4</b>        | <b>DISCUSSION</b>   | <b>92</b>  |
| <b>CHAPTER 4:</b> | <b>GENERAL SUMMARY</b>  | <b>95</b>  |
| <b>CHAPTER 5:</b> | <b>FUTURE DIRECTIONS</b>  | <b>99</b>  |
| <b>REFERENCES</b> |   | <b>102</b> |
| <b>VITA</b>       |   | <b>120</b> |

| <b>LIST OF FIGURES</b>  | <b>Page</b>  |
|---|--------------|
| <b>CHAPTER 1</b>  |              |
| <b>Figure 1:</b> Arp2/3 promotes actin polymerization                                       | <b>22</b>    |
| <b>Figure 2:</b> Cytoskeletal structures of motility  | <b>25</b>    |
| <b>Figure 3:</b> Formation of invadopodia over gelatin substrate                            | <b>28</b>    |
| <b>Figure 4:</b> Signaling pathways of invadopodia formation                                | <b>30</b>    |
| <b>Figure 5:</b> Structure and regulation of c-Src  | <b>33</b>    |
| <b>Figure 6:</b> Src-dependent signaling pathways   | <b>34</b>    |
| <b>Figure 7:</b> N-WASp structure and regulation  | <b>38</b>    |
| <b>Figure 8:</b> Structure and isoforms of CIP4   | <b>40</b>    |
| <b>Figure 9:</b> F-BAR family of proteins   | <b>42</b>    |
| <b>Figure 10:</b> Ribbon diagram of dimerized BAR domains                                   | <b>43</b>    |
| <b>Figure 11:</b> Proposed model of CIP4-mediated invadopodia formation                     | <b>47</b>    |
| <b>CHAPTER 2</b>  |              |
| <b>Figure 12:</b> Dasatinib inhibits cell proliferation in sensitive cells                  | <b>54</b>    |
| <b>Figure 13:</b> Dephosphorylation of Src in response to dasatinib                         | <b>56</b>    |
| <b>Figure 14:</b> Basal Src activity does not correlate with sensitivity                    | <b>57</b>    |
| <b>Figure 15:</b> Dasatinib induces cell cycle arrest in sensitive cells                    | <b>59</b>    |
| <b>Figure 16:</b> Synergistic anti-proliferation with dasatinib and doxorubicin             | <b>61-62</b> |
| <b>Figure 17:</b> Doxorubicin cell cycle arrest dominates dasatinib                         | <b>65</b>    |
| <b>Figure 18:</b> Dasatinib induces cytoskeletal deregulation in sensitive cells            | <b>66</b>    |
| <b>Figure 19:</b> Effects of dasatinib on cytoskeletal proteins                             | <b>67</b>    |
| <b>Figure 20:</b> Dasatinib impairs migration and invasion of MDA-MB-231                    | <b>69</b>    |
| <b>Figure 21:</b> Invadopodia and invasion impaired with dasatinib, doxorubicin combination | <b>71</b>    |
| <b>CHAPTER 3</b>  |              |
| <b>Figure 22:</b> Overexpression of CIP4 in invasive breast cancer cell lines               | <b>81</b>    |
| <b>Figure 23:</b> Upregulation of CIP4 mRNA in triple-negative cell lines                   | <b>82</b>    |

|  |              |
|--|--------------|
| <b>Figure 24:</b> Subcellular localization of endogenous CIP4                          | <b>83</b>    |
| <b>Figure 25:</b> Depletion of CIP4 impairs migration, not proliferation               | <b>84-85</b> |
| <b>Figure 26:</b> CIP4 interacts and increases activation of N-WASp downstream of EGFR | <b>86</b>    |
| <b>Figure 27:</b> CIP4 enriched at invadopodia of MDA-MB-231 cells on gelatin          | <b>87</b>    |
| <b>Figure 28:</b> CIP4 required for formation and function of invadopodia              | <b>89</b>    |
| <b>Figure 29:</b> CIP4 required for basal and EGF-dependent invasion                   | <b>91-92</b> |

#### **CHAPTER 4**

|   |            |
|---|------------|
| <b>Figure 30:</b> Proposed model of CIP4-mediated invadopodia formation ( <i>repeated</i> ) | <b>198</b> |
|---|------------|

| <b>LIST OF TABLES</b>  | <b>Page</b> |
|--|-------------|
| <b>Table 1:</b> Comparison of podosomes and invadopodia                          | <b>27</b>   |
| <b>Table 2:</b> Viability and proliferation of dasatinib-treated cells           | <b>55</b>   |
| <b>Table 3:</b> Synergy between dasatinib and doxorubicin                        | <b>63</b>   |
| <b>Table 4:</b> Comparison of invasive and non-invasive breast cancer cell lines | <b>80</b>   |



## **ABBREVIATIONS**

|           |  |
|-----------|--|
| 7-AAD     | 7-Amino-actinomycin D                          |
| apFRET    | Acceptor photobleaching FRET                   |
| Arp2/3    | Actin-related proteins 2/3                     |
| ATP       | Adenosine triphosphate                         |
| BrdU      | Bromodeoxyuridine                              |
| BSA       | Bovine serum albumin                           |
| Cdc42     | Cell division control protein 42               |
| CDK       | Cyclin-dependent kinase                        |
| CFP       | Cyan fluorescent protein                       |
| CI        | Combination index                              |
| CIP4      | Cdc42-interacting protein 4                    |
| CME       | Clathrin-mediated endocytosis                  |
| CRIB      | Cdc42/Rac-interactive binding                  |
| CSF-1R    | Colony stimulating factor 1 receptor           |
| Csk       | c-Src kinase                                   |
| DMSO      | Dimethyl sulfoxide                             |
| ECM       | Extracellular matrix                           |
| EFC       | Extended FCH (Fes/CIP4 homology)               |
| EGFR      | Epidermal growth factor receptor               |
| ELISA     | Estrogen receptor                              |
| ERM       | Exrin-radixin-moesin                           |
| F-BAR FCH | (Fes-CIP4 homology)- BAR (Bin-Amphiphysin-Rvs) |

|          |  |
|----------|--|
| FAK      | Focal adhesion kinase                    |
| FBP17    | Formin binding protein 17                |
| FCH      | Fes/CIP4 homology                        |
| FITC     | Fluorescein isothiocyanate               |
| FRET     | Fluorescence resonance energy transfer   |
| GAP      | GTPase-activating protein                |
| GDP      | Guanosine diphosphate                    |
| GEF      | Guanine nucleotide exchange factor       |
| GTP      | Guanosine-5'-triphosphate                |
| HB-EGF   | Heparin-binding EGF-like growth factor   |
| HER2     | Human Epidermal growth factor Receptor 2 |
| HGF      | Hepatocyte growth factor                 |
| HNSCC    | Head and neck squamous cell carcinoma    |
| HR1      | Homology region-1                        |
| I-BAR    | Inverse-BAR (Bin-Amphiphysin-Rvs)        |
| IC50     | Half maximal inhibitory concentration    |
| IL-8     | Interleukin-8                            |
| MAPK     | Mitogen-activated protein kinase         |
| mDia     | Mammalian Diaphanous-related             |
| MLC      | Myosin light chain                       |
| MMP-2,-9 | Matrix metalloproteinase-2, -9           |
| mRNA     | Messenger ribonucleic acid               |
| MTOC     | Microtubule-organizing center            |

|           |  |
|-----------|--|
| MTT       | 3-(4,5-Dimethylthiazol-2-yl)-2,5-diphenyltetrazolium bromide |
| N-WASP    | Neuronal-WASP (Wiskott Aldrich Syndrome protein)             |
| NFκB      | Nuclear factor-kappaB  |
| p130CAS   | p130(Crk-associated substrate)                               |
| PARP      | Poly(ADP-ribose) polymerase                                  |
| PDGFR     | Platelet-derived growth factor receptor                      |
| PI        | Propidium iodide   |
| PI3K      | Phosphoinositide 3-kinase                                    |
| PI(4,5)P2 | Phosphatidylinositol 4,5-bisphosphate                        |
| PIP3      | Phosphatidylinositol (3,4,5)-trisphosphate                   |
| PR        | Progesterone receptor  |
| ROCK      | Rho-associated coiled-coil-forming protein kinase            |
| ROI       | Region of interest   |
| RSV       | Rous sarcoma virus   |
| SFK       | Src family kinase  |
| SH2,SH3   | Src homology 2,3   |
| siRNA     | Small interfering RNA  |
| STAT3     | Signal transducer and activator of transcription 3           |
| TGFα      | Transforming growth factor alpha                             |
| Tks5/FISH | Tyrosine kinase substrate 5/five SH3 domains                 |
| Toca-1    | Transducer of Cdc42-dependent actin assembly                 |
| TRITC     | Tetramethyl rhodamine iso-thiocyanate                        |
| Tyr       | Tyrosine   |

|      |  |
|------|--|
| WAS  | Wiskott Aldrich Syndrome                 |
| WASP | Wiskott Aldrich Syndrome protein         |
| WAVE | WASP family verprolin-homologous protein |
| WH2  | WASP homology domain-2                   |
| WIP  | WASP-interacting protein                 |
| YFP  | Yellow fluorescent protein               |

## **CHAPTER 1: INTRODUCTION**

### **1.1 BIOLOGY OF BREAST CANCER**

#### ***1.1.1 Etiology***

Breast cancer is the most commonly diagnosed cancer in American women, affecting nearly 200,000 new patients every year. Currently, there are more than 2.5 million women living in the US with a history of breast cancer diagnosis. Five-year survival rates for patients diagnosed with localized or regional disease are encouraging: 98.3% and 83.5%, respectively. However, for the women presenting with metastatic disease, the five-year survival drops to a dismal 23.3% (2). Thus, targeting of metastatic disease represents an important area of research with strong clinical implications.

Although having a mother or sister with breast cancer significantly increases a woman's risk of developing breast cancer (3), less than 5% of breast cancer cases can be attributed to family history of the disease (4, 5). This leaves the vast majority of breast cancers as occurring due to environmental effects or unknown genetic factors. Age is a primary risk factor; 65% of patients are over the age of 55 at diagnosis (2). Hormone therapy, ionizing radiation, breast density, obesity, and excessive alcohol intake all increase the lifetime risk of developing breast cancer, whereas pregnancy (especially early), breast-feeding, and exercise are associated with decreased risk (6, 7). Many of these risk factors hinge on the role of hormones, especially heightened levels of estrogen, in the development of breast cancer (8).

In general, cancer is defined as the uncontrolled growth of cells, which may or may not spread to other parts of the body. The seminal paper by Hanahan and Weinberg describes the "Hallmarks of Cancer": uncontrolled growth, evasion of death (apoptosis), self-sufficiency in growth signals, insensitivity to anti-growth signals, angiogenesis, and tissue invasion/metastasis (9). Through a variety of mechanisms, cancer cells acquire these basic capabilities in a multi-step process known as tumorigenesis.

As a whole, “breast cancer” is really a collection of diseases with a wide array of etiologies. Tumors arise from the epithelial cells of the mammary ducts (ductal carcinoma) or glands (lobular carcinoma). However, this histological distinction does not correspond with the clinically important molecular subtypes (10). Recent molecular profiling further separates breast cancers into subtypes based on gene expression signatures. Cancers of the luminal subtype express hormone receptors and, due to newer targeted therapies, have a generally good prognosis. In contrast, basal type tumors lack estrogen and progesterone hormone receptors, making them refractory to popular targeted therapies. This combined with the higher rate of aggressiveness and invasiveness associated with basal tumors leads to a generally poor prognosis (10). Overlapping this basal subtype are the “triple-negative” cancers, which lack the estrogen and progesterone receptors (ER and PR, respectively) as well as the human epidermal growth factor 2 (HER2/*neu*/ErbB2), and are currently the subject of intense research. Identification of this three-gene signature is clinically important in assigning therapy regimens, although some studies now suggest an expansion to five genes with the inclusion of epidermal growth factor receptor 1 (EGFR) and cytokeratin 5/6 (11). Cancer stem cell populations have been identified in breast cancers, and these subtypes might represent tumors arising from stem cells at different stages of differentiation (10).

### ***1.1.2 Clinical impact of metastatic disease***

Metastatic tumors in organs distant from the primary cancer account for the majority of breast cancer deaths. Fewer than 5% of patients diagnosed with metastatic breast cancer achieve complete remission (12). Early-stage, non-invasive breast cancers, or ductal carcinoma in situ (DCIS), are diagnosed in nearly 50,000 women every year, with approximately 30% of these patients presenting with invasive disease in the ipsilateral breast within the next 6 to 10 years (12). Identification of biomarkers to predict the occurrence of invasive disease would have a profound impact on the treatment of these patients. Additionally, treatment plans for women diagnosed with locally invasive disease could be tailored based on these markers, advising whether localized radiation or systemic therapy is more suitable. These methods would spare

many patients from the unnecessary toxicity of systemic chemotherapies and target only the most high-risk patients with aggressive treatments. Furthermore, identification of pro-invasive pathways also presents novel targets for the development of anti-metastatic therapies best suited to these early-stage and locally invasive subtypes.

### **1.1.3 EGFR and HER2 oncogenesis in breast cancer**

Oncogenes are mutated genes that promote tumorigenesis. In breast cancer, the family of ErbB receptor tyrosine kinases (RTKs) are potent oncogenes whose expression in tumors inversely correlates with the clinical prognosis (13). The epidermal growth factor receptor (**EGFR/HER-1/ErbB1**) is activated by its ligand, EGF (as well as TGF $\alpha$ , HB-EGF, amphiregulin, and others) upon which it dimerizes and becomes phosphorylated. Active EGFR dimers trigger downstream signaling pathways with a wide range of outcomes, including proliferation, survival, and migration. Classically, EGFR activates the PI-3K/Akt and Ras/Raf/MAPK pathways. Activation of Akt leads to cell survival via phosphorylation and inhibition of the pro-apoptotic Bcl-2 family of proteins and cell cycle arrest through inactivation of the p21 and p27 cell cycle inhibitors. EGFR can also activate the STAT family of transcription factors, specifically STAT3 in breast cancer, promoting transcription of genes for proliferation (c-myc) and cell-cycle progression (p21 and cyclin D1) (14). In addition to the classical signaling cascades resulting from EGFR activation, EGFR can also translocate to the nucleus to act directly as a transcriptional regulator (14). Overexpression as well as the appearance of activating mutations in EGFR has been identified in a variety of cancers, leading to the development of several EGFR-targeted inhibitors. Specific small molecule inhibitors of EGFR, such as gefinitib (Iressa®; AstraZeneca) and erlotinib (Tarceva®; Genentech) are approved for treatment of lung and metastatic colorectal cancers, but have shown only moderate effects in various trials for breast cancer.

The second member of the ErbB family, **HER2/neu (ErbB2)** has no identified ligand, but is activated by heterodimerization with other family members. Functioning as a co-receptor with the other ErbB receptors, many of the transformative signaling

pathways activated by EGFR are also activated by HER2. However, ligand dissociation rates from HER2-containing heterodimers are slower than without HER2, leading to prolonged ErbB signaling (15). Amplification and/or overexpression, which occur almost entirely in ductal carcinomas, are found in approximately 20-30% of invasive breast cancers (16, 17). Activating mutations may also be present which lead to constitutive activation. Overexpression of HER-2/*neu* is associated with more aggressive disease, faster proliferation, and decreased sensitivity to chemotherapy. Anti-HER2 therapies such as trastuzumab (Herceptin®; Genentech) have had high rates of success in HER2-overexpressing cancers.

#### **1.1.4 *Src in breast cancer***

The Src family kinases (SFKs) are involved in the regulation of many signaling pathways affecting cell growth, migration, adhesion, and survival. (18-21). C-Src is the cellular homolog of the potent v-Src oncogene identified as the transforming protein encoded by the Rous Sarcoma Virus. (RSV). Hyper-activation or overexpression of Src kinases is associated with transformation through increased proliferation and decreased cell-cell adhesion (22-25, 26, 27) . Breast cancers exhibit significantly increased tyrosine kinase activity compared to normal breast tissue, most of which can be attributed to elevated activation of c-Src (28, 29). Activating mutations in Src may result in increased kinase activity (up to 20-fold) with or without a concomitant increase in protein expression (29-32). Src associates with several oncogenes in breast cancer, including Her-2/*neu* and EGFR, and amplifies the transformative signaling (33-35). Src is commonly overexpressed with EGFR overexpression (33).

Treating breast cancer cells with Src-targeted inhibitors (dominant-negative proteins or pharmaceutical inhibitors) decreases cell proliferation and migration in a variety of human cancer cells, including breast cancer (36-40).

## **1.2 THE ACTIN CYTOSKELETON**



Many cellular functions, including maintenance of cell shape, polarity, division, adhesion, intracellular trafficking, and motility are dependent on the cytoskeletal system. The cytoskeleton can translate cues from the extracellular environment into changes in gene expression and differentiation. The structural and regulatory components of the cytoskeleton are highly conserved across all organisms, attesting to its importance in the most basic cellular functions. Because the cytoskeleton utilizes a system of multimeric filaments, it can rapidly respond to changing extracellular cues to change shape by rearranging the building block subunits. Migrating cells generate discrete structural organelles, such as lamellipodia, podosomes, and invadopodia, which are driven by the force of elongating cytoskeletal filaments. Many accessory proteins participate in the regulation of filament dynamics, linking the intracellular signaling to a functional output (41-44).

In addition to providing the mechanical drive for cellular migration, the actin cytoskeleton also provides the forces required for endocytosis, pathogen invasion, cytokinesis, and organelle transport within the cell. Studies of actin “comets” used for propulsion by invasive *Listeria* in mammalian cells have provided excellent models for investigating the molecular requirements of actin filament polymerization (45).

### ***1.2.1 Actin filament structure and dynamics***

The actin cytoskeleton, like the microtubules, is a dynamic system of small, diffusible subunits that self-assemble into polarized filaments with a dynamic (plus) end. Individual chains are then cross-linked by accessory proteins into larger structures to create specialized mechanical or functional organelles (41, 43, 45).

Components: Actin filaments (microfilaments) are 2-stranded, helical filaments built from globular actin monomers (G-actin). These are the thinnest and most flexible of the cytoskeletal filaments, with a diameter of approximately 5-9 nm. Actin filaments not only provide tracks for intracellular trafficking, but also are critical in the force generation required for cellular motility and shape change. Each actin monomer added to the filament is bound to a molecule of ATP, which is hydrolyzed by the enzymatic G-actin after

its incorporation. Filamentous actin (F-actin) is dispersed throughout the cell, but is highly concentrated at the cortex, a region just below the plasma membrane, allowing for rapid formation of migratory protrusions at the cell surface. Traditionally, the more dynamic plus end has been termed the “barbed” end and the more stable, minus end the “pointed” end (41, 43, 45).

Kinetics: Filament formation occurs in three main phases: nucleation, elongation, and steady state. Although subunits will self-assemble spontaneously, small oligomers are highly unstable and will dissociate before elongation can proceed. This initial “seeding” of the nascent filament is the rate-limiting step or “lag-phase”.

Once successful nucleation has occurred, subunits will rapidly assemble in the “growth-phase.” The filament will continue to elongate until it reaches the “equilibrium phase,” a steady state in which subunits will continue to assemble and disassemble without changing the length of the filament. In a phenomenon known as treadmilling, subunits are added and progress through a filament when both ends of the filament are exposed and are in areas of unequal critical concentrations, allowing subunit addition at one end at the same rate at which the opposite end is losing subunits. This activity is important to the dynamic responsiveness of the actin network. In response to a stimulus, a small shift in the rates of association or dissociation can produce a rapid change in filament length. By coupling spontaneous assembling filaments to the plasma membrane, cells have developed a method of using very little energy to accomplish energetically unfavorable mechanical work (41, 45).

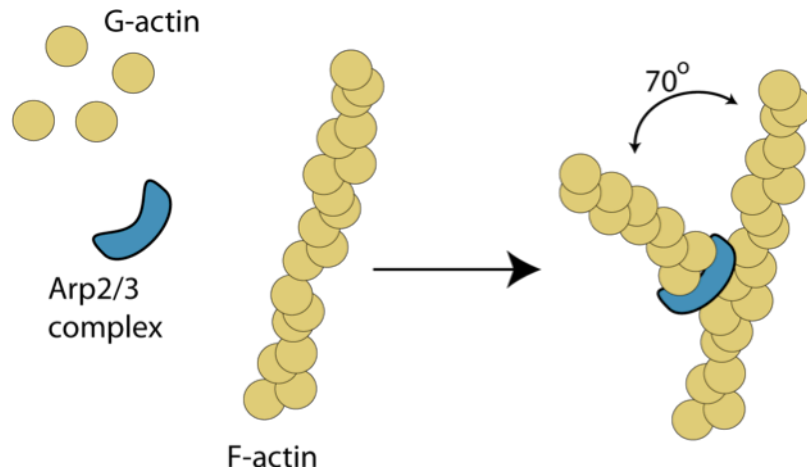


**Figure 1: Arp2/3 complex promotes actin polymerization through dendritic nucleation.** Arp2/3 complex of proteins facilitates nucleation of nascent actin filament, resulting in a branched actin structure with filaments at 70-degree angles.

**Nucleation:** Spontaneous nucleation of nascent filaments is a slow process, but can be facilitated by accessory proteins (**Figure 1**). There are three primary proteins which promote actin nucleation: the Arp complex, the formin proteins, and spire. Formins, which include mDia1 and mDia2, dimerize via shared FH2 domains to form a ring structure from which actin filaments spontaneously elongate. The formin ring remains bound to the growing plus-end and moves processively, blocking access by other capping proteins. Regulatory inputs by signaling molecules can alter the function of formins at the plus-end. Spire functions as a single protein that contains four WH2 domains to bind and stabilize a tetramer of actin monomers. After elongation, spire dissociates from the filament, but can re-bind to cross-link actin filaments with microtubules (42).

The best-characterized nucleator of actin filaments, however, is the Arp complex (Arp 2/3), an aggregate of 7 proteins. Arp 2 and Arp 3 are structurally similar to actin monomers and mimic a stable actin dimer. Five structural Arp proteins (ArpC 1-5) support the pseudo-dimer. Although the Arp 2/3 complex can promote nucleation freely, actin filaments are often formed from Arp complexes bound to the side of existing actin filaments. This model of dendritic nucleation describes the ability of Arp complex to initiate new branches of actin that protrude off the mother filament at a 70° angle,

forming web-like networks. In migrating cells, this multi-directional polymerization allows the cell to more quickly respond to extracellular cues and “steer” in any direction by altering the localized activation state of the Arp complex (41-44, 46, 47).

Organization of individual filaments into larger structures requires cross-linking accessory proteins. Actin filaments can be arranged in to either bundles of closely tied, parallel fibers or looser webs of short filaments with more flexibility. Stress fibers are contractile actin bundles linked together by alpha-actinin and myosin to provide tension between the cytoskeleton and anchoring focal adhesions. Web-like networks of actin interlink short actin filaments at right angles to provide a flexible rigidity to the cell periphery. Filamin-actin networks are found in lamellipodia and are required to maintain a migratory phenotype (41-44, 46).

These actin structures must be tied to the plasma membrane for effective shape change. This function is provided by the ERM family of proteins, named for the three charter members: ezrin, radixin, and moesin. These proteins contain a conserved actin-binding C-terminus and an N-terminal domain that anchors to transmembrane glycoproteins. Commonly, this is CD44, the receptor for the extracellular matrix component hyaluronan. ERM proteins exist in 2 conformations, open and closed, depending on intracellular cues. Elevated levels of PIP<sub>2</sub> open the conformation, permitting oligomerization and cross-linking (41-44, 46). Membrane associated proteins are discussed in more detail in section 1.5.2.

### ***1.2.2 Cytoskeletal structures of motility***

Cellular migration and invasion are critical to the development and survival of any organism. During embryogenesis, cells migrate, individually and as epithelial sheets, as they differentiate into new tissues. Notably, individual neural crest cells migrate long distances along the neural tube to colonize a wide variety of cell types in vertebrates. Gastrulation, the process in which the three embryonic germ layers are positioned, requires sheets of cells to move in a coordinated fashion. But these cell migrations are not limited to development; there are many motile cells that maintain the adult body as well.

Lymphocytes such as macrophages and neutrophils must home to sites of bacterial invasion, osteoclasts and osteoblasts crawl through bone, degrading and replacing tissue, and fibroblasts roam the stroma remodeling collagen networks. With the singular exception of swimming sperm, all motile cells in the human body migrate by crawling, a process which requires a dynamic and responsive network of sensors, signaling molecules, and structural filaments (41, 44, 48).

While the protrusive force at the leading edge of a migrating cell is provided by elongation of actin filaments, the microtubule network is also critical for efficient cell movement. Polarity is a pre-requisite for directional migration, and microtubules provide the asymmetric network that reorients the Golgi towards the leading edge. While disruption of microtubules does not impair the formation of protrusions, their distribution is scattered and does not result in a net directional migration. This is the result of lost polarity in signaling pathways and intracellular trafficking. Cdc42 activation not only controls actin polymerization, but also induces microtubule polarity and centrosome reorientation through the Par6/aPKC (atypical protein kinase C) complex (49, 50). Microtubules, as well as intermediate filaments, contribute to the turnover of adhesions, which is necessary for cellular migration.

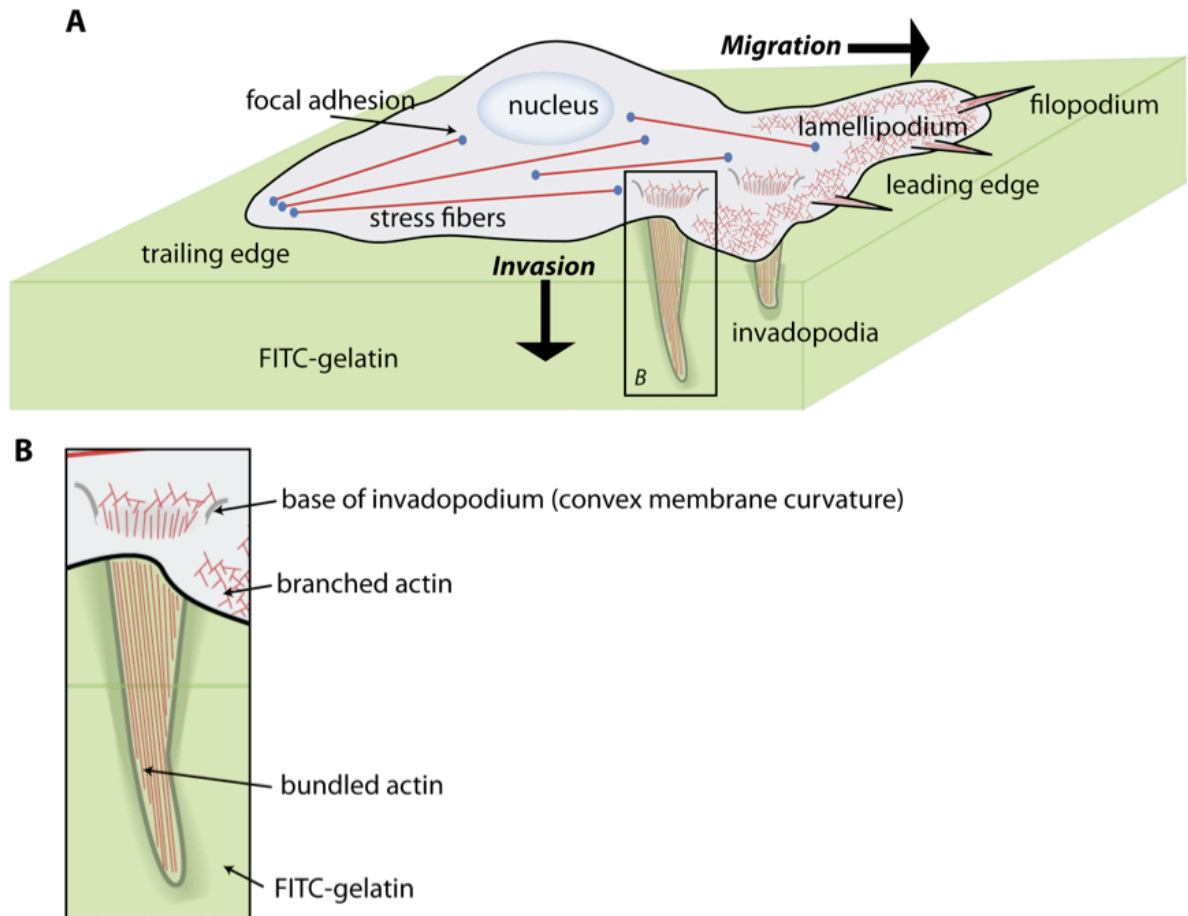


**Figure 2: Cytoskeletal structures of motility. A)** Three-dimensional rendering of a cell as it migrates across and invades a matrix-like substrate. The lamellipodium, which is enriched in highly branched actin filaments, is at the leading edge of the cell. From the lamellipodium emerge filopodia, sensory structures of bundled actin. Contractile stress fibers terminate at focal adhesions, which are being dissolved at the trailing edge of the cell. Invadopodia, also formed of bundled actin, emanate from the ventral face of the cell to invade and degrade the gelatin substrate. **B)** Higher-magnification view of an active invadopodia as it degrades a layer of FITC-gelatin. Bundled actin stretches the length of the invadopodia, but is dependent upon the branched actin at the base within the cell body.

Specialized structural organelles are formed by both motile and non-motile cells to interact with the surrounding environment (**Figure 2**). **Microvilli** are short protrusions of bundled actin from the apical face of absorptive epithelial cells in the gut, which greatly increase the available cell surface. Villin cross-linking is specific to microvilli. Crawling cells utilize a variety of specialized structural organelles to sense their environment and

locomote forward (**Figure 2**). The initial phase of migration requires forward protrusion, driven by polymerization and re-organization of actin into uni- or multi-dimensional arrangements. Along the leading edge of a migrating cell, a broad, flat extension known a **lamellipodium** expands out parallel to the substrate and adheres to propel the cell forward. These structures have been well studied in frog and fish keratocytes, demonstrating the dendritic nucleation model of Arp2/3-mediated actin branching. Microinjection of fluorescent-actin into these structures has demonstrated array treadmilling, in which the filaments turnover within the network (51). Just behind the branched actin of the lamellipodium, resides a more stable, progressive lamellum. **Ruffles** are similar sheet-like protrusions of the membrane, but are distinguished from lamellipodia by their lack of substrate adhesion, resulting in migration of the ruffle rearward up the dorsal surface of the cell (42). Whereas lamellipodia provide the main thrust of migration, **filopodia** serve as “directional sensors” to sense the extracellular environment at the far leading edge. Filopodia are thin (less than 200nm in diameter), finger-like projections of bundled actin that are extended by migrating fibroblasts and neural growth cones.

Three-dimensional actin growth at the leading edge creates **pseudopodia**, which are short protrusions seen primarily in amoebae and neutrophils. Adhesive structures anchoring the migrating cell to the underlying substrate must also be dynamic; new adhesions must be established at the leading edge of the lamellipodium while older adhesions along the rear of the cell must be broken for retraction of the cell body. Protruding lamellipodia that fail to adhere are swept up on the dorsal face of the cell as membrane ruffles and carried back to the cell body. Focal adhesions link the extracellular matrix to the stress fibers of the actin cytoskeleton via transmembrane integrins. Sensing the substrate and tensions, integrins cluster and activate the focal adhesion kinase (FAK) via Src (tyrosine kinase). This signaling pathway is critical for cell survival, growth, proliferation, and migration (43, 52, 53).

|                 | <b>Podosomes</b>  | <b>Invadopodia</b>                |
|-----------------|---|-----------------------------------|
| Cell type       | Macrophages,<br>osteoclasts<br>Endothelial cells  | Invasive cancer cells             |
|                 | Src-transformed fibroblasts   |                                   |
| Components      | Bundled F-actin<br>Actin-associated (cortactin, N-WASp, Arp2/3)<br>Adhesion (FAK, talin, paxillin, vinculin)<br>Src family kinases, phosphotyrosine |                                   |
| Number / cell   | 20 – 100  | 1 – 10                            |
| Size (max)      | 1 $\mu\text{m}$ x 0.4 $\mu\text{m}$   | 8 $\mu\text{m}$ x 5 $\mu\text{m}$ |
| Persistence     | 2 – 12 min  | Up to 1 hr                        |
| ECM degradation | +   | +++                               |

**Table 1: Comparison of podosomes and invadopodia.** Despite sharing many of the same components, podosomes and invadopodia are differentiated by their size, behavior, and the cells in which they are found.

Some adult cells must invade tissues to perform their normal functions. These cells have developed specialized cytoskeletal structures to facilitate their unique method of migration. **Podosomes** are finger-like extensions found on the basal surface of the cell that mediate adhesion to the extracellular substrate via integrins. Podosomes are built of a central core of bundled F-actin around which lies a characteristic ring of accessory proteins that includes adhesion-related proteins such as integrins and vinculin. Also within the actin-dense core are actin-regulators such as (N-)WASp and Arp2/3. Cortactin is also present in podosomes, possibly acting as a scaffolding protein for N-WASp and Arp2/3 (54). Whereas podosomes are described primarily in monocyte-derived cells such as macrophages and osteoclasts, similar structures known as **invadopodia** have been described in Src-transformed fibroblasts and cancer cells (**Table 1**) (41, 42, 44, 54-58).



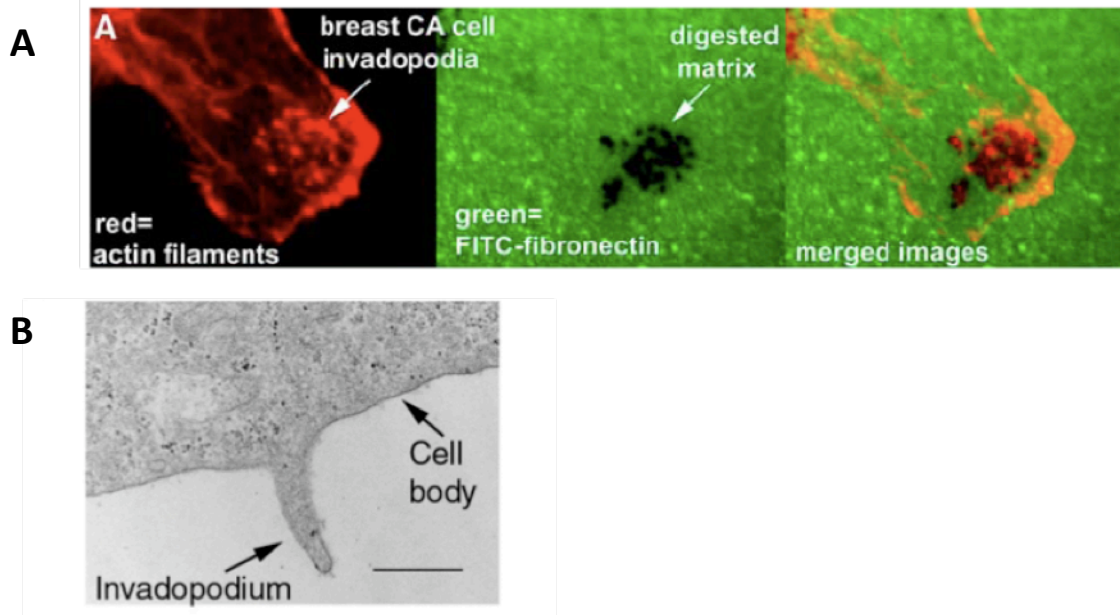


**Figure 3: Formation of invadopodia over gelatin substrate. A)** Formation of invadopodia by breast cancer cell grown on FITC-fibronectin substrate Reprinted with kind permission from Springer Science+Business Media: Clinical and Experimental Metastasis, Invadopodia: specialized cell structures for cancer invasion, 23, 2006, 97-105, A.M. Weaver, Figure 1. **B)** Electron micrograph of invadopodia invading gelatin layer from a cancer cell. Scale bar = 500 nm. Reprinted from Current Biology, 18 (9), A.M. Weaver, Invadopodia, R362-4, Copyright (2008), with permission from Elsevier.

### 1.2.3 Structure and signaling of invadopodia

The terms podosome and invadopodium have been used interchangeably in reference to protrusive structures formed by Src-transformed fibroblasts (59-61). Some reports have speculated podosomes to be precursors to invadopodia, although no evidence has been found to support this theory. Others argue them to be distinct organelles, dependent on the cell type or extracellular environment. Invadopodia are typically much larger, longer-lived, and fewer in number. Both are enriched in matrix-metalloproteases, specialized proteins for ECM degradation, although invadopodia are much more capable of degrading matrix (**Figure 3**) (41, 42, 44, 54-58, 62, 63). **Table 1** summarizes the common features and differences between podosomes and invadopodia (54).

Although the membrane protrusion of invadopodia is driven by bundled actin, this structure is dependent on a base of branched actin similar to the actin structures found in lamellipodia. Because of their similar structures, it's no surprise that podosomes and invadopodia would share many of the same actin regulatory proteins, including Arp2/3, N-WASp, cortactin, cofilin, and dynamin-2. In addition to cortactin and N-WASp, several other Src-targeted proteins, like FAK, p130Cas, and Tks5/FISH, are also common to both (54, 58). A high concentration of phospho-tyrosine is found in invadopodia (64), suggesting elevated Src activity. In the dynamic podosomes, microtubules are critical to their rapid turnover and patterning. The more stable nature of invadopodia, however, limits their reliance on the microtubule network for formation. Intracellular trafficking along microtubule networks may be necessary for delivery of proteinases for matrix degradation (53, 54).

Cortactin: The role of cortactin in invadopodia formation has been studied in more detail and is required for the early-stages of formation (56, 65, 66). Studies have implicated cortactin as a central scaffolding protein that brings together many of the proteins required for invadopodia maturation (55, 56, 65, 67, 68). Cortactin, in synergy with N-WASp, potentiates Arp2/3 activation and stabilizes Arp2/3-dependent branched actin structures (69). More recently, Clark *et al* also demonstrated a role for cortactin in targeting the metalloproteases MMP2 and MMP9 for secretion (56).

Cdc42/NWASp: Overexpression of components of this pathway, including Cdc42 and Arp2/3 subunits, has been described in invasive mammary tumors (70). Using MTLn3 mammary rat adenocarcinoma cells, Yamaguchi (68) demonstrated that endogenous N-WASp localizes to invadopodia and is required for invadopodia formation (per siRNA and dominant negative experiments). Using a FRET-based biosensor, Lorenz (71) demonstrated that N-WASP is unfolded, and therefore active, at the base of nascent invadopodia. Other WASP family members WAVE1 and WAVE2 do not localize to invadopodia (68). Nck1, an upstream activator of N-WASp, and WIP, the WASP-interacting protein which binds and stabilizes (N-)WASP, also concentrate at invadopodia

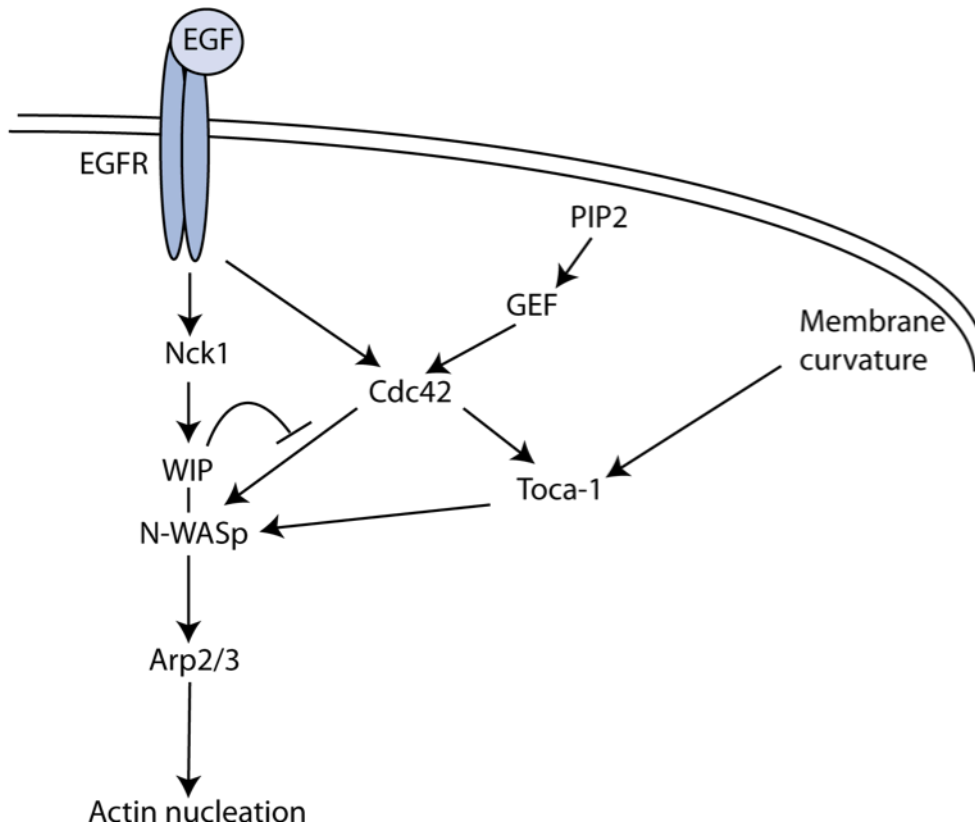


**Figure 4: Signaling pathways of invadopodia formation.** The WIP-NWASp complex is activated downstream of EGFR through Nck1 and Cdc42. Toca-1 also increases N-WASp activation in response to curved membranes. N-WASp activity promotes Arp2/3, leading to branched actin nucleation, a requirement for early invadopodia formation.

and are required for their formation (68). Active, GTP-bound Cdc42 is also required for invadopodium formation (68).

In cultured cells, invadopodia are routinely identified by co-localization of degraded substrate with actin and cortactin. Similarly, N-WASP and Cdc42 are co-localized with invadopodia (54, 55, 65, 68, 71).

EGFR: EGF stimulation promotes the formation of invadopodia, presumably through this Cdc42-N-WASP pathway (**Figure 4**) (68, 71). EGF stimulation of cells

expressing an N-WASp biosensor elicits a spike in N-WASp activation at the cell periphery in response to EGF stimulus (71). Inhibition of EGFR (using AG1478) decreased invadopodia formation in rat mammary adenocarcinoma cells (68). This correlates with previous studies showing that EGFR inhibitors block invasion of cancer cells (72, 73). Most recently, DesMarais *et al* demonstrated that cells preferentially form early stage invadopodia on the side closest to an EGF source (74).

ECM remodeling: In addition to becoming motile, invading cancer cells also acquire the ability to break through the basement membrane separating the tumor from the endothelial cells of nearby blood vessels. Invadopodia are also sites of concentrated protease secretion, allowing them to degrade the extracellular matrix and facilitate cellular migration through a basement membrane (55, 68, 75, 76). ECM degradation is mediated by matrix-metalloproteases and both transmembrane proteases (MT1-MMP and seprase) and secreted proteinases (MMP2 and MMP9) are enriched at invadopodia (56).

In vitro modeling: The formation of invadopodia can be visualized in detail in cells grown in culture over a gelatin matrix (**Figure 3**), and studies have demonstrated a strong correlation between formation of these structures *in vitro* and metastasis *in vivo* (66, 77, 78). Only invasive tumor cells form Invadopodia, with the basal-type breast cancer cell line MDA-MB-231 being one of the most extensively studied human lines (54, 58). Most studies of invadopodia have been carried out using carcinoma cell lines, specifically MTLn3 rat adenocarcinoma and MDA-MB-231 breast cancer cell lines. However, invadopodia have also been observed in primary human HNSCC tumors cultured on a fibronectin substrate (56). Recently, DesMarais *et al* also demonstrated the formation of early stage invadopodia by MTLn3 cells grown on glass without any gelatin or fibronectin substrate (74).

## 1.3 SRC

### 1.3.1 History of Src research

The first form of Src (v-src) was identified as the virally-encoded transforming gene responsible for chicken sarcomas. Peyton Rous isolated the causative virus in 1911 from filtered fluids extracted from the tumors and demonstrated the induction of new tumors in healthy chickens injected with the virus. Infection of cultured cells also induced transformation, leading to the search for the oncogenic mechanism of the virus, now called Rous sarcoma virus (RSV). By 1977, the encoded v-Src protein was isolated by Joan Brugge and Ray Erikson, the first and one of the most potent oncogenes identified. Transfection of v-Src into cultured cells induces shifts in gene expression, alters cellular morphology and adhesion, and increases migration.

Research by Michael Bishop and Harold Varmus identified a cellular form, dubbed c-Src, in normal chicken cells. This normal version of Src, homologs of which have been identified in nearly every species, is known as a proto-oncogene, the non-mutated precursor of an oncogene. Src was also the first tyrosine kinase to be characterized and functions in a wide variety of signal transduction pathways. Under normal conditions, c-Src is non-transforming. However, activating mutations in c-Src can shift the regulatory balance and induce some hallmarks of transformation such as anchorage- and growth factor-independent growth. The potent transforming effects of v-src demonstrate the need for tight regulation of this kinase in normal cells. Therefore, much subsequent research focused on the comparative structure and regulation of the v- and c-Src kinases (79).

### ***1.3.2 Structure and regulation of Src***

The regulation of Src is dependent on its structure, which is comprised 2 protein-interaction domains, SH2 and SH3, and a catalytic domain (**Figure 5**). Activity of normal c-Src is tightly regulated through the auto-inhibitory folding that results from the intramolecular interaction between the short, regulatory domain at the carboxyl terminus and the internal SH2 domain. This conformation is controlled by the balance of two tyrosine phosphorylation sites: Tyr416 (Tyr419 in human Src) and Tyr527 (Tyr530 in human Src). Phosphorylation of Tyr527/530 in the regulatory domain by Csk (C-terminal Src kinase) inactivates Src by maintaining the auto-inhibitory interaction with the SH2

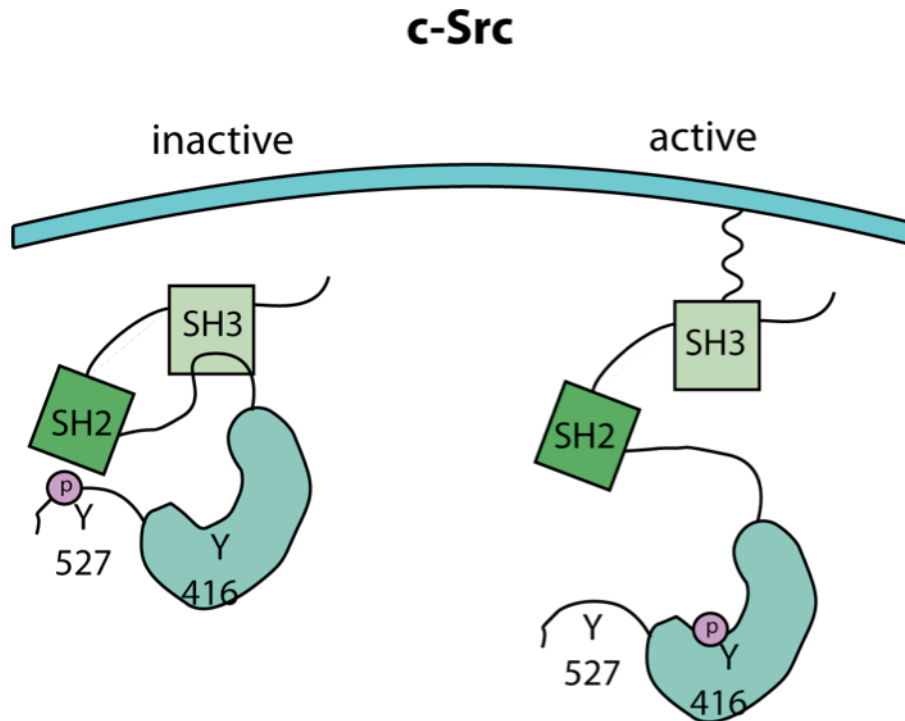


**Figure 5: Regulation of c-Src.** Intramolecular interactions between Tyr527 in the regulatory domain and the internal SH2 domain, as well as between the SH3 and linker region, maintain inactive Src in its closed conformation. Dephosphorylation of Tyr527 alleviates the interaction and allows for auto-phosphorylation of Tyr416 in the kinase domain of open, active Src.

domain. An additional intramolecular interaction between the SH3 domain and the short linker region between the SH2 and catalytic domains further strengthens the closed conformation. Tyr416/419 in the kinase domain is auto-phosphorylated in active, open Src. An analogous tyrosine residue is found within the activation loop of all other tyrosine kinases. The constitutive activity of v-Src results from the loss this tight regulation due to the deletion of the regulatory domain, keeping Src in the open, active conformation.

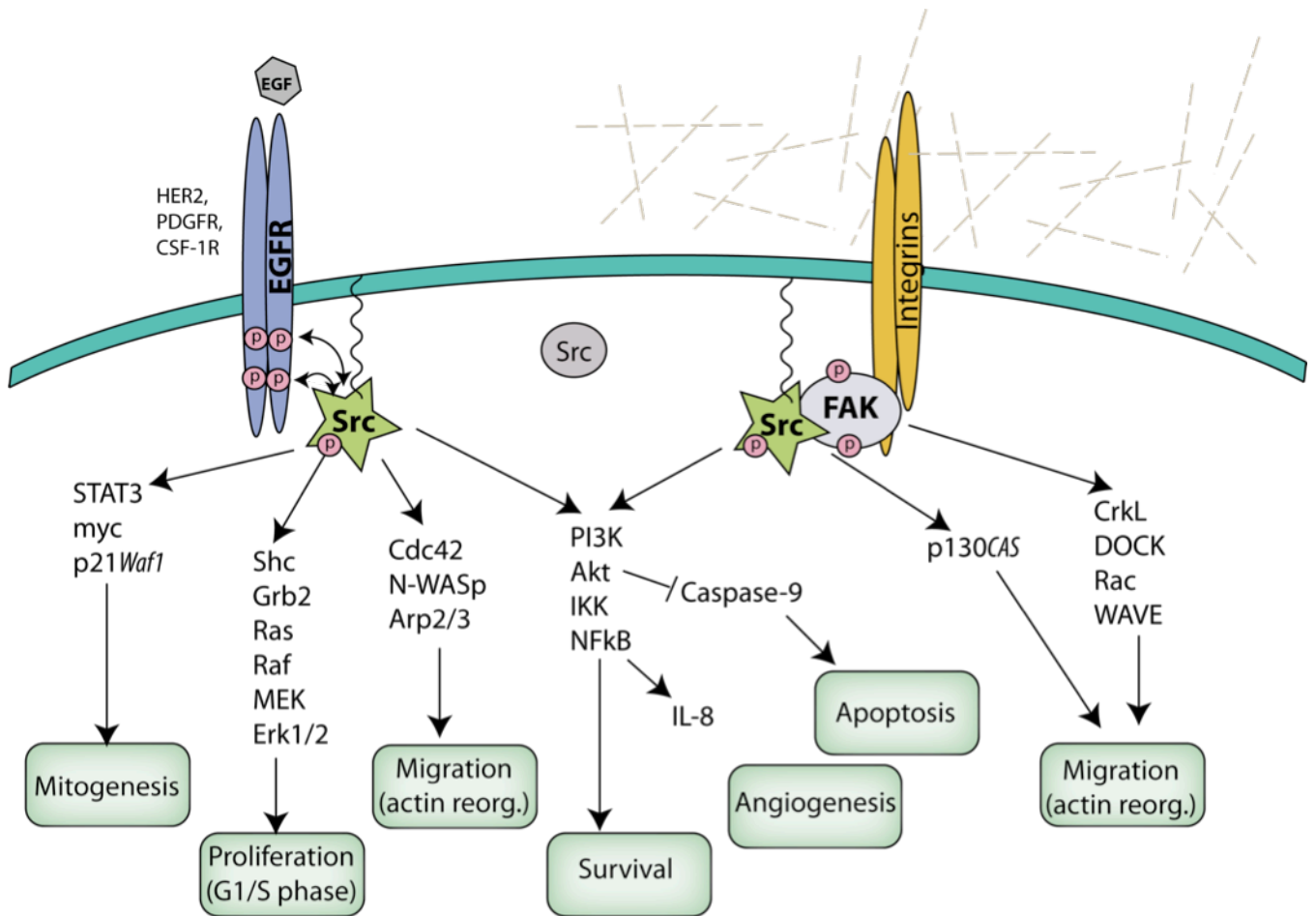


**Figure 6: Src-dependent signaling pathways.** Src activity is critical to many signaling pathways, leading to a wide variety of cellular functions, including mitogenesis, proliferation, survival, angiogenesis, apoptosis, and actin reorganization. Active growth factor receptors, such as EGFR, promote Src activation. Src may also be activated in complexes with FAK downstream of integrins.

### 1.3.3 Src and cytoskeletal reorganization

The tyrosine kinase function of Src is involved in many signaling pathways, including those that control the cytoskeleton (**Figure 6**). The cytoskeleton plays a large role in modulating the activity of Src. Intracellular localization of Src correlates with its activation state. Inactive Src is sequestered at the perinuclear region of the cell in

association with the microtubule network. However, active Src translocates to the plasma membrane where it associates with actin via the SH3 domain. Myristilation at the amino-terminus also interacts with the plasma membrane. This translocation is not dependent on an intact Src kinase domain (80). Src is recruited to focal adhesions through its interaction with the **F**ocal-**a**dhesion **k**inase (FAK), which stabilizes the open conformation of Src and encourages Src activity. The FAK-associated adaptor protein p130<sup>CAS</sup> may play a similar role (81). Src-null fibroblasts and osteoclasts have severe cytoskeletal defects, including lost adhesion and rounding. These phenotypes can be rescued even by kinase-deficient Src mutants, indicating a kinase-independent role for Src in maintaining the cytoskeleton. However, rescue of migratory defects does require the activity of Src at the plasma membrane and at focal adhesions (82). Phosphorylation of Src-targets at peripheral adhesion sites, such as FAK and p190rho-GAP, is necessary for focal-adhesion turnover, a pre-requisite of cellular migration. Fibroblast that are deficient in either FAK or Src are non-motile and have enlarged adhesions, presumably due to lost turn-over (81). FAK is also capable of phosphorylating N-WASp at Tyr256 leading to actin nucleation through the Arp2/3 complex (83). Additionally, cells that are lacking a kinase-competent Src are unable to polarize towards a chemoattractant (81).

Src also phosphorylates the actin cross-linking protein cortactin, which stabilizes Arp2/3-mediated actin assembly (81). Src phosphorylation of cortactin decreases its ability to bind actin, leading to impaired cytoskeletal rearrangement (84). Recent studies of cortactin have demonstrated its central role in the organization of specialized invasive structures (56, 65, 66).

## **1.4 CELLULAR REGULATION OF CDC42 AND N-WASP ACTIVITY**

### **1.4.1 *Rho GTPases***

The Rho family of GTPases is a subset of the larger Ras family of proteins, which function as integration points for the control of cytoskeletal regulatory proteins. Rho GTPases are important in many cellular functions, including cell cycle progression, cell division, cell polarity, and migration. (Reviewed by (85) and (86)). Although there are



over 20 known members of the Rho GTPase family, there are three that are well characterized: Cdc42 (cell division cycle 42), Rac1 (Ras-related C3 botulinum toxin substrate 1), and RhoA (Ras homologous member A). These molecular switches are downstream of several different G-protein coupled receptors and receptor tyrosine kinases (87)

Switching mechanism of small GTPases. GTPases exist in two states: the inactive, GDP-bound state and the active, GTP-bound state. In the active state, GTPases bind and regulate effector proteins. Upon hydrolysis of the bound GTP molecule, the GTPases revert to an inactive conformation. Although GTPases possess the intrinsic ability to hydrolyze GTP, specific GTPase-activating proteins (GAPs) promote GTPase hydrolytic activity and subsequent inactivation. Alternatively, guanine nucleotide exchange factors (GEFs) catalyze the opposite reaction, in which a GDP molecule is exchanged for a GTP molecule to activate the GTPase again. Activation of small GTPases is blocked by guanine nucleotide dissociation inhibitors (GDIs), which sequester GDP-bound forms of the small G proteins in the cytosol. Constitutively active GTPase mutants impair the hydrolytic activity of the GTPases, thereby locking them in the GTP-bound state (85, 86, 88).

Rho GTPase activation induces a variety of cellular behaviors, including transcriptional regulation and cell cycle progression. Cytoskeletal reorganization for polarity and migration are heavily dependent on the regulation provided by RhoGTPases.

#### ***1.4.2 Cdc42 Functions and Effector Proteins***

Polarity Polarization is fundamental to many cellular processes, including division, secretion, and migration, and is typically dependent on external signals. Polarity is also established by localized recruitment of Cdc42 to activated receptors, as well as activated cell adhesion molecules (89). Cell-cell contact activates Cdc42 through nectin and E-cadherin leading to generation of apical and baso-lateral surfaces (90). Cdc42 is also critical to the polarization of T cells towards the immunological synapse formed during interaction with an antigen-presenting cell. Upon activation of the T-cell receptor, Cdc42 and its effector protein WASP are recruited to promote localized actin polymerization and

generation of the synapse. Additionally, the MTOC and Golgi are re-oriented towards the synapse for the delivery of secretory vesicles, a process that is dependent on Cdc42 activity (89). Chemotactic cells also polarize in a similar manner to soluble factors. Chemokines such as EGF and PDGF bind and activate cell surface receptors, recruiting Cdc42 to the plasma membrane and activating Cdc42 via the Src pathway (91-93). For motile cells, the initial step in mesenchymal-type migration is polarization to define the regions of protrusion at the leading edge and retraction of the cell body at the trailing edge.

Migration Active, GTP-bound Rac accumulates at the leading edge of migrating cells and establishes a positive-feedback loop between PIP<sub>3</sub> and PI3-kinase (63). Activation of PI3K results in increased PIP<sub>3</sub> at the plasma membrane and activation of Rac and Cdc42. In advancing lamellipodia, Rac induces actin polymerization via the effector protein WAVE and activation of the Arp complex. Rac can also activate the LIM-kinase in lamellipodia to phosphorylate and inhibit cofilin activity effectively stabilizing actin filaments. Downstream of Rac and Cdc42, the cross-linking protein IQGAP may function to stabilize the actin meshwork. Although Cdc42 is not required for formation of lamellipodia, it does contribute to the protrusion of filopodia from the leading edge. This occurs through the activation of the Cdc42 effector protein, N-WASp, a promoter of Arp2/3 activation and actin polymerization. Rho functions primarily in contractile forces filaments and also participates in lamellipodia activity in hepatocyte growth factor (HGF)-stimulated KB cells. Interestingly, there is also complex cross talk between Rho, Rac, and Cdc42. In general, the cell body retraction at the rear of the cell is dependent on Rho signaling through ROCK and MLC phosphorylation to create actin-myosin contractile bundles (42, 86, 88).

Effector proteins Active GTPases mediate their responses through a wide variety of effector proteins. Many of these proteins have been identified through yeast 2-hybrid screens and contain the classical Cdc42/Rac-interactive binding (CRIB) domain. Rac and Cdc42 share many of the same targets, such as IQGAP and PAK1-3, which mediate actin reorganization, cell-cell adhesion, and stress-fiber formation. Cdc42 plays a unique role in

filopodia and invadopodia formation through its effects on the WASP/N-WASP proteins (85, 88).

### 1.4.3 N-WASP Family and Regulation

WASP family Wiskott-Aldrich Syndrome (WAS) is a rare, X-linked disorder characterized by eczema, thrombocytopenia, and immunodeficiency. Mutations in the gene for the WAS protein (WASP) typically result in premature truncation of the protein, leading to severe platelet and immune system defects. WASP expression is restricted to hematopoietic cells, while the closely related neural-WASP (N-WASP) is ubiquitously expressed. Another related set of proteins was named the WASP family verprolin homologous protein (WAVE) 1-3, also known as SCAR1-3 (suppresses abnormalities of cAR loss) (94, 95). N-WASP was the first to be linked with actin polymerization as an intermediate effector between Cdc42 and Arp2/3 (96).

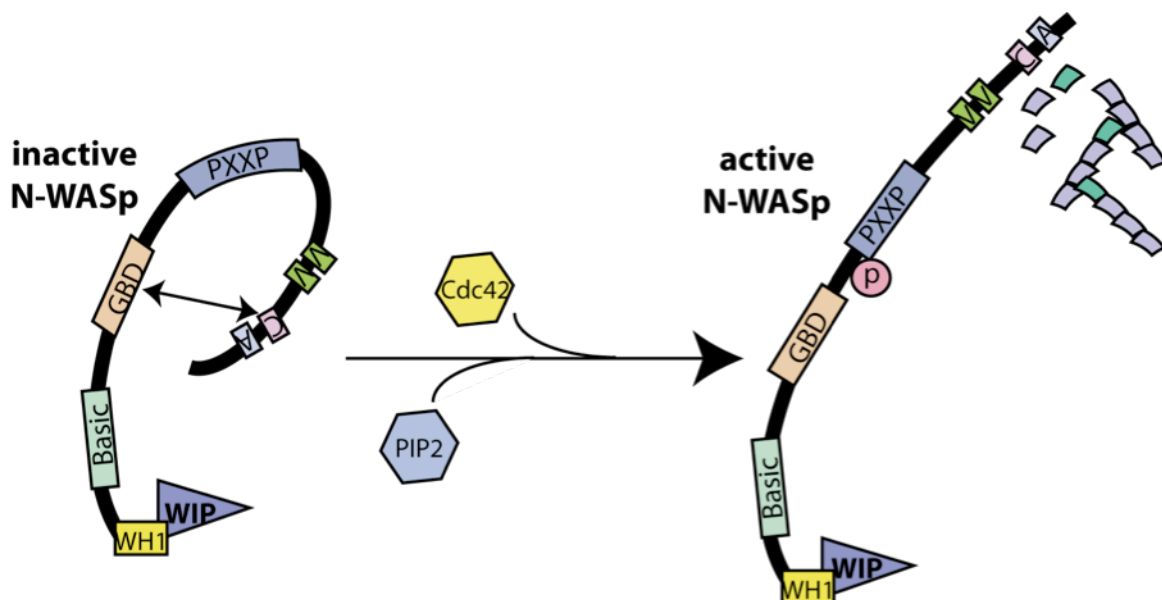


**Figure 7: N-WASp structure and regulation.** Intramolecular interaction between the connecting regions (C) and the GTPase-binding domain (GBD) maintain N-WASp in a closed, inactive state. Cdc42 and PI(4,5)P<sub>2</sub> cooperatively relieve the inhibitory conformation, activating N-WASp. Open N-WASp, which is accessible to phosphorylation by Src, is able to activate Arp2/3 and induce actin polymerization.

Conserved across the five family members (WASP, N-WASP, WAVE1-3) is the C-terminal

WCA domain (**Figure 7**). This is actually a collection of three distinct regions, the WH2 (W) domain, a connecting region (C), and the acidic domain (A). N-WASP is the only family member that varies from this organization by having a second WH2 domain, although its function is unknown. The WH2 domain, in close proximity to the Arp2/3 binding site within the acidic A region, binds actin monomers. The connecting (C) region is responsible for the auto-inhibitory folding conformation by binding to a central CRIB domain. Binding of active Cdc42 to the CRIB (also known as GBD, GTPase binding domain) displaces the C region, opening and activating N-WASP (95, 97). Once open, N-WASP can bind Arp2/3, increasing Arp2/3's affinity for ATP and promoting actin nucleation (47, 94, 98). Flanking the CRIB domain are poly-lysine (BR, basic region) and poly-proline domains to which other regulatory proteins and adaptors bind. PI(4,5)P<sub>2</sub> binds to the BR and with Cdc42 can synergistically activate N-WASP. SH3-containing adaptor proteins such as Nck2 and Grb2 bind the proline-rich region, presumably to link N-WASP to activated receptor tyrosine kinases (RTKs) such as epidermal growth factor receptor (EGFR). The tyrosine kinases Src and Fyn also bind here, although the function of N-WASP's tyrosine phosphorylation sites is still not understood. N-WASP may be able to integrate the signaling pathways of GTPases with tyrosine kinases in the regulation of actin nucleation (95, 97, 99, 100). The Cdc42-interacting protein, CIP4, also interacts with N-WASP through the proline-rich domain via its own SH3 domain (101, 102). The WASP interacting protein (WIP) binds to N-WASP at the WH1 domain and can interfere with Cdc42-mediated activation of N-WASP (103). However, its presence also seems to be required for efficient activation of N-WASP by Toca-1 (**transducer of Cdc42-activation-1**) (104, 105).

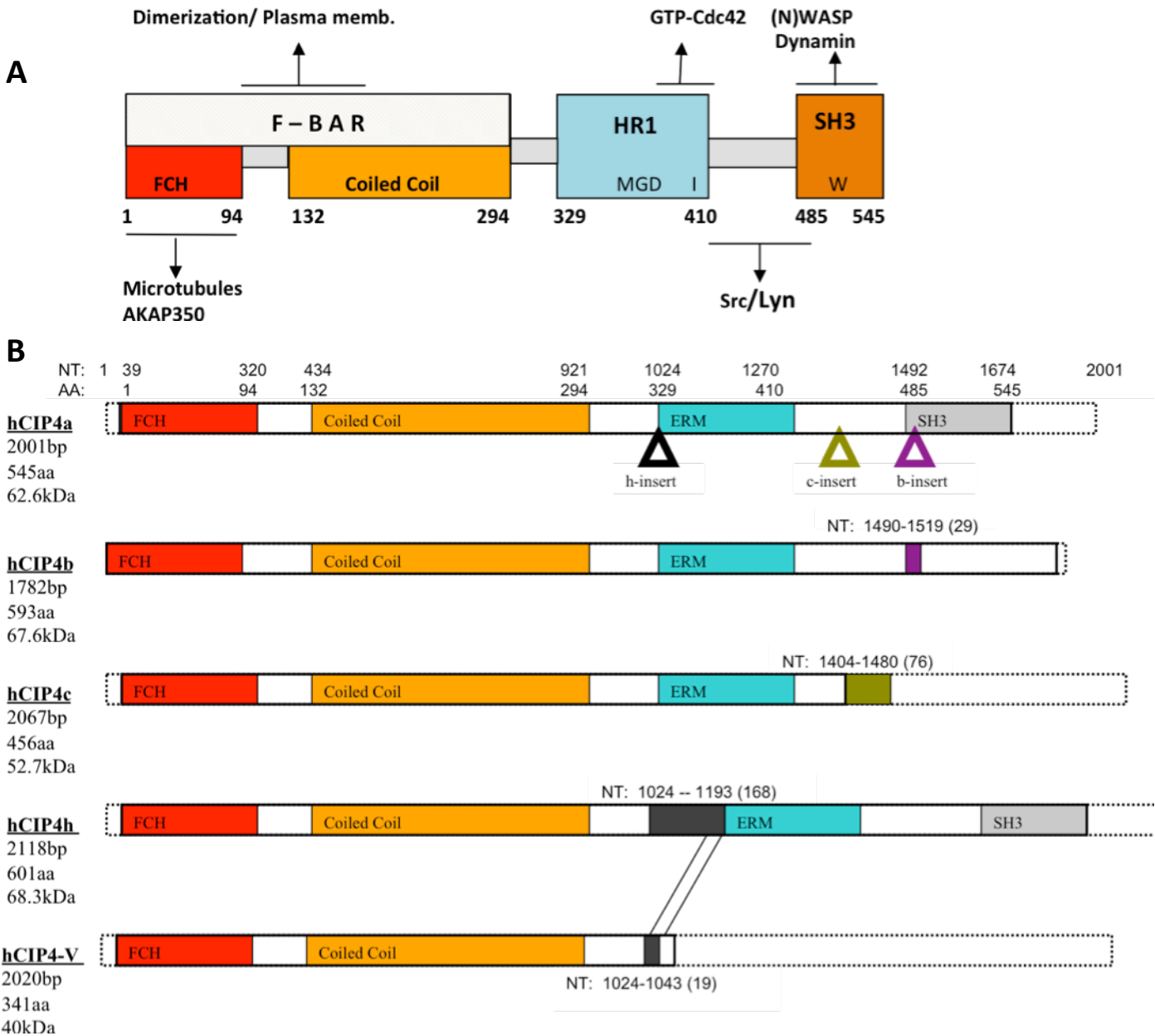


**Figure 8: Structure and isoforms of CIP4. A)** Domains and protein interactions of human CIP4a. Amino acid positions are shown below each domain. MGD, I, and W are conserved residues amongst CIP4 and Toca-1. Mutations in MGD or I abrogate binding to Cdc42, where as mutation of W in the SH3 impairs N-WASp interaction. **B)** Structure of CIP4 isoforms. Dotted outline represent mRNA, solid outline represents protein. Inserts, represented by triangles under CIP4a, are the result of retained intronic sequences. Resulting isoforms are also diagrammed.

## 1.5 CIP4 AND THE F-BAR FAMILY

### 1.5.1 Characterization of CIP4

The Cdc42-interacting protein **4** (**Figure 8a**) was originally identified through yeast-2-hybrid screens for novel binding partners of the RhoGTPase Cdc42 (101), WASP (106), and the Src family kinase Lyn (102). It was immediately characterized by its unique amino-terminal coiled-coil domain, which was termed FCH (**F**ER-**C**IP4 **h**omology), analogous to the coiled-coil domain of the actin-associated protein Cdc15 in *S. pombe*. Subsequently, the carboxyl-terminal SH3 domain was shown to interact with WASp and mediate its binding to microtubules (106). Interaction between CIP4 and N-WASp is necessary for podosome formation in macrophages (107). Alternative isoforms of CIP4 have been identified that lack a functional SH3 domain due to retained intronic sequences near the Cdc42 binding region (**Figure 8b**) (102, 108, 109).

The HR1 domain, an internal coiled-coil motif with homology to the protein kinase C, mediates binding of CIP4 to GTP-Cdc42, not a classical Cdc42-binding CRIB domain. Point mutation of the isoleucine at 398 within the HR1 abrogated Cdc42 binding (106). Two proteins closely related to CIP4 have since been identified, namely **F**ormin **b**inding **p**rotein **17** (FBP17) and **t**ransducer **o**f **C**dc42 **a**ctivation **1** (Toca-1). These proteins share similar FCH and SH3 domains and bind N-WASp and dynamin via their SH3 domains (**Figure 9**) (105, 110). Toca-1 and FBP17 also share similar HR1 regions, however mutation of the analogous isoleucine in Toca-1 did not interrupt Cdc42 binding, but required triple mutation of the adjacent MGD sequence (105). FBP17 does not bind Cdc42 (111). Toca-1 also potentiates the Cdc42-dependent activation of N-WASp mediated actin nucleation (105, 110). Functional studies of these proteins are still limited.

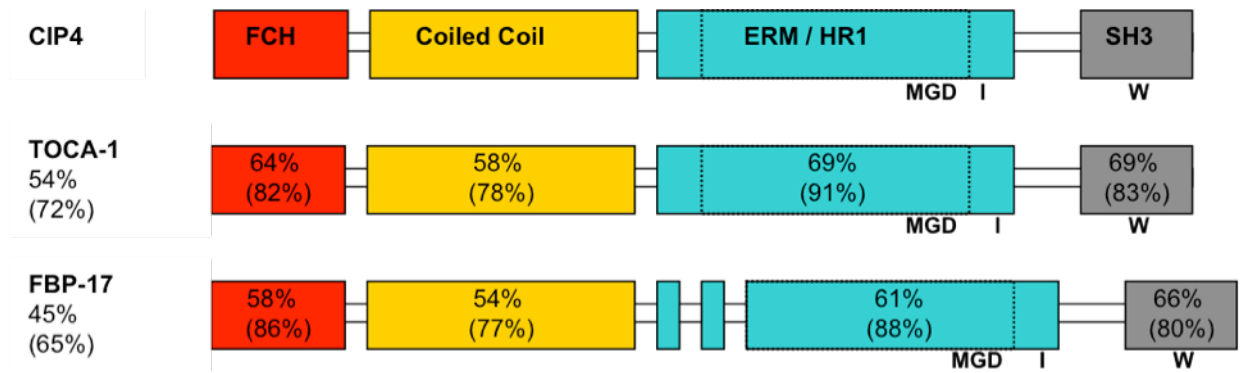


**Figure 9: F-BAR family of proteins.** Homology of CIP4, Toca-1, and FBP17 at protein and mRNA (parentheses) sequence levels. Significant conserved residues are noted: MGD and isoleucine (I) residues in HR1 domain are necessary for Cdc42 binding. Conserved tryptophan (W) is critical for N-WASp interaction.

Recently, our understanding of the N-terminal region has evolved greatly. Tsujita *et al* demonstrated the weak homology of the coiled-coil domain to the BAR (Bin-amphiphysin-Rvs) family of proteins. Like other members of the BAR family, this structure can induce the tubulation of membranes (112, 113). In tandem, the N-terminal **FCH** and **BAR** regions comprise the F-BAR domain (also known as EFC for **e**xtended **FCH**), a subgroup of the larger BAR family that is characterized by a shallower curvature (112, 114, 115). BAR proteins (lacking the FCH) and I-BAR proteins (inverse-BARs) function by the same mechanism, but have different degrees of curvature, producing different diameters of membrane tubules (116, 117).

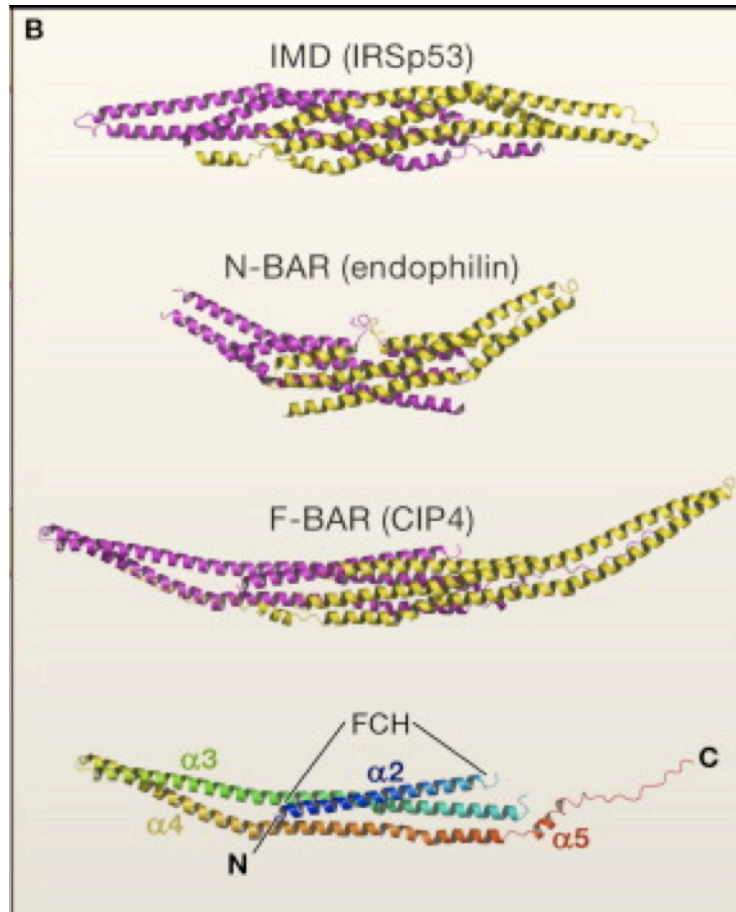


**Figure 10: Ribbon structure of dimerized BAR domains.** From top: I-BAR (IMD/IRSp53), BAR/N-BAR (endophilin), and F-BAR (CIP4). Bottom diagram indicates individual helices and FCH region of F-BAR domains. Reprinted from Cell, 129, K. Fütterer and L.M. Machesky, “Wunder” F-BAR Domains: Going from Pits to Vesicles, 655-657, Copyright (2007), with permission from Elsevier.

### 1.5.2 BAR Domains and membrane curvature

Effective cell shape change requires not only the forces provided by the actin cytoskeleton, but also molding of the cell membrane. Proteins of the BAR (**B**in-**a**mphiphysin-**R**vs) superfamily, which are capable of binding and/or inducing membrane curvature, are the convergence point for RhoGTPase signaling, actin remodeling, and membrane dynamics. The BAR structure that is shared by all members of the superfamily is defined as a coiled-coil region with a positively charged surface. The 3 repeated alpha-helices of each domain form a hydrophobic, curved structure (**Figure 10**) that mediates



dimerization and interacts with the negatively-charged lipid membranes, preferably phosphatidylserine (118). In most members of the BAR family, this cationic face rests on the concave side of a crescent-shaped structure. This arrangement is typical of the “classical” BAR and F-BAR (FCH-BAR) subfamilies, whereas proteins of the I-BAR family are inverted with a positively charged convex surface (**Figure 10**) (112, 114, 115). The subfamilies of the BAR superfamily are characterized by the degree of curvature created in the dimerized molecule, which specializes the proteins to a distinct membrane structure. For instance, the BAR proteins are associated with endocytic vesicles, whereas the F-BAR proteins, which have a shallower curvature, are associated with the thinner neck of vesicles as they separate from the plasma membrane (116, 119). The unique inverted structure of I-BAR proteins is associated with the opposite curvature found in membrane protrusions (120, 121). Homologous proteins are conserved in yeast; Cdc15 in fission yeast is found at the contractile actomyosin ring as daughter cells separate (122, 123).

Overexpression of BAR domains, either in isolation or within full-length proteins, is sufficient to induce membrane tubulation (112, 113, 124). However, some studies suggest that BAR domains are “curvature sensing” and bind membranes which are already deformed (125). These two arguments are not mutually exclusive: BAR domains binding to curved membranes will be induced to dimerize, recruiting additional BAR-containing proteins, and in turn inducing additional membrane curvature (116). These mechanisms may also be repeated in caveolae-dependent endocytosis.

Aside from their membrane-interacting regions, BAR proteins also commonly associate with the actin cytoskeleton and cytoskeletal regulatory proteins such as N-WASP/WAVE and dynamin. The interaction between BAR proteins and the cytoskeleton has been best described in clathrin-mediated endocytosis, specifically in the recruitment of dynamin to promote membrane scission (115, 126, 127). F-BAR proteins CIP4 and FBP17 both bind N-WASP and dynamin-2 via carboxy-terminal SH3 domains. Toca-1 and FBP17 are both inducers of membrane curvature-dependent actin polymerization (126, 127).

### 1.5.3 TOCA-1 and Actin Polymerization

N-WASp activation is dependent on its interaction with GTP-Cdc42 and PIP<sub>2</sub> (**Figure 7a**) (for detailed discussion, see section 1.4.3). Similar to CIP4, Toca-1 binds GTP-Cdc42 through the internal HR1 motif and interacts with N-WASp via the C-terminal SH3 domain (105). Actin polymerization assays can be used to infer the activation state of N-WASp by quantifying the rate of pyrene-actin assembly in cell-free systems. Using this method, Ho *et al* demonstrated that depletion of Toca-1 from *xenopus* egg extracts decreased N-WASp-mediated activation of Arp2/3 and actin polymerization (**Figure 7b**) (105). Whereas purified wild-type Toca-1 rescued the phenotype, mutated Toca-1 proteins, deficient in either N-WASp or Cdc42 binding, were unable to restore actin polymerization. A constitutively active mutant of N-WASp does not require Toca-1 to induce actin polymerization, confirming that N-WASp is downstream of Toca-1 (105). These results were also repeated by observing actin comet formation on the surface of endomembrane vesicles in the presence of Toca-1 depleted cell extracts (105). Takano *et al* utilized liposomes to demonstrate that FBP17 and Toca-1 induce activation of N-WASp (in complex with WIP) and actin polymerization that is dependent on membrane curvature (127). Interestingly, this effect was dependent on a conserved sequence of acidic residues adjacent to the SH3 domain, suggesting the conformation of FBP17/Toca-1 is critical to its function.

## 1.6 HYPOTHESIS AND MODEL

F-BAR proteins are known to function at the plasma membrane to sense and induce membrane curvature through dimerized BAR domains, amphipathic crescent shaped regions at the N-terminus. CIP4 and Toca-1 also bind the RhoGTPase Cdc42 through a central HR1 domain and N-WASp via their c-terminal SH3 domains. While F-BAR proteins have typically been implicated in endocytosis, I propose that there is also a role for the concave-binding regions of F-BAR proteins in membrane protrusion. FBP17, which is closely related to CIP4 but unable to bind Cdc42, contributes to podosome formation in macrophages (128). Toca-1, which is structurally very similar to CIP4, stimulates Arp2/3-mediated actin polymerization through Cdc42-dependent activation of

N-WASp (105). Cell-free models demonstrated that liposome binding of FBP17 and Toca-1 increased N-WASp-mediated actin polymerization, suggesting a role for F-BAR proteins in cytoskeletal reorganization at curved membranes (127). The study by Takano *et al* highlights the importance of an acidic region adjacent to the SH3 domain and presents a model in which this motif repels the lipid bilayer, forcing the SH3 domain away from the plasma membrane and the F-BAR domain. Given the high degree of similarity between CIP4 and Toca-1, I propose that CIP4 functions in an analogous manner. The Corey lab demonstrated that Src family kinases bind and phosphorylate CIP4 at a site adjacent to this acidic motif. Therefore, it is likely that Src phosphorylation of CIP4 contributes to the conformation of CIP4 by modulating the electrostatic repulsion.

My preliminary data indicates a correlation between CIP4 expression and the invasiveness of breast cancer cell lines *in vitro*, suggesting that CIP4 might play a role in cellular motility. **Therefore, I propose a model in which CIP4 functions as a scaffolding protein that facilitates N-WASp activation by stabilizing the open conformation, which increases its interaction with active Cdc42 at areas of membrane curvature and leads to localized actin polymerization at invasive cytoskeletal structures (Figure 11).** In this model, CIP4 binds the lipid membrane, dimerizes via the F-BAR domains, and induces membrane curvature. Activation of EGFR and Src leads to the phosphorylation of CIP4, strengthening the electrostatic repulsion that forces the SH3 domain away from the membrane and the F-BAR domain. This spring-like conformation acts as a scaffold to maintain the open conformation of N-WASp by tethering the poly-proline region of N-WASp away from the membrane-bound basic domain. By stabilizing this open conformation, CIP4 increases access by Cdc42 and Src to the regulatory domains of N-WASp, potentiating N-WASp activation and leading to Arp2/3-mediated actin polymerization. Through this proposed mechanism, CIP4 targets actin polymerization to areas of membrane curvature, a critical function in invadopodia formation.



## CHAPTER 2: SRC PROMOTES MIGRATION AND INVASION OF BREAST CANCER CELLS

### 2.1 INTRODUCTION

c-Src is a non-receptor tyrosine kinase that is involved in many distinct signaling pathways (**Figure 6**). The structure of Src combines a carboxy-terminal kinase domain with SH2 and SH3 interaction domains. This arrangement allows it to function as a kinase within larger, multi-protein complexes, most notably the FAK-Src complex. In response to ECM-interaction, the **f**ocal-**a**dhesion **k**inase (FAK) is recruited to the cytoplasmic tail of  $\beta$ -integrins via talin and paxillin.  $\beta$ -integrins also bind the SH3 domain of Src, encouraging interaction between FAK and Src's SH2 domain. FAK auto-phosphorylation at Tyr397 is associated with activation, although Src also phosphorylates FAK at multiple tyrosine sites, including Tyr576 in the kinase domain and Tyr925. Paxillin is also phosphorylated by Src. The FAK-Src complex phosphorylates several targets leading to increased migration and cytoskeletal rearrangement. The p130<sup>CAS</sup> (**C**rk-**a**ssociated **s**ubstrate) adaptor protein promotes migration after phosphorylation by FAK and Src (20, 33, 129). Also downstream of FAK-Src are Crk and the closely related CrkL, which interact with p130<sup>CAS</sup>. Activation of CrkL induces Rac/Cdc42 signaling to promote integrin dependent migration via WAVE/N-WASp and Arp2/3 (20).

In addition to the integrin-mediated c-Src signaling through FAK, Src also modulates signaling from receptor tyrosine kinases like EGFR, HER2, PDGFR, and CSF-1R. Src's interaction and synergism with the oncogenic potential of EGFR have been well described (33). After EGF-induced dimerization and transphosphorylation of EGFR, Src is recruited and phosphorylates the cytoplasmic tails of EGFR at Tyr 845 and Tyr1101. This amplifies the activation of EGFR targets such as PI-3K, Shc, and MAPK. PI-3K signaling through the Akt/IKK/NF $\kappa$ B cascade results in inhibition of apoptosis via caspase-9 inactivation and cell survival. Furthermore, NF $\kappa$ B-dependent increases in IL-8 encourage angiogenesis.

c-Src encourages EGFR-dependent tumorigenesis through potentiation of signaling. Given that Src is overexpressed or hyperactive in a variety of human cancers, Src-targeted therapies have been widely investigated for the treatment of cancers. Several

small-molecule inhibitors that inhibit Src also inhibit the Abl tyrosine kinase due to the structural similarity between their ATP-binding domains. Dasatinib (BMS-354825, Sprycel<sup>®</sup>, [N-(2-chloro-6-methylphenyl)-2-[[6-[4-(2-hydroxyethyl)-1-piperazinyl]-2-methyl-4-pyrimidinyl]amino]-5-thiazole-carboxamide] is a recently developed inhibitor of Src/Abl that is orally active. Dual Src/Abl inhibitors like dasatinib were initially approved for BCR-Abl+ leukemias that were refractory to imatinib therapy. Like other small-molecule inhibitors, dasatinib is capable of inhibiting its target at low concentrations, making it a more favorable clinical option. *In vitro* testing demonstrated that the kinase activities of Src and Abl are 50% inhibited with less than 1.0 nM of dasatinib. Increasing the dasatinib dose leads to inhibition of other tyrosine kinases (p38, Akt, and FAK) and receptor tyrosine kinases (PDGFR, c-kit, and Ephrin) (130). In lung and prostate cancer cell lines, low-dose (nanomolar) treatment with dasatinib inhibited proliferation (37, 130-132). Dasatinib has also shown mixed efficacy in breast cancer cell lines: “triple-negative” cell lines, which lack ER, PR, and HER2, are more sensitive to dasatinib than other hormone receptor-positive lines (133). However, the molecular pathways mediating this selectivity have not been previously been investigated.

To identify the molecular pathways that differentiate dasatinib-sensitive from dasatinib-resistant breast cancer cell lines, I investigated the effects of dasatinib on three cell lines that had been previously screened for their response to dasatinib in growth assays. Reliable measures of response are an important component in the clinical evaluation of tumors treated with targeted therapies. Therefore, I also sought to identify biomarkers for dasatinib response by examining the inhibition of key Src-dependent signaling pathways. Given the critical role Src pathways play in cytoskeletal rearrangement, I evaluated the effects of Src inhibition on the migration and invasion of dasatinib-sensitive breast cancer cells.

## **2.2 MATERIALS AND METHODS**

### **2.2.1 Cell Culture**

Breast cancer cell lines were obtained from the ATCC via the labs of Drs Gordon

Mills and Janet Price (MD Anderson Cancer Center, Houston, TX). All cell lines were grown at 37°C and 5% CO<sub>2</sub>. MDA-MB-231 and T47D cells were grown in DMEM/F12 media (Invitrogen, Carlsbad, CA) supplemented with 10% fetal calf serum (Hyclone, Logan, UT), 100 U/mL penicillin, and 100 µg/mL streptomycin. MCF7 cells were maintained in MEM media (Invitrogen) supplemented with 10% fetal calf serum, 100 U/ml penicillin, 100 mg/ml streptomycin, 2mM L-glutamine, 0.1mM non-essential amino acids, 1mM sodium pyruvate, and MEM vitamin solution.

### ***2.2.2 Viability and Proliferation Assays***

For cell counting and trypan blue exclusion, cells were grown in the appropriate media plus dasatinib for up to 72 hours, collected by scraping, diluted in trypan blue dye, and counted with a Brightline hemocytometer (Hausser Scientific, Horsham, PA). Proliferation was determined using an MTT assay (#M5655, Sigma-Aldrich, St. Louis, MO). Cells were seeded at a density of 3-5x10<sup>3</sup> cells per well of 96-well plate with complete medium 24 hours prior to treatment. Cells were then treated for 24, 48, and 72 hours before MTT reagent was added and absorbance was read at 570nm, per manufacturer's instructions.

### ***2.2.3 Statistics and Combination Index***

Descriptive statistics including mean values and s.d. were calculated using Microsoft Excel or Prism software (GraphPad, La Jolla, CA). Statistical significance was determined by two-sample student t-tests (P1/40.05). Calculation of GI<sub>50</sub> (Dm) values, measures of sigmoidicity (m), correlation coefficients (r), and combination indices (CI) of multi-drug treatments were performed using the CalcuSyn software (Biosoft, Cambridge, UK). Degree of cooperation between dasatinib and doxorubicin was determined from the combination index (CI) as follows: CI >1 indicates antagonism; CI = 1 indicates additivity; 1 > CI > 0.3 indicates synergy; 0.3 > CI > 0.1 indicates strong synergy (134, 135).

### ***2.2.4 Immunoblotting***

Cells were grown in complete media overnight, treated with dasatinib for 2–48 h, and washed in ice-cold PBS. Whole-cell lysates were obtained from cells collected by

scraping, and lysed in 1% NP-40 buffer supplemented with the appropriate proteinases and phosphatase inhibitors. Protein concentrations were determined by a Bradford assay and equal amounts of each sample were either prepared for loading by boiling in Laemmli sample buffer. Western blot analysis was performed with whole cell lysates or immunoprecipitated samples resolved by SDS-PAGE and transferred onto Immobilon-P Transfer Membranes (Millipore Corp, Billerica, MA, USA). The membranes were blocked overnight with blocking buffer (5% milk or 5% BSA, depending on the antibody, with 0.1% Tween-20). The blots were incubated with primary and then secondary antibodies for 1 h each at room temperature. Immunoreactive bands were visualised by enhanced chemiluminescence (Amersham, Piscataway, NJ, USA). Membranes were then stripped for 30 min at 37°C using Stripping buffer (Pierce, Rockford, IL, USA), reblocked, and probed for actin, GAPDH, or the nonphosphorylated protein being analysed as loading controls. Densitometric analysis was performed using the NIH software, ImageJ (Macintosh platform, Bethesda, MD, USA), to determine the ratio of phosphorylated protein to total protein. For Src-pY416: c-Src, IC<sub>50</sub> values were calculated based on exponential regressions of the plotted ratios using Microsoft Excel. For IC<sub>50</sub> values of Src inhibition, ratio values of Src-pY416 to total Src were generated by exponential regression (Microsoft Excel).

### ***2.2.5 Cell Cycle and Cell Death Assays***

Cell cycle distribution was analyzed by plating cells at a density of  $3-4 \times 10^5$  cells per 10cm culture dish with complete medium 24 hours prior to treatment. Cells were then treated with dasatinib for 48 hours, collected, fixed in 70% ethanol, washed, and stained with a 5% propidium iodide solution. Samples were detected with a FACSCalibur (Becton Dickinson, Franklin Lakes, NJ) and analyzed with FlowJo software (Tree Star, Inc., Ashland, OR). Annexin-V and propidium iodide staining were performed with a flow cytometric apoptosis detection kit (BD Pharmingen, San Jose, CA) per the published manual and analyzed by FACSCalibur. BrdU and 7-AAD staining and analyses were performed per the manufacturer's published protocols (FITC Flow Kit, BD Biosciences).

### ***2.2.6 Immunofluorescence and Invadopodia Imaging***



Cells were grown and treated on glass chamber slides or glass coverslips, fixed in 4% formaldehyde, permeabilized with 0.1% TritonX-100, blocked in 1% BSA, and stained with anti-alpha-tubulin (Sigma, St. Louis, MO) and Alexa-488 fluorescent phalloidin (Molecular Probes, Carlsbad, CA). Tubulin staining was detected with a Cy3-conjugated donkey anti-mouse antibody (Jackson ImmunoResearch). Slides were prepared using ProLong Antifade mounting media (Molecular Probes), and imaged with a Nikon Eclipse TE2000U microscope and MetaMorph imaging software (Molecular Devices, Toronto, Canada). Invadopodia were analyzed by seeding cells on a thin layer of FITC-labeled gelatin (VWR, West Chester, PA) as previously described (56). Cells were allowed to invade for 20 hours, and the slides were then processed as described above, stained first for cortactin and then with Cy3-anti-mouse. Invadopodia were counted from 10 random fields in each sample (blinded) and averaged.

### ***2.2.7 Migration and Invasion Assays***

Migration was measured by wound healing assay, in which cells were grown to 80% confluence in 6-well plates, streaked with a sterile pipette tip, and allowed to recover in dasatinib-treated media. After 6 hours, plates were visualized at 10x magnification and migration determined by measuring wound width (in pixels) using the MetaMorph imaging software (Molecular Devices, Toronto, Canada). Invasiveness was determined using Matrigel invasion chambers with an 8mm-pore membrane (BD Biosciences, San Jose, CA) seeded with  $2.5 \times 10^4$  cells each. Dasatinib-treated media was used in both the upper and lower chambers, with serum added only to the lower chamber. Cells were allowed to invade for 24 hours through the Matrigel, at which point the inserts were removed and the membranes scrubbed and fixed in methanol. Invading cells were then stained and mounted on slides with Prolong Antifade with DAPI (Molecular Probes, Carlsbad, CA). Membranes were then visualized with an epifluorescent microscope (Nikon, Tokyo, Japan), and quantification of invading cells (visualized as DAPI-stained nuclei) was determined in 6 random fields per sample.

## 2.3 RESULTS

### 2.3.1 *Dasatinib inhibits proliferation and metabolism of MDA-MB-231 cells*

Building on the observations by Finn *et al* that triple-negative and basal-type breast cancer cell lines were more sensitive to dasatinib (133), I compared three representative breast cancer cell lines. MDA-MB-231 is a well-characterized, triple-negative, basal-subtype breast cancer cell line. MCF-7 and T47D are luminal-subtype breast cancer cell lines that are positive for ER and PR. To determine the  $IC_{50}$  for the anti-proliferative effects of dasatinib, a dose-response curve was created for each cell line by treating cells with dasatinib for 48 hours and quantifying metabolic activity using an MTT assay (**Figure 12a**). MDA-MB-231 cells were the most responsive ( $IC_{50} = 0.16 \mu M$ ), while T47D demonstrated moderate growth inhibition ( $IC_{50} = 0.45 \mu M$ ) and MCF7 showed very little response ( $IC_{50} = 12.3 \mu M$ ). To confirm these results, cells were grown in dasatinib for 72 hours and counted at 24, 48 and 72 hours (**Figure 12b**). Again, MDA-MB-231 were the most sensitive; a dose-dependent increase in doubling-time was significant ( $p < 0.01$ ) after 72 hours for all three doses ( $0.05 \mu M$ ,  $0.1 \mu M$ , and  $1.0 \mu M$ ), where as only the highest dose for MCF7 was significant at 72 hours. Using cell-counting data, the calculated  $IC_{50}$  values for MDA-MB-231 and MCF7 cells were  $0.33 \text{ mM}$  and  $0.99 \text{ mM}$ , respectively, a three-fold difference in sensitivity. Again, T47D were moderately sensitive.

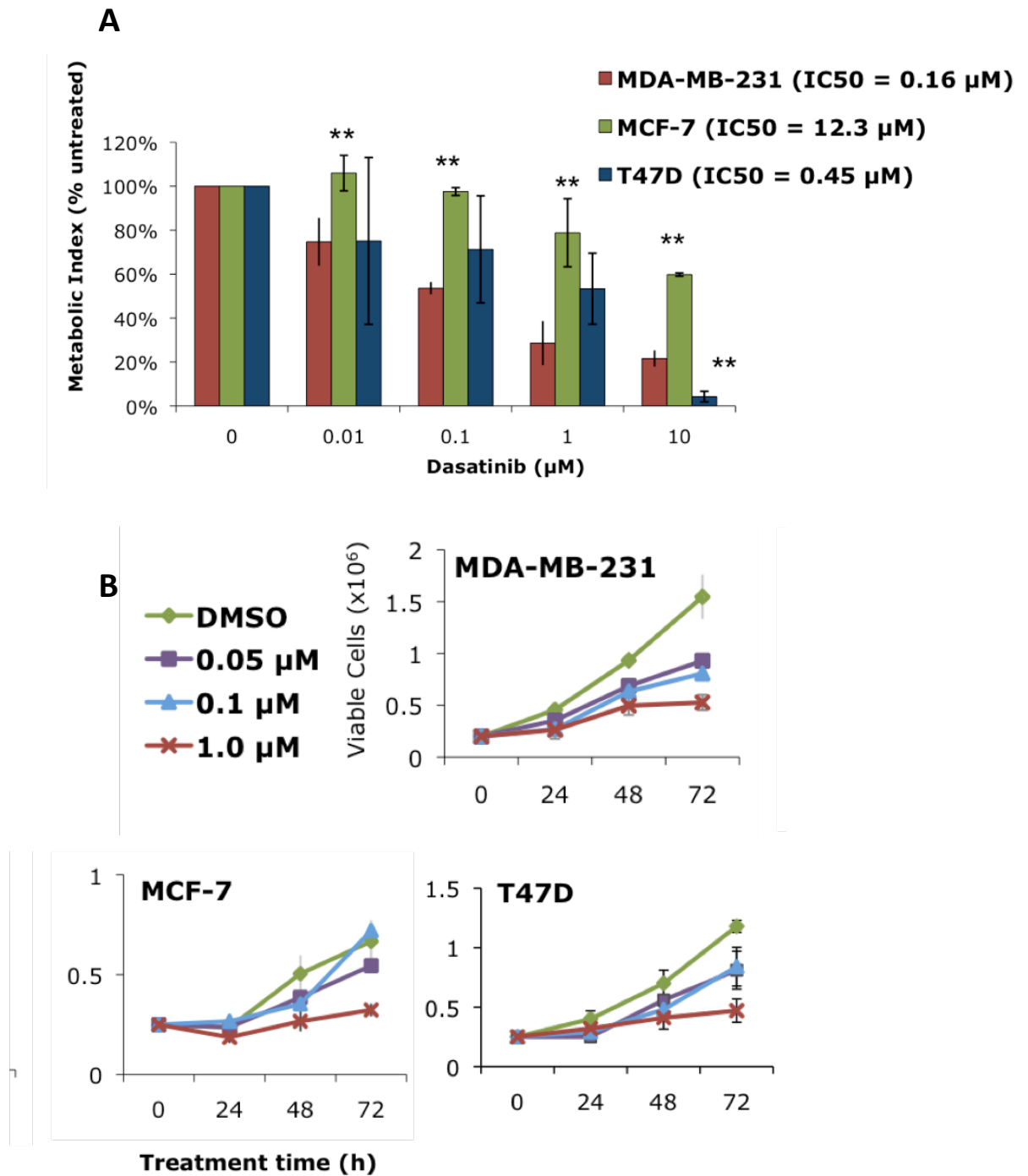


**Figure 12: Dasatinib inhibits cell proliferation in sensitive cells. A)** MTT assay of MDA-MB-231, MCF7, and T47D after dasatinib treatment. **B)** Cell counting for 72 hours of dasatinib treatment.

Because the calculated IC<sub>50</sub> values were higher when based on cell counting, I examined the viability using trypan-blue exclusion and replication rates using BrdU uptake. Replicating MDA-MB-231 cells were significantly reduced from 35% to 12% with 100 nM dasatinib (**Table 2**), whereas the BrdU uptake rates were not significantly altered in MCF7 or T47D cells. Interestingly, there was no significant decrease in viability of the MDA-MB-231 cells upon dasatinib treatment. This lack of cell death was confirmed using flow cytometric quantification of annexin-V and PI staining (data not shown). This is also demonstrated by western blotting for PARP cleavage products in whole cell lysates of MDA-MB-231 cells (**Figure 17b**).

|                        | MDA-MB-231  |          | MCF-7       |          | T47D        |          |
|------------------------|-------------|----------|-------------|----------|-------------|----------|
| 48 hr treatment        | % Viability | % BrdU + | % Viability | % BrdU + | % Viability | % BrdU + |
| DMSO                   | 93.9        | 35.0     | 75.7        | 61.6     | 65.8        | 32.8     |
| 0.01 $\mu$ M Dasatinib | 93.2        | 35.7     | 67.7        | 57.0     | 63.8        | 30.6     |
| 0.1 $\mu$ M Dasatinib  | 92.0        | 11.6     | 62.5        | 62.1     | 71.5        | 25.9     |

**Table 2: Viability and proliferation of dasatinib-treated cells.**

### ***2.3.2 Src inhibition does not correlate with proliferative inhibition by dasatinib***

Previous studies of dasatinib have demonstrated that decreases in phospho-Src may serve as biomarkers for responsiveness (136, 137), however, this has not yet been investigated in solid tumors. Therefore, I examined whether differential inhibition of Src was a biomarker in the breast cancer cell lines. Src activation is regulated by the balance of two main phosphorylation sites within in kinase domain: an activating site at Tyr416 (chicken nomenclature) and Tyr527 (chicken), an inactivating site whose phosphorylation maintains the inhibitory intra-molecular interaction with the SH2 domain (129). Using the dose-dependent dephosphorylation of Tyr416, I calculated the IC<sub>50</sub> values for Src inhibition in each cell line after 2 hours of dasatinib treatment. Despite the disparity in response for proliferation, there were no significant differences in Src inhibition between the three cell lines (**Figure 13a**). Dephosphorylation of Tyr416

(>75%) was accomplished with less than 100 nM of dasatinib in all three cell-lines, a dose achievable in clinical trials (138). Therefore, the phosphorylation status of Src is not an accurate biomarker for dasatinib-response in breast cancer cells.

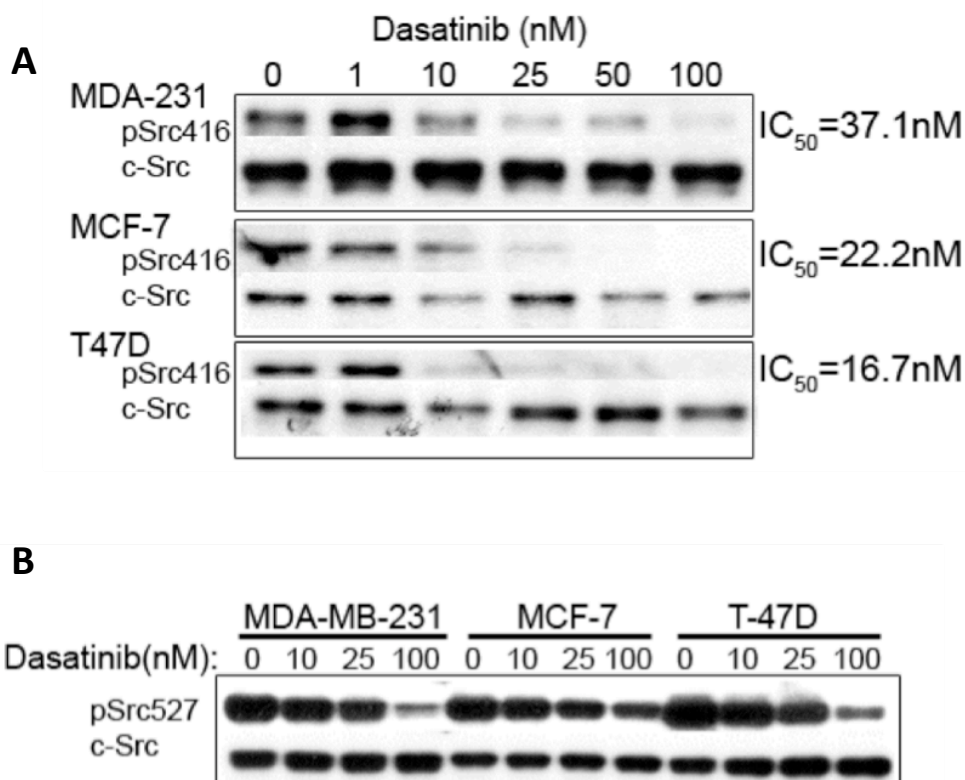


**Figure 13: Dephosphorylation of Src in response to dasatinib.** A) Phospho-Src Tyr416. B) Phospho-Src Tyr527.

The activation of Src is dependent upon the balance of two phosphorylation sites, the activating Tyr416 residue, as well as Tyr527, which maintains Src in its inactive, closed conformation. I examined the phosphorylation status of this inhibitory tyrosine, in response to dasatinib and found it to also be comparably inhibited across the three lines (**Figure 13b**). While this could affect the overall inhibition of Src, dephosphorylation of Src-Y527 was only significant at the doses 10-fold higher than that needed for Tyr416 inhibition. At this level of dasatinib dosing, off-target effects may be present like inhibition of Csk (C-terminal Src kinase) (139, 140).

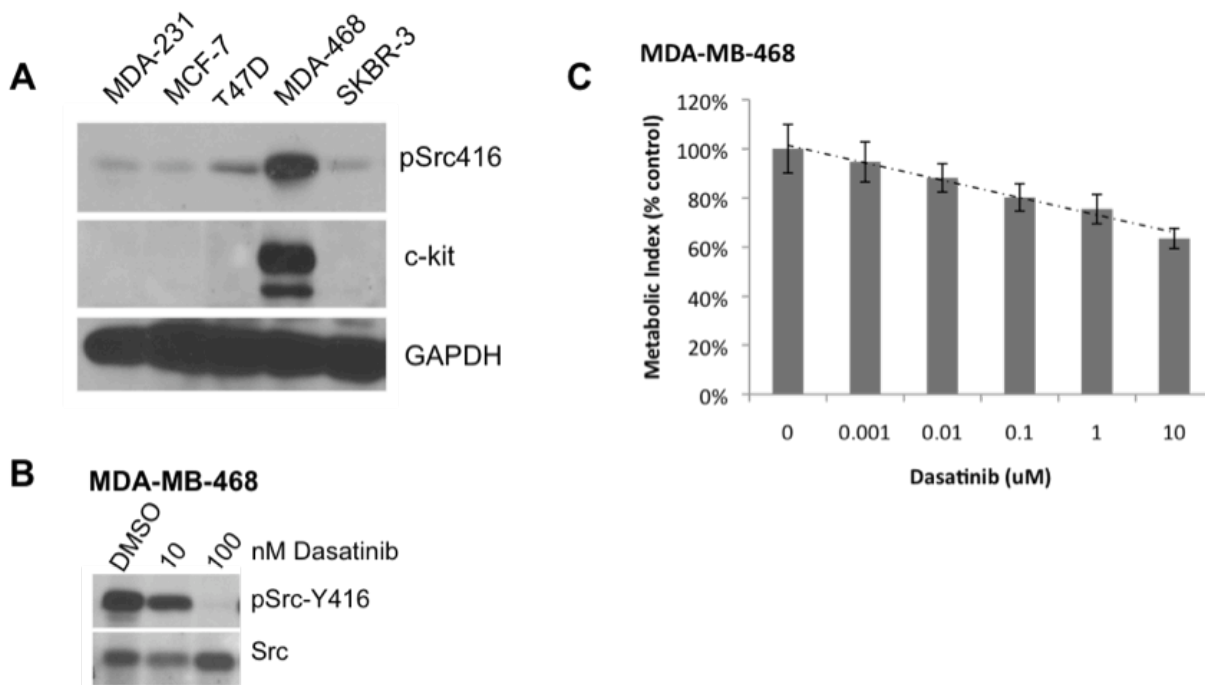


**Figure 14: Basal Src activity does not correlate with sensitivity.** A) Western blot for phospho-Src (Y416) and c-kit in untreated cell lines. B) Dephosphorylation of Src in dasatinib-treated MDA-MB-468 cells. C) MTT assay shows dasatinib-response of MDA-MB-468 cells.

Clinical applications of dasatinib will benefit from reliable predictors of response. To determine whether basal Src activity might predict response to dasatinib, I compared starting levels of phospho-Src (Y416) in a panel of breast cancer cells including MDA-MB-231, MCF7, and T47D (**Figure 14a**). Again, there were no dramatically different levels of Src phosphorylation that correlated with dasatinib-response. One cell line tested, MDA-MB-468, demonstrated high levels of phospho-Src (Y416), prompting me to check the dasatinib-responsiveness of this line. As with the initial three cell lines, phospho-Src (Y416) was completely inhibited by 100 nM dasatinib (**Figure 14b**), suggesting that the high level of basal Src activity did not confer resistance to dasatinib. However, the  $IC_{50}$  based on metabolic inhibition (MTT assay) was greater than 10  $\mu$ M (**Figure 14c**), similar to the MCF7 line, classifying it as a dasatinib-resistant cell line. Together, these results

demonstrate that basal phospho-Src levels and dasatinib-dependent dephosphorylation are not reliable markers of dasatinib sensitivity in breast cancer cell lines.

Because dasatinib has also been reported to inhibit c-kit, PDGFR, and EphA2 (130, 141-143), it is possible that the effects of dasatinib are dependent on their inhibition. To this end, also screened the cell line panel for expression of these alternative targets. The most-sensitive cell line, MDA-MB-231, did not express c-kit or PDGFR (**Figure 14a**) (144, 145), excluding them as potential targets. Again, only the MDA-MB-468 line expressed high levels of c-kit, also indicating that is not an appropriate predictive marker. The MDA-MB-231 cells did express high levels of the Ephrin receptor, however, but dasatinib treatment did not affect its phosphorylation status (data not shown) (146). Based on these results, these alternative targets of dasatinib were also unreliable predictors of response. However, it remains possible that other, unknown targets of dasatinib are being inhibited and could prove to be effective predictors or markers of response.

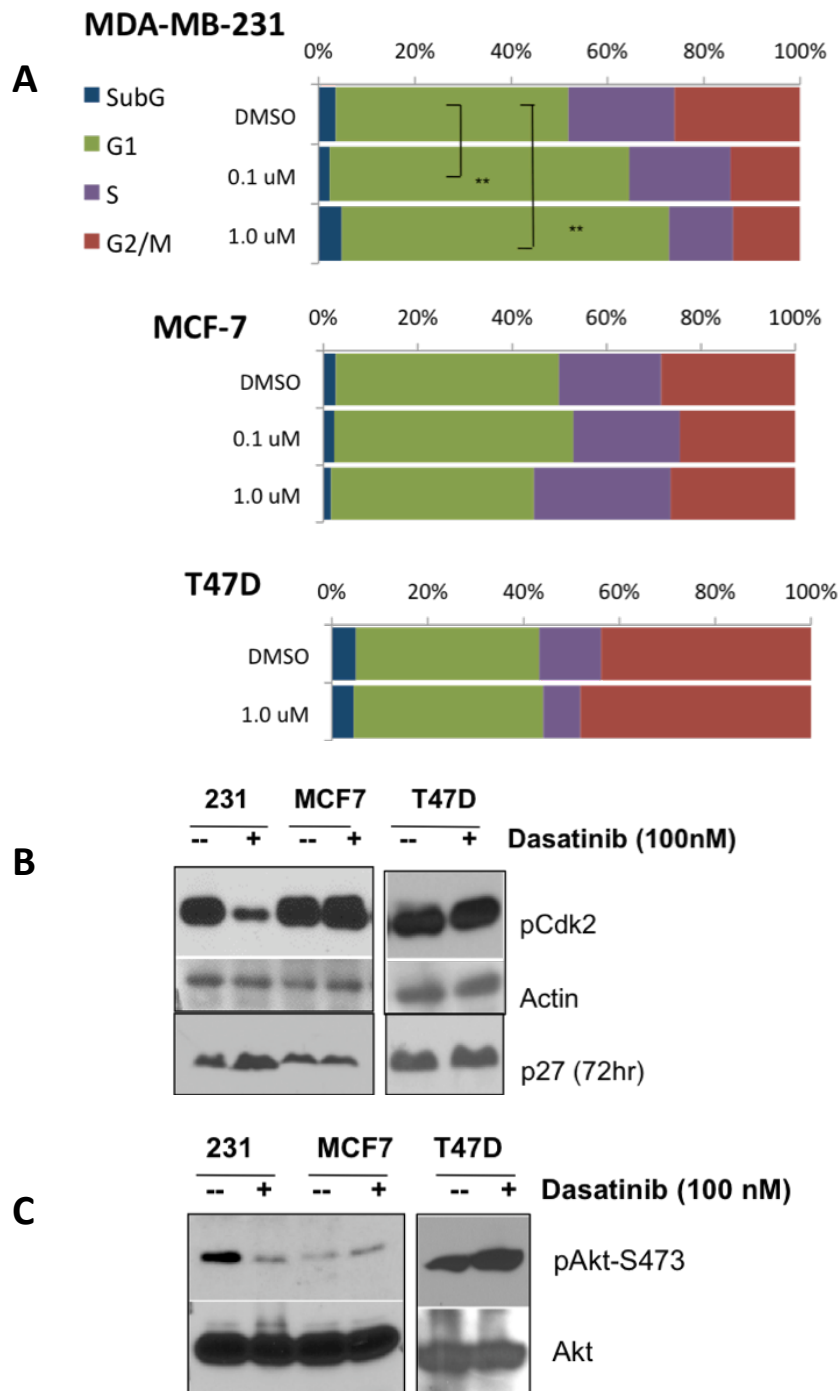


**Figure 15: Dasatinib induces cell cycle arrest in sensitive cells.** A) Cell cycle distribution after dasatinib treatment. Cells were treated with indicated doses of dasatinib for 48 hours, stained for DNA content, and analyzed by flow cytometry. Graphs illustrate the percentage of the population in each phase of the cell cycle. \*\* represents  $p < 0.01$  by t-test. B) Inhibition of pCdk2 and accumulation of p27 after dasatinib treatment. Accumulation of Src-targeted p27 and resulting inhibition of Cdk2 correlate with G1 arrest in dasatinib-sensitive MDA-MB-231 cells. C) Inhibition of Akt after dasatinib treatment. Dephosphorylation of Akt in response to dasatinib correlates with cell cycle arrest, and accumulation of p27, also a target of Akt.

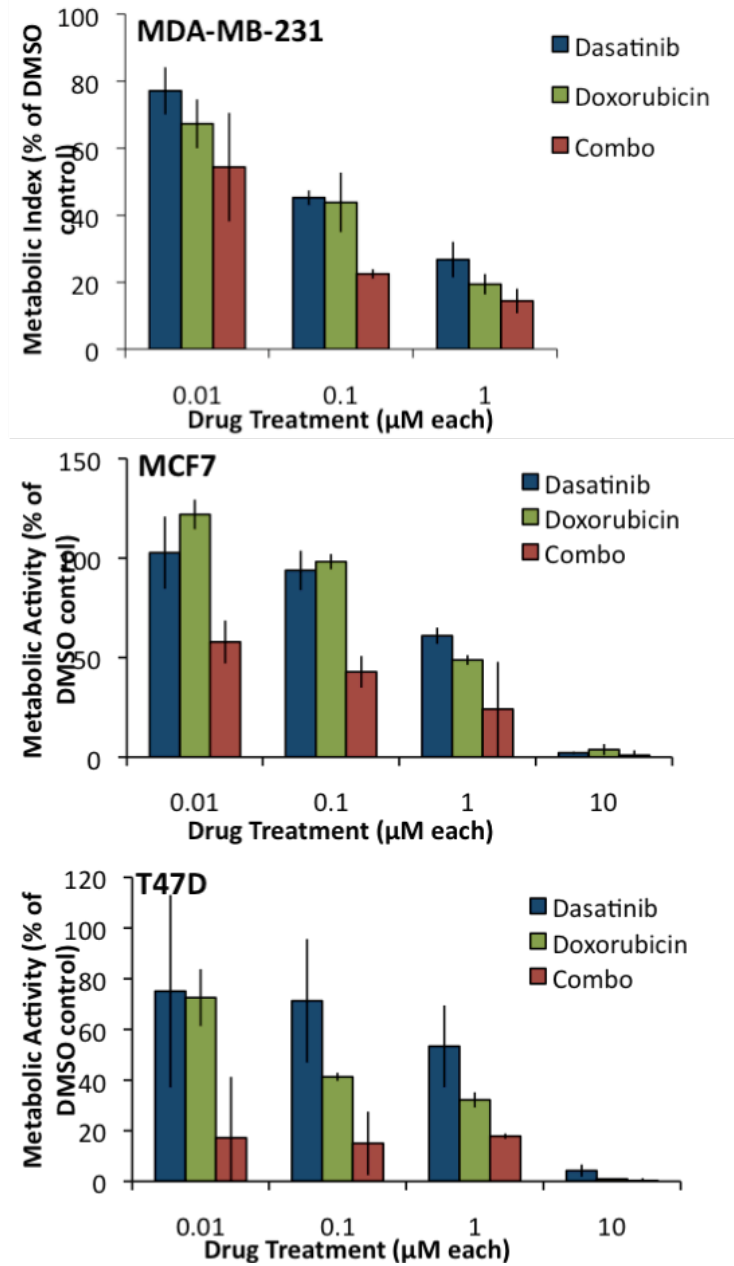


### **2.3.3 Dasatinib treatment induces $G_1$ arrest in MDA-MB-231 cells**

Because dasatinib impaired proliferation but did not result in cell death, I examined whether dasatinib could block cell cycle progression, which has not been previously demonstrated in solid tumors. Therefore, I employed flow-cytometry to create cell cycle distribution profiles for each cell line after 48 hours of treatment with dasatinib (**Figure 15a**). In keeping with the differences seen in proliferation, only the MDA-MB-231 cells exhibited a significant increase in  $G_1$  phase cells ( $p < 0.001$ ). This cell cycle inhibition was evident at 0.1 and 1.0  $\mu\text{M}$  of dasatinib (57% and 64%, respectively,  $p < 0.01$  by t-test), in comparison to the DMSO control (41% in  $G_1$ ). MCF7 and T47D cells did not undergo any significant cell cycle redistribution in response to dasatinib treatment. Supporting my previous observations that there was no cell death associated with dasatinib treatment, there was no significant accumulation of sub- $G_1$  cells in any cell line.

To further characterize the molecular pathways involved in the  $G_1$  arrest of MDA-MB-231 cells, I performed western-blots probing for the levels of phospho-Cdk2 (activating) and p27<sup>Kip1</sup>, proteins involved in promoting  $G_1$  to S-phase transition in cycling cells (**Figure 15b**). Confirming the cell-cycle data, only the MDA-MB-231 cells exhibited a decrease in phospho-Cdk2 after dasatinib treatment, an indicator of  $G_1$  arrest. Cdk2 activity is inhibited by p27, which is negatively regulated by Src through phosphorylation and targeting for degradation. Following dasatinib treatment, p27 accumulation was only seen in the MDA-MB-231 cells, explaining the decrease in Cdk2 activity. In addition to its regulation by Src, p27 is also negatively regulated by Akt. Because Akt is also downstream of Src, it is possible that Akt inhibition could contribute to p27 downregulation. To examine whether Akt was inhibited in response to dasatinib, I probed cells for phospho-Akt and found that Akt was inhibited only in the MDA-MB-231 cells (**Figure 15c**).

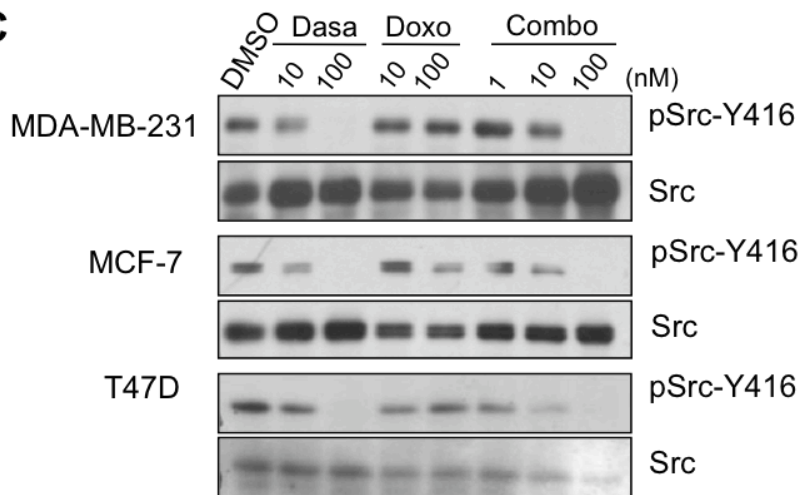
**A**



**Figure 16: Synergistic anti-proliferation with dasatinib and doxorubicin.** A) MTT assay in each cell line treated with dasatinib, doxorubicin, or 1:1 combination. B) Viability and proliferation rates after single and combination treatments. C) Dephosphorylation of phospho-Src (Tyr416) after single or combination treatments.

**B**

| MDA-MB-231 |       | % Viability | % BrdU |
|------------|-------|-------------|--------|
|            | DMSO  | 93.9        | 30.2   |
|            | Dasa  | 92.0        | 9.8    |
|            | Doxo  | 80.6        | 5.8    |
|            | Combo | 81.5        | 3.9    |
| MCF7       |       | % Viability | % BrdU |
|            | DMSO  | 75.7        | 61.6   |
|            | Dasa  | 62.5        | 62.1   |
|            | Doxo  | 52.0        | 15.6   |
|            | Combo | 36.4        | 15.3   |
| T47D       |       | % Viability | % BrdU |
|            | DMSO  | 65.8        | 32.8   |
|            | Dasa  | 71.5        | 25.9   |
|            | Doxo  | 59.2        | 29.4   |
|            | Combo | 76.4        | 19.5   |

**C**

#### ***2.3.4 Combination treatment of dasatinib and doxorubicin synergistically inhibits metabolism***

Small molecule inhibitors are most likely to be used in combination with other chemotherapeutics to maximize their efficacy. Therefore, we tested the effects of dasatinib in combination with a doxorubicin, a commonly used chemotherapeutic in breast cancer to determine whether the two drugs might synergize. Doxorubicin (Adriamycin ®) is an anthracycline antibiotic that intercalates into DNA, inhibiting

| MDA-MB-231      |                       |      |      | CI Values at: |      |      |
|-----------------|-----------------------|------|------|---------------|------|------|
| Drug            | IC <sub>50</sub> (nM) | m    | r    | ED50          | ED75 | ED90 |
| Dasatinib       | <b>158.95</b>         | 0.36 | 0.98 | N/A           | N/A  | N/A  |
| Doxorubicin     | <b>137.93</b>         | 0.37 | 0.99 | N/A           | N/A  | N/A  |
| 1:1 Combination | <b>34.95</b>          | 0.36 | 0.99 | <b>0.47</b>   | 0.51 | 0.54 |

| MCF-7           |                       |      |      | CI Values at: |      |      |
|-----------------|-----------------------|------|------|---------------|------|------|
| Drug            | IC <sub>50</sub> (nM) | m    | r    | ED50          | ED75 | ED90 |
| Dasatinib       | <b>12365.00</b>       | 0.72 | 0.97 | N/A           | N/A  | N/A  |
| Doxorubicin     | <b>150.49</b>         | 0.50 | 0.97 | N/A           | N/A  | N/A  |
| 1:1 Combination | <b>7.59</b>           | 0.37 | 0.93 | <b>0.05</b>   | 0.11 | 0.23 |

| T47D            |                       |      |      | CI Values at: |      |      |
|-----------------|-----------------------|------|------|---------------|------|------|
| Drug            | IC <sub>50</sub> (nM) | m    | r    | ED50          | ED75 | ED90 |
| Dasatinib       | <b>453.34</b>         | 0.87 | 0.94 | N/A           | N/A  | N/A  |
| Doxorubicin     | <b>292.89</b>         | 1.03 | 0.91 | N/A           | N/A  | N/A  |
| 1:1 Combination | <b>6.59</b>           | 0.56 | 0.77 | <b>0.04</b>   | 0.08 | 0.19 |

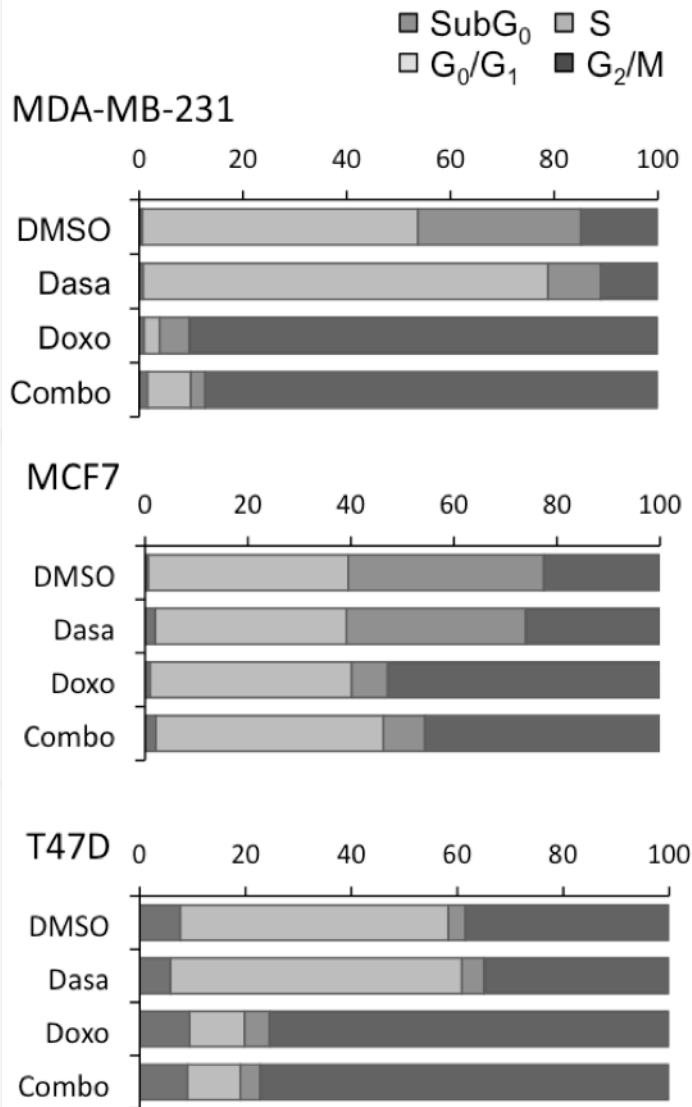
**Table 3: Combination indices demonstrate synergy between dasatinib and doxorubicin in anti-proliferation.**

replication machinery. I repeated MTT assays using dasatinib alone, doxorubicin alone, and dasatinib and doxorubicin together (1:1) at three doses (**Figure 16a**). The metabolic inhibition of MDA-MB-231 cells with doxorubicin was comparable to that seen with dasatinib treatment at an equivalent dose (IC<sub>50</sub> = 160 nM vs. 140 nM). Simultaneous treatment resulted in a moderate degree of synergism that lowered the IC<sub>50</sub> for each drug to 35 nM. To statistically evaluate the level of cooperating between the two drugs, I use the CI (combination index), a calculated measure of drug interaction in which values less than 1 indicate synergy. The CI for combination treatment of dasatinib and doxorubicin in MDA-MB-231 cells was 0.47, indicating moderate synergy. Synergism between dasatinib and doxorubicin was also seen in treatment of MCF7 and T47D cells. Interestingly, the degree of synergism was considerably stronger in these cells, which were only moderately sensitive to dasatinib alone, as compared with the MDA-MB-231 cells. The CI values for 50% inhibition of MCF7 and T47D were 0.05 and 0.04, respectively (**Table 3**). For MCF7 cells, this degree of synergism lowered the IC<sub>50</sub> doses from 12.4  $\mu$ M

(dasatinib) and 150 nM (doxorubicin) to just 7.6 nM of each drug. In T47D cells, this combination lowered the individual doses from 453 nM and 293 nM for dasatinib and doxorubicin, respectively, to 6.6 nM for each drug when combined. These results represent a 95% decrease in the dose of doxorubicin required for 50% metabolic inhibition of MCF7 cells and a 98% decrease in T47D cells. Given the toxic side effects of doxorubicin, this synergy could have a profound effect on the clinical use of a currently used chemotherapeutic.

To determine whether the synergistic effects between dasatinib and doxorubicin could also be seen in the viability or replication rates, I again counted cells using trypan-blue exclusion and flow-cytometric quantification of BrdU uptake (**Figure 16b**). Combination treatment in MDA-MB-231 cells did not increase the percentage of dead cells over the rate seen with doxorubicin alone. The combination treatment did, however, further reduce the rate of BrdU uptake from 5.8% (doxorubicin alone) to 3.9%. In contrast, MCF7 cells demonstrated no significant reduction in BrdU uptake with combination treatment, but did exhibit a decrease in viability from 52% (doxorubicin alone) to 36.4%. Although there was obviously a dramatic effect on proliferation, combination treatment did not result in any increased effect on the dephosphorylation of Src (**Figure 16c**). Whereas I demonstrated that dasatinib treatment of breast cancer cells results in a G<sub>1</sub>-phase arrest, doxorubicin has previously been shown to cause G<sub>2</sub>/M arrest in actively growing cells (147). To determine whether the cycle-arresting effects of one drug were dominant, I again used flow-based cell-cycle analysis of cells treated with either 100 nM of each drug alone or in combination (**Figure 17a**). In all three cell lines, the G<sub>2</sub>/M arrest characteristic of doxorubicin treatment was the prevalent effect after combination treatments. After 48 hours of combination treatment, 82.6% of live MDA-MB-231 cells were arrested in G<sub>2</sub>/M phase, but this was not significantly different than the arrest seen with doxorubicin alone (82.1% in G<sub>2</sub>/M). Consistent with G<sub>2</sub>/M arrest, accumulation of the CDK inhibitor p21<sup>WAF1</sup> was evident after doxorubicin or combination treatment in all three cell lines (**Figure 17b**). Only minimal PARP cleavage was evident after doxorubicin treatment and no increase was seen after combination treatment (**Figure 17b**), further confirming my previous results that any cell-death is occurring through a non-apoptotic mechanism.

**A**



**B**

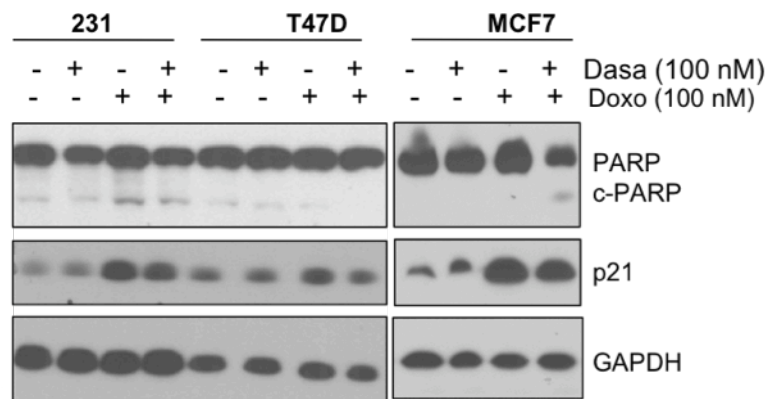


**Figure 17: Doxorubicin cell cycle arrest dominates dasatinib.** A) Cell cycle distribution of treated cells. B) Cycle arrest through p21 accumulation and lack of apoptosis.

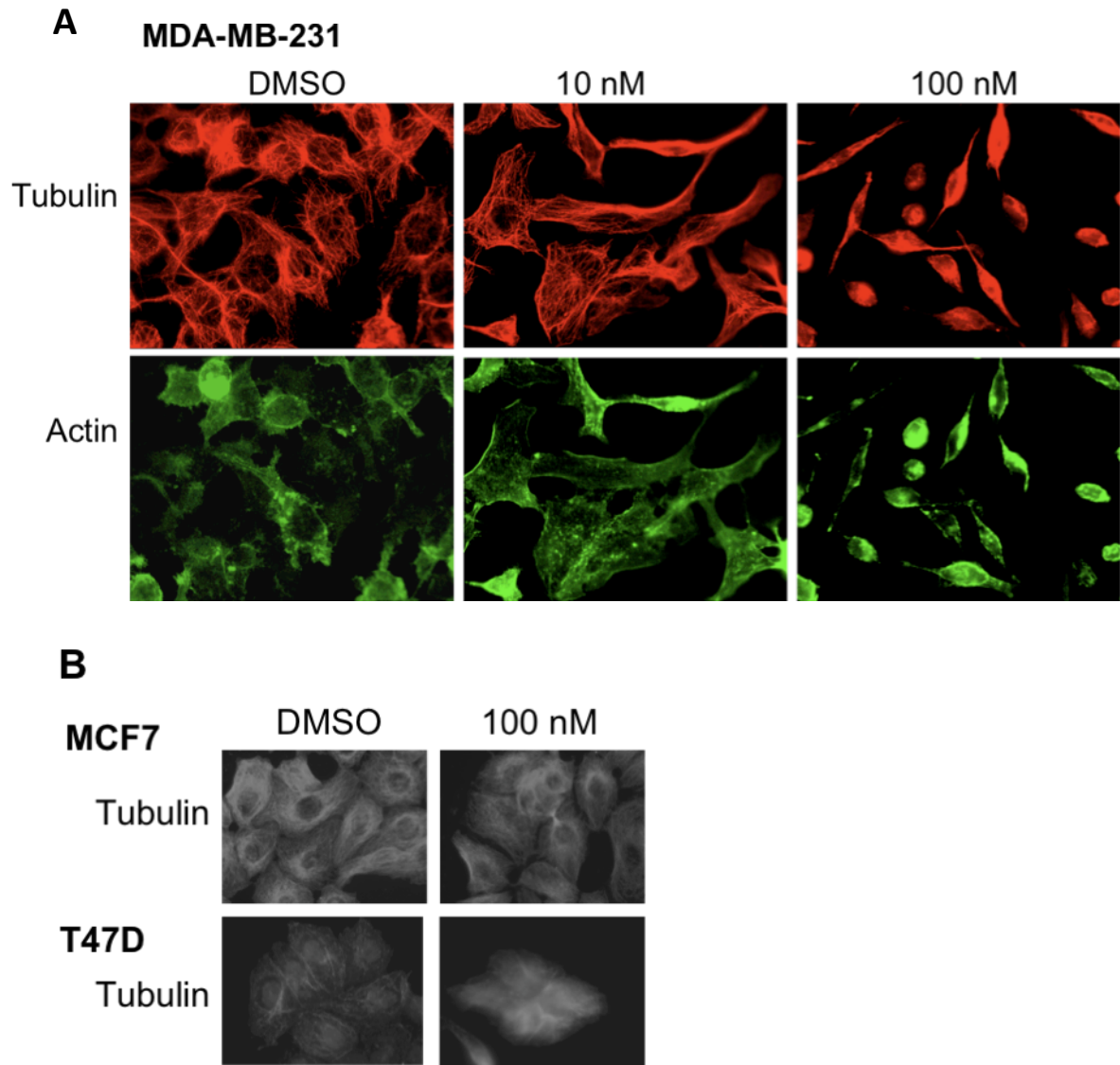


**Figure 18: Dasatinib induces cytoskeletal deregulation in sensitive cells.** A) Tubulin and actin cytoskeleton of sensitive MDA-MB-231 cells. B) Tubulin staining of dasatinib-resistant MCF7 and T47D cells.

### ***2.3.5 Dasatinib-sensitive cells undergo cytoskeletal contraction***

MDA-MB-231 cells are characterized as basal-subtype, which also indicates a more mesenchymal-like phenotype (148). As such, these cells grow as spindle-shaped cells with extensive cell protrusions and are highly migratory and invasive in cell culture. Dasatinib

treatment was sufficient to disrupt their morphology, resulting in a cell that was still attached, but severely rounded and contracted (**Figure 18a**), as demonstrated by immunofluorescence microscopy of cells probed for tubulin and actin. The morphology of MCF7 and T47D cells, which are of the luminal subtype and maintain a more epithelial-like shape in culture, was not affected by dasatinib treatment (**Figure 18b**). This is consistent with the relatively resistant nature of these cells to dasatinib treatment.

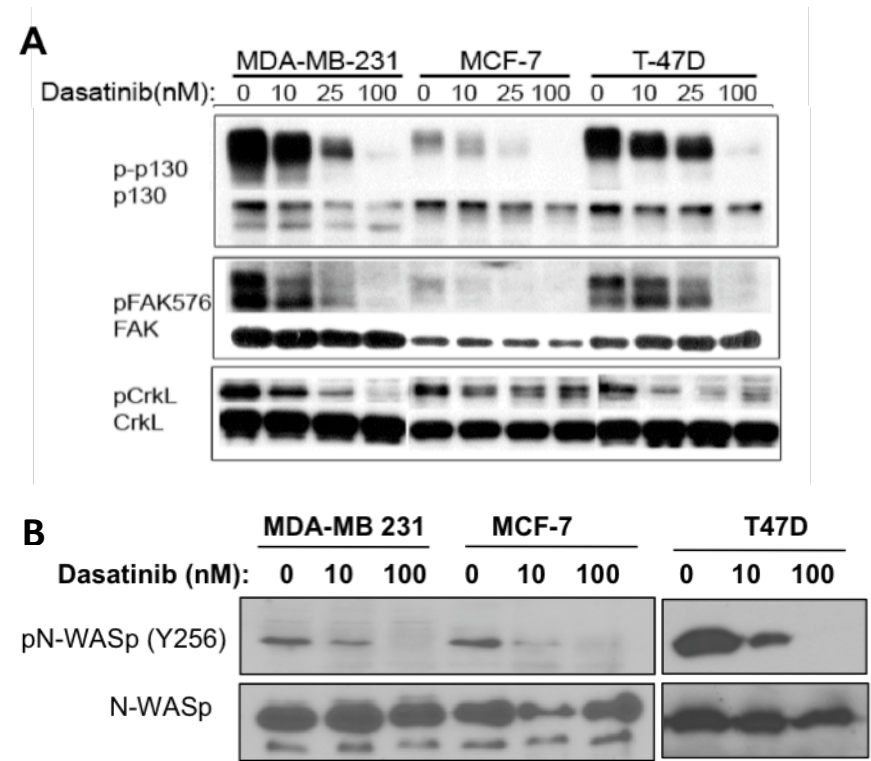


**Figure 19: Effects of dasatinib on cytoskeletal proteins.** A) Dephosphorylation of cytoskeletal-associated proteins p130, FAK, and CrkL with dasatinib. B) Dephosphorylation of actin regulator N-WASp. C) Akt inhibition in sensitive MDA-MB-231 cells.

In an effort to differentiate the molecular pathways involved in the variable response to dasatinib, I probed the cell line panel for the active forms of Src substrates commonly implicated in cytoskeletal rearrangement. The adaptor protein p130<sup>CAS</sup>, which is phosphorylated by Src downstream of integrin activation, was comparably inhibited in all three cell lines (**Figure 19a**). Similarly, phosphorylation of FAK at the Src-targeted activating site, Tyr576, was comparably inhibited in all three lines. Consistent with this



was the observation that N-WASp, a target of both FAK and Src that mediates Cdc42-dependent Arp2/3 activation and actin nucleation, was inhibited in all three lines (**Figure 19b**). It should be noted, however, that MCF7 cells exhibited lower basal phosphorylation of p130<sup>CAS</sup> and FAK (Y576) than either the MDA-MB-231 or T47D cells. The residual phosphorylation after 100 nM of dasatinib treatment, however, was equal despite the starting levels. Of the proteins tested here, only inhibition of CrkL, the Cas-related kinase, was variable across the cell lines. Dephosphorylation of CrkL at Tyr207 was strongest in the MDA-MB-231 cells and weakest in the MCF7 cells, a pattern similar to that seen with the anti-proliferative effects of dasatinib. Thus, further investigation of CrkL (Tyr207) phosphorylation may be warranted as a potential marker for dasatinib response in breast cancer cells.

As opposed to the integrin-mediated signaling of Src through FAK, Src can also target the Akt survival pathway through regulation of PI-3K. Therefore, I probed dasatinib-treated cells for phospho-Akt to determine whether this might contribute to the effects of dasatinib (**Figure 15c**). Indeed, MDA-MB-231 cells were the only line in which dasatinib induced the dephosphorylation of Akt at Ser473. As is common in mesenchymal-type cells, the MDA-MB-231 cells exhibit heightened levels of basal phospho-Akt. This suggests that aberrant activation of Akt in basal-subtype cells may predispose the cells to the anti-proliferative effects of dasatinib. It should be noted that while Akt can be directly inhibited by dasatinib at high concentrations, the dose used in this experiment (100 nM) is well below the published IC<sub>50</sub> for Akt (>50  $\mu$ M). Thus, dephosphorylation of Akt may serve as an effective biomarker for the response of breast cancer cells to dasatinib.

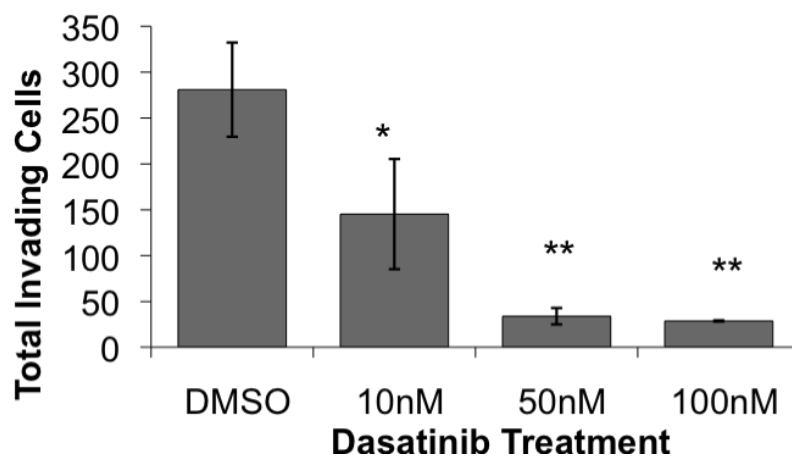
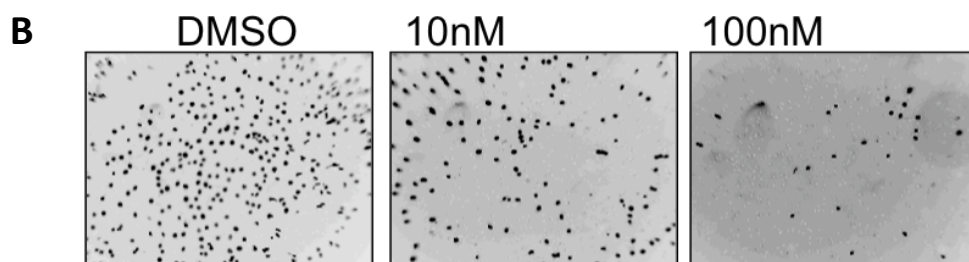
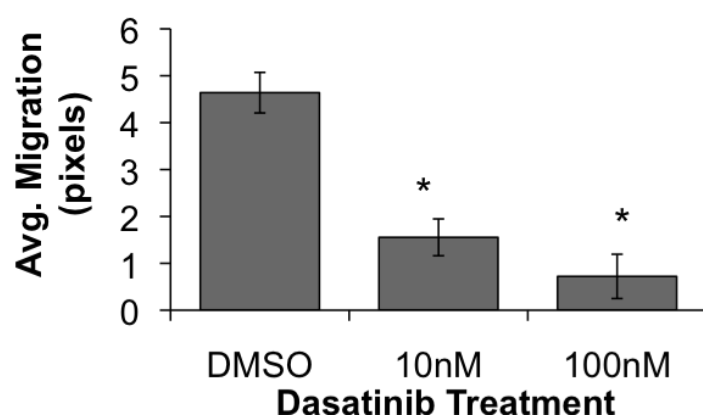
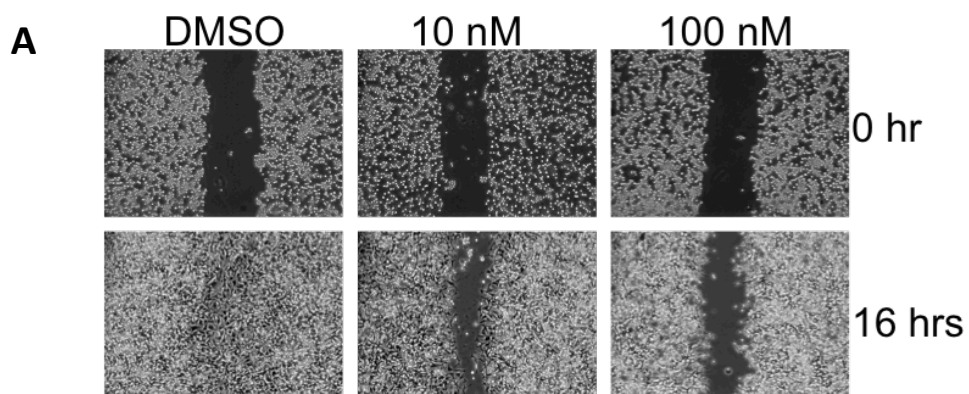


**Figure 20:** Dasatinib impairs migration and invasion of MDA-MB-231. A) Wound healing assay after dasatinib pre-treatment. B) Matrigel-coated Boyden chamber assay after dasatinib pre-treatment.

### **2.3.6 Migration and invasion are inhibited by dasatinib treatment**

Given the highly dynamic morphology of MDA-MB-231 cells and the dasatinib-induced inhibition of cytoskeletal proteins (**Figure 19**), I investigated whether dasatinib could inhibit cellular migration and invasion of MDA-MB-231 cells. To accomplish this, I quantified wound-healing (scratch) assays to compare the 2D migration of cells after pretreatment with dasatinib (**Figure 20a**). Whereas control-treated (DMSO) cells were able to repopulate the denuded area within 16 hours, this migration was significantly inhibited with both doses (10 nM or 100 nM) of dasatinib ( $p < 0.05$ ). As a measure of 3D invasion and the ability of cells to degrade and penetrate a Matrigel layer, I used a Boyden chamber assay (**Figure 20b**). Treatment with dasatinib greatly reduced (88% reduction at 50 nM) the number of cells that had successfully invaded to lower chamber ( $p < 0.01$ ). Because MCF7 and T47D cells are resistant to migration at a wound and are unable to invade Matrigel, they were not tested in these assays. It should also be noted that, because of the relatively short time-point at which these assays were completed, the effects are not the result of impaired proliferation.

Previous studies have demonstrated the contribution of specialized cytoskeletal structures known as invadopodia to the penetration of cells through extracellular matrix (54, 58, 76). These finger-like projections are bundles of actin, which efficiently degrade the extracellular matrix via secreted and transmembrane proteinases. In cultured cells, invadopodia can be visualized grown over a thin layer of FITC-labeled gelatin. Using this method, I counted the number of invadopodia formed per cell after dasatinib treatment (**Figure 21a**) and found a dramatic decrease (more than 10-fold) from an average of 5.4 (DMSO-treated) to 0.4 invadopodia per cell ( $p < 0.05$  by t-test).

Because of the strong anti-proliferative synergy between dasatinib and doxorubicin, I also tested the effects of combination treatment on the migration and invasion of MDA-MB-231 cells (**Figure 21b**). Using the same methods as with individual treatment, I observed a small decrease in migration (approximately 20%) with doxorubicin. However, this was significantly improved with combination-treated cells ( $p < 0.05$ ). Although the results were not statistically significant, this may even represent a small improvement on the inhibition seen with dasatinib alone. In the Matrigel-coated

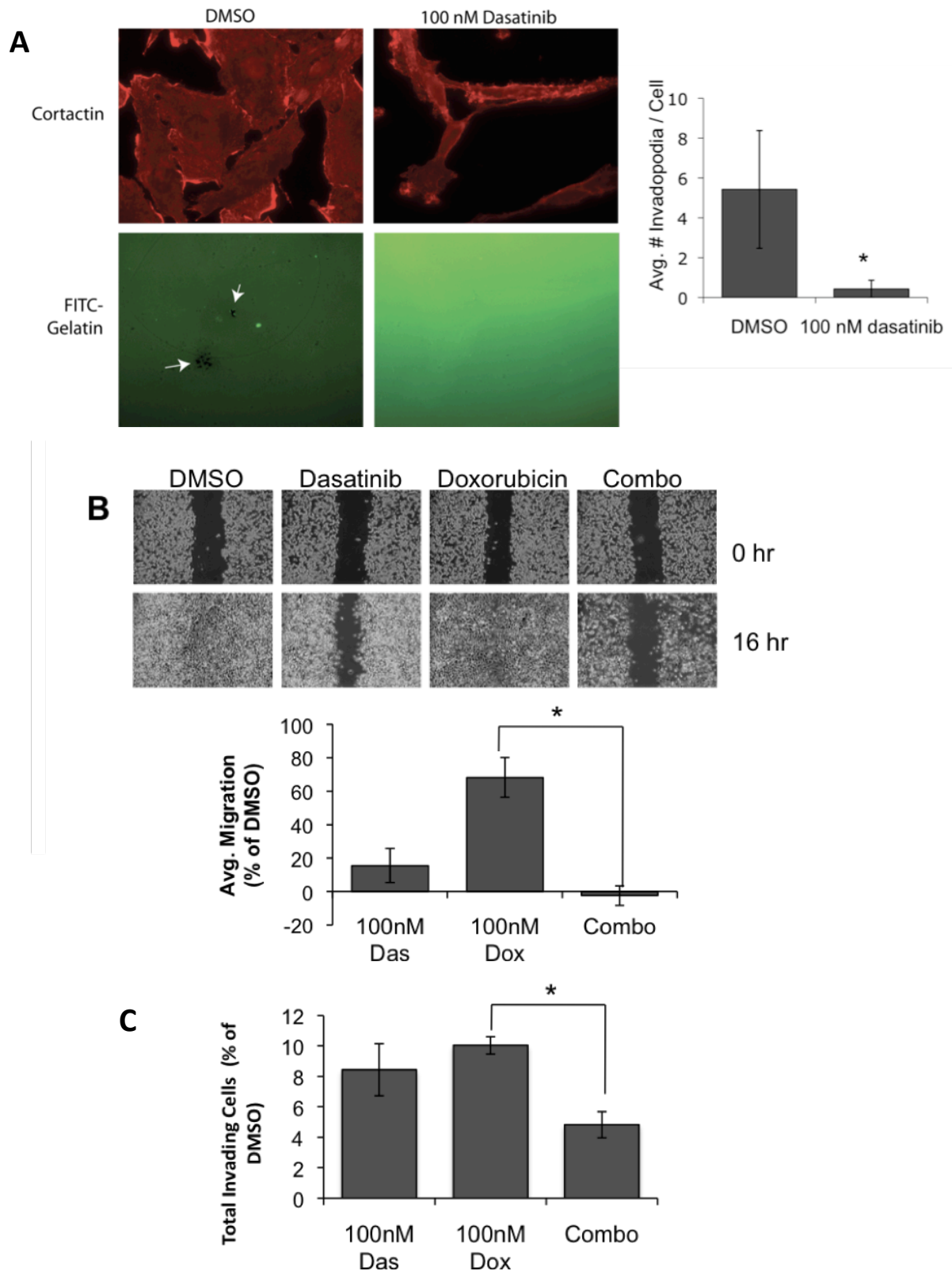


**Figure 21: Invadopodia and invasion impaired with dasatinib, doxorubicin combination.** A) MDA-MB-231 cells grown over FITC-gelatin. Active invadopodia within each cell degrade the gelatin (arrows) after overnight incubation. B) Wound healing-assay after pretreatment with dasatinib, doxorubicin, or combination. C) Quantification of Matrigel invasion assay after pretreatment with single or combination drugs.

invasion assay, doxorubicin treatment alone resulted in impaired invasion comparable to dasatinib alone (approximately 90% inhibition). Combination treatment, however, significantly reduced the number of invading cells to approximately 5% of the untreated controls (**Figure 21c**,  $p < 0.05$ ). These data further support the investigation of dasatinib-doxorubicin combination treatments to impair the proliferation, migration, and invasion of breast cancer cells.

## 2.4 DISCUSSION

c-Src is commonly overexpressed or hyperactive in human cancers, including breast cancer. Because of its role at the crossroads of many pathways leading to proliferation, survival, and migration, downregulation of Src is an attractive therapeutic target in the treatment of cancer. New small molecule inhibitors like dasatinib (Sprycel®) target both Src and Abl and are significant because of their relatively high selectivity and high affinity, making low clinical doses possible. Although dasatinib targets primarily Src and Abl at low, nanomolar concentrations, it can directly target other tyrosine kinases, such as Akt, PDGFR, c-kit, and Ephrin receptor, at higher concentrations. At the concentrations of dasatinib used in this study, however, it is unlikely that dasatinib is directly affecting the activity of other tyrosine kinases. Furthermore, I demonstrated that, in the breast cancer cell lines within this work, there are negligible levels of expression and/or activation of other potential targets of dasatinib, including c-kit, EphA2, and Abl.

In these experiments, I investigated the effects of dasatinib on a small panel of breast cancer cell lines in an attempt to determine the molecular pathways underlying the variable responsiveness of basal versus luminal subtype cells to dasatinib that had previously been described (133). Three breast cancer cell lines were tested for their response to dasatinib in proliferation, inhibition of Src signaling, migration, and invasion. Furthermore, I investigated the effects of combining dasatinib treatment with doxorubicin (Adriamycin), a common chemotherapeutic used in breast cancer.

Initially, I found that the MDA-MB-231 cell line, which is triple-negative (lacking ER, PR, and HER2) and basal sub-type, was significantly more sensitive to the anti-proliferative effects of dasatinib than the ER-, PR-positive, luminal subtype MCF7 and T47D cell lines. However, Src inhibition, as measured by dephosphorylation of the Tyr416 activation site, was consistent in all three lines. This indicated that Src activation is not a reliable marker for dasatinib response, despite previous reports in other cell systems (136, 137). Although some loss of phosphorylation was also evident at the inactivating site of Src (Tyr527), this occurred at a much higher dose than that required for Tyr416 dephosphorylation and also did not correspond with anti-proliferative effects of dasatinib. At high doses, dasatinib may also inhibit other tyrosine kinases like PDGFR and c-kit, however these kinases were not present in MDA-MB-231 cells. Although the activation of Abl in MDA-MB-231 cells has previously been reported (149), I was unable to detect any basal phosphorylation of Abl in the breast cancer cell lines tested in these experiments (data not shown). Interestingly, Gonzalez *et al* demonstrated decreases in proliferation of MCF-7 cells employing dominant-negative and siRNA-mediated inhibition of Src that were not evident with dasatinib-mediated Src inhibition (40) suggesting that the non-pharmacological methods of Src inhibition may have stronger effects than dasatinib.

Because there was no difference in the inhibition of Src to explain the differences in anti-proliferative effects, I screened other potential markers of response. Others have reported downregulated mRNA levels of caveolin and moesin after dasatinib treatment of sensitive cells (133, 150). After dasatinib treatment of MDA-MB-231 cells, however, I was unable to detect and change in the protein levels of caveolin or moesin, indicating that actual protein levels may not be suitable markers of response (data not shown). I did identify a Src substrate, CrkL, for which dephosphorylation correlated with proliferative inhibition. CrkL is an adaptor protein that associates with p130<sup>CAS</sup> and is phosphorylated at Tyr207 by FAK-Src complex. This leads to activation of Rac, WAVE/WASp, and Arp2/3 and ultimately actin remodeling. In the dasatinib-sensitive MDA-MB-231 cells, phospho-CrkL (Y207) was decreased by 76%, compared with decreases of only 17% and 34% in

the MCF7 and T47D cells, respectively. This observation warrants further exploration of CrkL activity as a marker for dasatinib response in breast cancer cells.

Downstream of EGFR, Src activation also modulates activation of the PI-3K signaling cascade, leading to activation of the Akt/IKK/NFκB survival pathway (151). The more mesenchymal-like MDA-MB-231 cells demonstrated high basal levels of Akt phosphorylation (S473), which was strongly inhibited by 100 nM dasatinib treatment. Neither basal activity or dasatinib-dependent inhibition were evident in MCF7 or T47D cells, suggesting that the phosphorylation status of Akt could be a biomarker to predict or measure response to dasatinib in breast cancer cells. Kinase assays have demonstrated that dasatinib is capable of directly inhibiting Akt activity, however the IC<sub>50</sub> reported in kinase assays is much higher (> 50 μM) than the 100 nM doses used in these experiments. Because several experiments in this study did not indicate any increases in apoptosis, it is unlikely that dasatinib is affecting cell survival pathways. Rather, Akt-mediated effects on the cell cycle regulators Cdk2 and p27<sup>Kip1</sup>, may explain these results (152-154).

The vast majority of breast cancer related deaths are the result of metastasis, a complex process that requires the acquisition a migratory and invasive phenotype by otherwise non-motile epithelial cells. Therefore, it is important that therapeutics be identified that effectively inhibit the migration and invasion of cancer cells. Several Src substrates, such as FAK, CrkL, and N-WASp, are intimately involved in adhesion and reorganization of the cytoskeleton. Consequently, dasatinib treatment dramatically altered the morphology of the mesenchymal-like MDA-MB-231 cells in culture. In assays measuring migration (wound-healing) and invasion (Matrigel-coated Boyden chambers), MDA-MB-231 cells were greatly impaired (>90% inhibition) by nano-molar doses of dasatinib. The formation of invadopodia, protrusive structures specialized in matrix degradation, is a critical component of efficient cellular invasion (54, 58, 155). Dasatinib-treatment of MDA-MB-231 cells significantly decreased formation of invadopodia, explaining the loss of cellular invasion. However, invasion is a complex process and it cannot be excluded that other functions that contribute to invasion, such as matrix metalloprotease activation and secretion, may also be inhibited after dasatinib treatment. The loss of branched actin structures in dasatinib-treated cells suggests a loss in actin

polymerization, the driving force behind cell motility, which may be sufficient to abrogate any cell migration or invasion.

All of the doses of dasatinib used in this study are below the achievable plasma concentrations determined in Phase I clinical trials and are therefore clinically relevant (138). Although small-molecule inhibitors are potent therapeutics, it is unlikely that they will be used as single-drug regimens. Previous studies have demonstrated that hyperactive Src signaling impaired doxorubicin-induced senescence (156). Based on this, I compared the anti-proliferative effects of dasatinib or doxorubicin alone with combination treatments and found very strong synergistic effects. Doxorubicin alone induces cell cycle arrest at the G<sub>2</sub>/M transition due to inhibition of topoisomerase II. Based on cell cycle analysis, it was evident that the growth arrest effects of doxorubicin were dominant in combination treatments. In MCF7 and T47D cells, which are only moderately responsive to dasatinib alone, the dose of doxorubicin could be reduced by up to 44-fold by combining treatment with an equal dose of dasatinib. Therefore, dasatinib sensitizes cells to the G<sub>2</sub>/M-arrest induced by doxorubicin. Vigneron *et al* suggests a Src-dependent blockage of p21<sup>WAF1</sup> induction in response to doxorubicin.(40). However, I did not observe an additive effect on p21 accumulation after combination treatment (data not shown), indicating that the protective effects of Src are occurring through other regulators of the G<sub>2</sub>/M checkpoint. Additionally, combination treatments significantly reduced the migration and invasion of MDA-MB-231 cells beyond the levels achieved with doxorubicin treatment alone. This suggests that combination treatments might also impair the metastasis of cancer cells *in vitro*. All dosing of dasatinib and doxorubicin was done simultaneously and in equimolar amounts. Adjustments to the dose and schedule of treatment may affect the observed synergistic effects and should be carefully studied. All together, these data strongly support the further investigation of multidrug regimens combining dasatinib with traditional chemotherapeutics such as doxorubicin.



## **CHAPTER 3: CIP4 IS REQUIRED FOR MIGRATION AND INVASION OF BREAST CANCER CELLS**

### **3.1 INTRODUCTION**

Metastatic tumors are responsible for the majority of all breast cancer deaths. Therefore, considerable research is aimed at predicting and preventing invasive behavior in cancer cells. Metastasis is a complex, multistep process in which cancer cells must break away from a larger tumor mass, invade the surrounding tissue, enter, survive, and exit the circulatory system (either lymphatic or blood), and finally survive and proliferate in a distant organ (157). The initial steps in this cascade require a transition to a motile, mesenchymal-like phenotype. Many proteins involved in cell proliferation, apoptosis/survival, and motility have been identified with this “invasive signature” (158). EGFR and several downstream proteins which lead to actin polymerization, including Cdc42, subunits of the Arp2/3 complex, and cofilin are upregulated in rat models of mammary carcinoma (158).

EGFR activation directs actin polymerization, targeting the cell towards higher concentrations of EGF. EGFR signaling, which is potentiated by Src activity, induces Arp2/3-dependent dendritic nucleation through a cascade of G-proteins and WASP/WAVE family members (33, 158). In the case of lamellipodia, branched actin networks are nucleated in response activation of Rac and WAVE. Bundled-actin structures such as filopodia and invadopodia are dependent on Cdc42 and N-WASp activation (42, 86, 88).

N-WASp activation is regulated through auto-inhibitory folding that is relieved by its interaction with active Cdc42 and PI(4,5)P<sub>2</sub> (159). Phosphorylation of Tyr256 by Src family kinases, which occurs only in the open conformation, increases N-WASp activity (97, 160-162). A central proline-rich region adjacent to the Src phosphorylation site interacts with the SH3 domain of CIP4 (101, 102). CIP4 was originally identified as a binding partner of both GTP-Cdc42 and Src family kinases (101, 102).

CIP4 is a member of the F-BAR family of proteins, with FBP17 and Toca-1, that dimerize via alpha-helical BAR domains into amphipathic, crescent-shaped structure that

sense and induce membrane curvature (116, 119). FBP17 has been implicated in podosome formation (128) and Toca-1 potentiates N-WASp activation and actin polymerization (105) (97, 163). Recently, Takano *et al* demonstrated that the increase in N-WASp activation and actin polymerization that occurs with FBP17 and Toca-1 is dependent on the presence of curved lipid membranes (127).

N-WASp activity has been reported at invadopodia, specialized membrane protrusions driven by actin polymerization that promote cellular invasion and remodeling of the extracellular matrix (54, 58, 71). Expression of N-WASp and Cdc42 are both required for invadopodia formation (68). My work demonstrated that Src inhibition also impairs the formation of invadopodia in human breast cancer cells (**Figure 21a**). Although many cytoskeletal proteins have been identified in invadopodia, little attention has been paid to the role of membrane deforming proteins in the formation of invadopodia.

## **3.2 MATERIALS AND METHODS**

### **3.2.1 Cell Culture**

Breast cancer cell lines were obtained from the ATCC via the labs of Drs Gordon Mills and Janet Price (MD Anderson Cancer Center, Houston, TX). All cell lines were grown at 37°C and 5% CO<sub>2</sub> with 10% fetal calf serum (Hyclone, Logan, UT), 100 U/ml penicillin, and 100 mg/ml streptomycin. MDA-MB-231 and T47D cells were grown in DMEM/F12 media (Invitrogen, Carlsbad, CA). MCF7 cells were maintained in MEM media (Invitrogen) supplemented with 10% fetal calf serum, 2mM L-glutamine, 0.1mM non-essential amino acids, 1mM sodium pyruvate, and MEM vitamin solution. All other cell lines were maintained in DMEM with 4500 mg/L glucose and 10% fetal calf serum

### **3.2.2 siRNA-mediated knockdown of CIP4 and N-WASp expression**

MDA-MB-231 cells were transiently transfected with 10 nM of CIP4 or N-WASp-directed or non-targeting siRNA (Qiagen) using the HiPerFect transfection reagent (Qiagen). Decreases in protein expression were verified by western blotting of whole cell

lysates, as described in Section 2.2.4. After 72 hours, cells were replated for the appropriate functional assay.

### ***3.2.2 Immunofluorescence and Invadopodia imaging***

Cells were grown on glass coverslips, fixed in 3.7% formaldehyde (30 minutes), permeabilized with 0.1% TritonX-100 (5 minutes), and blocked in 1% BSA (30 minutes), each at room temperature. Samples were incubated with mouse  $\alpha$ -CIP4 antibody overnight at 4° C, followed by Cy3- or Cy5-conjugated anti-mouse and TRITC-phalloidin for 1 hour at room temperature. Cells were re-fixed in 3.7% formaldehyde. Slides were prepared using ProLong Antifade with DAPI mounting media (Molecular Probes), and imaged with either a Nikon Eclipse TE2000U microscope with MetaMorph imaging software (Molecular Devices, Sunnyvale, CA) or Nikon A1 Confocal Microscope with Nikon NIS-Elements software (Melville, NY).

Gelatin was labeled with FITC (Sigma) in 0.1 M bicarbonate buffer (pH 9.0), dialyzed extensively against PBS, and stored at 4° C. FITC-gelatin was crosslinked with 0.5% glutaraldehyde (10 minutes on ice and 30 minutes at room temperature) and reduced with 1 mg/mL sodium borohydride (5 minutes at room temperature). Cells were plated on FITC-gelatin-coated dishes in complete media and allowed to invade for 16-20 hours, then processed as described above. Samples were stained with TRITC-phalloidin. Invadopodia were counted from 6 to 10 random fields in each sample and averaged over multiple experiments. Gelatin degradation was quantified using the Macnification software (Orbicule BVBA, Heverlee, Belgium).

### ***3.2.3 Migration and Invasion Assays***

Migration was measured by wound healing assay, in which cells were grown to 80% confluence in 6-well plates and streaked with a sterile pipet tip to create a wound. The wound width was measured at marked locations immediately after wounding and again after 24 hours of recovery time. Measurements were taken at multiple points along the length of the wound to create an average for each individual wound, and samples were tested in triplicate. Invasion assays were performed using Matrigel invasion chambers (BD Biosciences, Bedford, MA) seeded with  $2.5 \times 10^4$  cells per well. Complete

media was used in both the upper and lower chambers, with or without 100 ng/mL EGF added only to the lower chamber. Cells were allowed to invade for 24 hours through the Matrigel and 8 mm-pore membrane, at which point the inserts were removed, the upper side of the membranes were scrubbed. The cells were then fixed in methanol, rinsed in distilled water (1 minute each), air-dried, and mounted on slides with ProLong Antifade with DAPI (Molecular Probes). Membranes were visualized with Zeiss epifluorescence microscope to count the number of invading cells in 9 random fields per sample. Samples from multiple experiment were averaged.

### **3.2.4 Acceptor-photobleaching FRET**

Acceptor photobleaching FRET (apFRET) was used to quantify the EGF-dependent interactions between CIP4/N-WASp. All images were recorded using a Zeiss LSM 510 confocal microscope using a 63X, 1.3 NA objective. apFRET was applied largely as described previously where bleach settings are defined empirically (164, 165). Briefly, a cell expressing YFP-CIP4 and CFP-N-WASp was selected and 3 regions of interest (ROIs) were drawn for YFP bleaching and controls. The large ROI (ROI 3) was scanned 10 times using routine scanning settings. The bleach ROIs (ROI1) region was then bleached at 100% intensity for 1000 iterations or approximately 3 min. One ROI (ROI 2) was drawn to measure any potential for off-target bleaching, which accounted for less than 1% of changes in YFP and CFP. Following the bleach, 10 more scans were taken using the prebleach settings. The FRET efficiency (increase in CFP upon YFP bleaching) was calculated using the following equation:

$$\eta_{FRET} = 1 - \frac{I_{CFP, initial}}{I_{CFP, after photobleaching}}$$

Furthermore, the distance between fluorophores was calculated by solving the equation for r:

$$\eta_{FRET} = \frac{R_0^6}{R_0^6 + r^6}$$

Control experiments were performed to validate the apFRET protocol. These included vector controls (CFP, YFP) co-transfected with either YFP-CIP4 or CFP-N-WASp, respectively. In these control experiments, the false positive increase in CFP or CFP-N-WASp upon bleaching YFP-CIP4 or YFP, respectively, ranged from 1-6%.

|                     | Hs578T             | MDA-MB-231       | MCF7               | SKBR3           |
|---------------------|--------------------|------------------|--------------------|-----------------|
| Growth in Matrigel  | Invasive           | Invasive         | Spherical          | Spherical       |
| Growth in nude mice | Metastatic to lung | Locally invasive | Primary tumor only | Non-tumorigenic |
| Invasion assay      | 80-100%            | 100%             | 20-40%             | >20%            |
| Matrix degradation  | 80-100%            | 80-100%          | 0%                 | 0%              |

**Table 4: Comparison of invasive behaviors in breast cancer cell lines**

### 3.3 RESULTS

#### 3.3.1 Invasive breast cancer cell lines express high levels of CIP4

To determine whether CIP4 expression levels correlated with invasiveness, I compiled a panel of breast cancer cell lines of varying invasiveness. Based on previous studies, MDA-MB-231 and Hs578T cells are highly invasive in *in vitro* Boyden chamber assays (1) and also invade and metastasize in nude mice (**Table 4**) (66). In contrast, MCF7, T47D, and SKBR3 cells are weakly or non-invasive *in vitro* (1). These two groups correspond with basal (MDA-MB-231 and Hs578T) and luminal (MCF7, T47D, and SKBR3) subtypes (1). Through immunoblotting, I found that CIP4 protein expression was elevated in the invasive lines as compared with the weakly- or non-invasive lines (**Figure 23a**). This trend was not seen with FBP17 or Toca-1 (**Figure 22a**). This difference was statistically significant ( $p < 0.05$ ) based on densitometric quantification (**Figure 22b**).

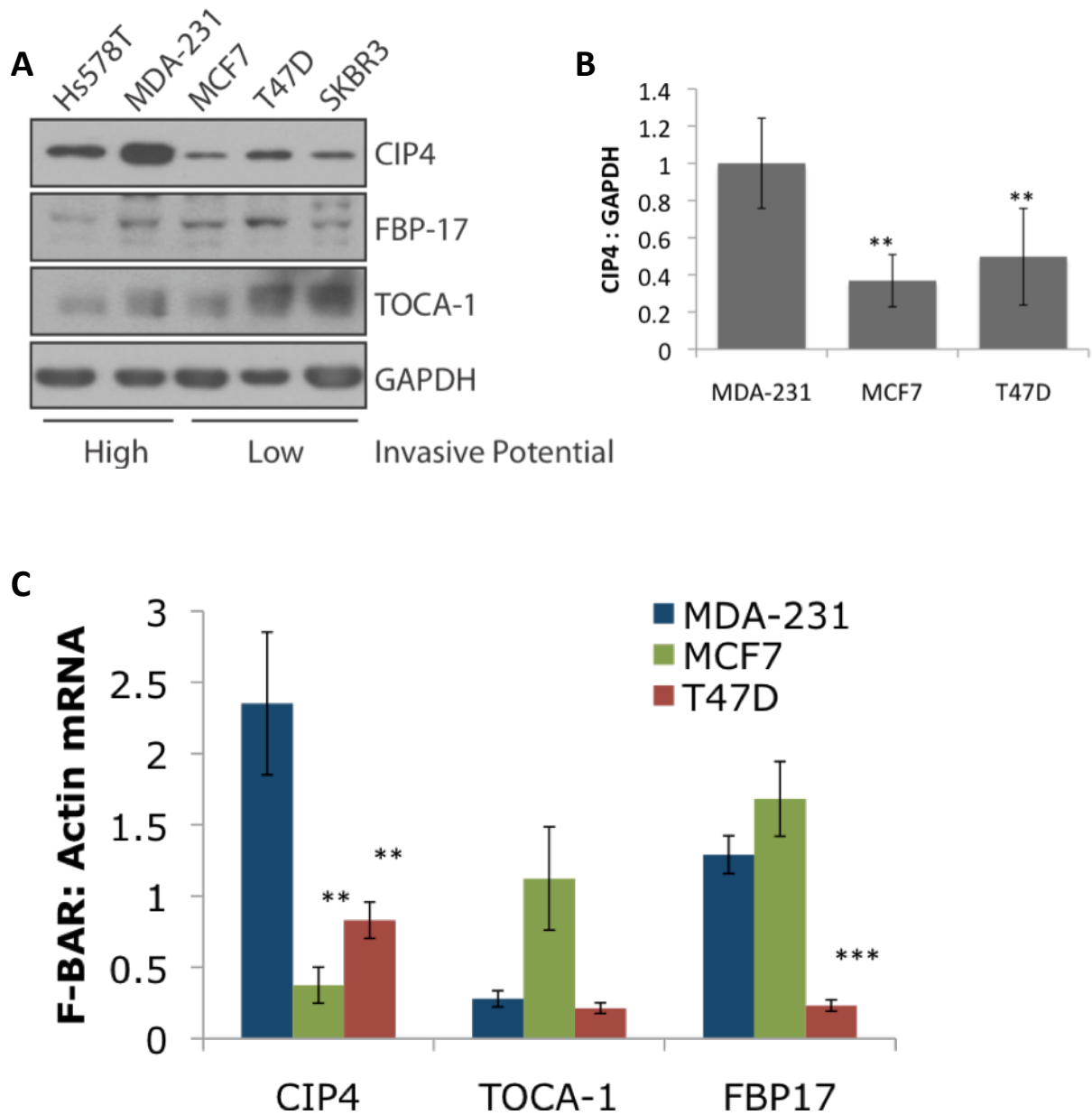


**Figure 22: Overexpression of CIP4 in invasive breast cancer cell lines.** A) Western blot of CIP4, FBP17, and Toca-1 in breast cancer cell line panel. B) Quantification based on densitometric analysis of western blot of CIP4. C) Quantitative PCR of CIP4, Toca1, and FBP17 mRNA.

Expression of CIP4 was also upregulated at the mRNA level in the MDA-MB-231 cells (**Figure 22c**), whereas this pattern was not evident with FBP17 or Toca-1. The average

CIP4 mRNA level was 6.3-fold higher in MDA-MB-231 cells compared with MCF-7 ( $p=0.009$ ) and 2.8-fold higher versus T47D ( $p=0.026$ ).

Our work in the Corey lab and others have identified multiple isoforms of CIP4 that lack functional SH3 domains due to retained intronic sequences (102, 109). Because this structure could have a profound impact on the function of CIP4, I used PCR amplification and digestion to determine whether any of these alternative isoforms were present in the breast cancer cell lines. I screened MDA-MB-231, MCF7, and T47D cell lines for the five CIP4 isoforms (**Figure 8b**), and found that only CIP4a, the ubiquitously expressed, full-length protein, was expressed (data not shown). Therefore, all discussion of CIP4 here refers to the CIP4a isoform.

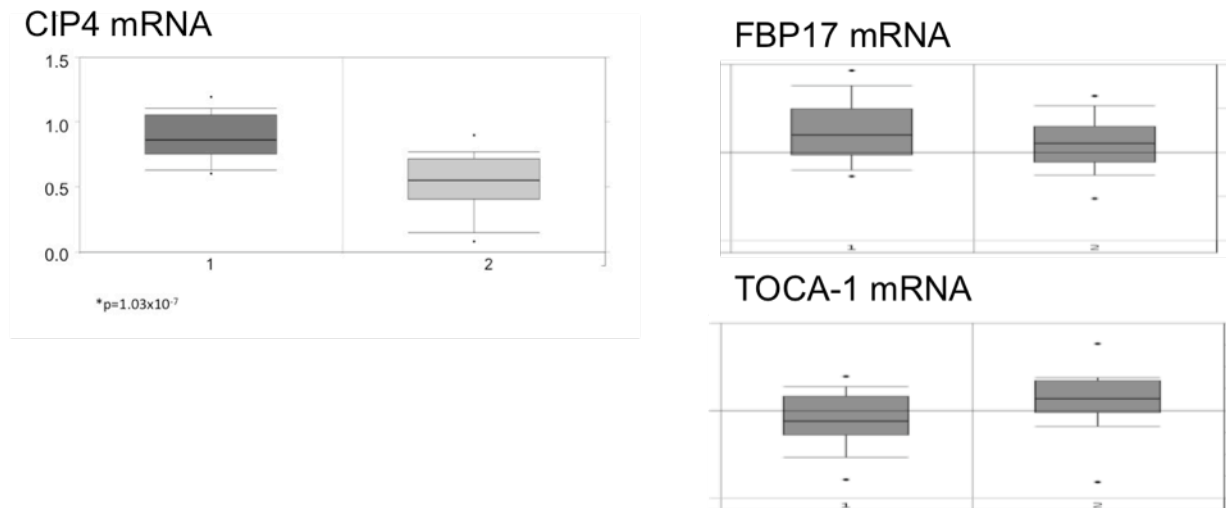


**Figure 23: Upregulation of CIP4 mRNA in triple-negative cell lines.** Gene analysis of 51 well characterized breast cancer cell lines, comparing triple-negative (Group 1) to other breast cancer cell lines (Group 2). From Neve (2006) and analyzed by Oncomine. (1)

MDA-MB-231 and Hs578t cell lines lack ER, PR, HER2, a phenotype known as “triple-negative” that is clinically relevant due to increased invasion, growth rate, and resistance to targeted therapies (166). To determine whether increased CIP4 expression was present in a larger set of triple-negative breast cancer cell lines, bioinformatic analysis of 51 well-characterized lines (1) was screened for CIP4 (**Figure 23**). CIP4 mRNA was significantly increased in the triple-negative group as compared with cell lines of

other biomarker status ( $p=1.03 \times 10^{-7}$ , t-test). Again, no significant difference was seen in the expression of FBP17 or Toca-1 (**Figure 23**).

Because of the membrane-binding properties conferred by the F-BAR domain, subcellular localization may affect its function. I compared the localization of endogenous CIP4 in MDA-MB-231 cells with MCF7 and MCF10a (non-cancerous mammary cell line) and found that CIP4 was enriched at the plasma membrane in only the invasive MDA-MB-231 cell line (**Figure 24**, arrows). MCF7 and MCF10a had little CIP4 at the plasma membrane.

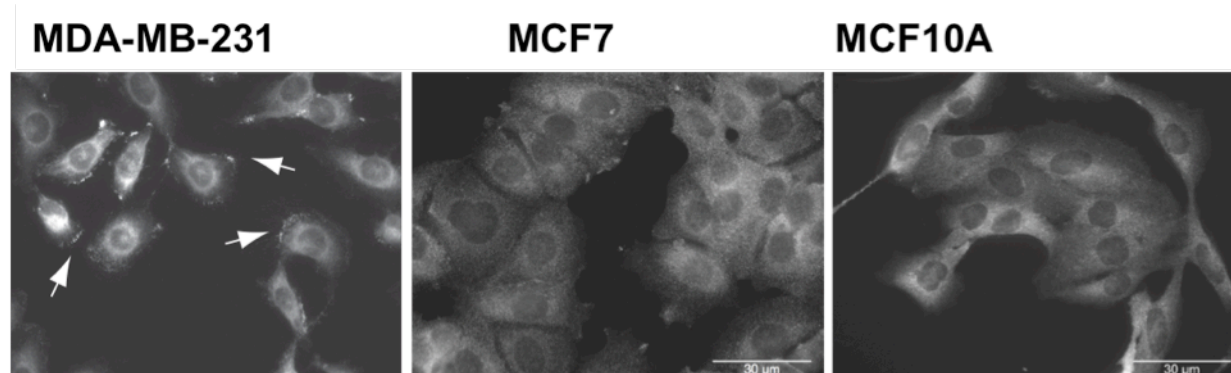


**Figure 24: Subcellular localization of endogenous CIP4.** Staining of unstimulated MDA-MB-231, MCF7, MCF10a.

### ***3.3.2 CIP4 promotes cellular migration in MDA-MB-231 cells***

To investigate whether CIP4 expression correlated with cellular motility in MDA-MB-231 cells, I examined its localization in actively migrating cells. It appears that endogenous CIP4 localizes to the lamellipodia in migrating cells (**Figure 25a**, arrows), suggesting a role in cell migration. Therefore, I used siRNA to specifically downregulate CIP4 (**Figure 25b**) and tested 2D migration with a wound-healing (scratch) assay. After 24 hours recovery, CIP4-depleted cells had repopulated significantly less of the denuded area compared with control cells (**Figure 25c**). Quantification indicated that the residual wounds in CIP4-knockdown cells were more than twice the width of the control wounds ( $p<0.001$ ). To exclude the possibility that this effect was an artifact of proliferative changes in CIP4-depleted cells, I also conducted MTT assays at 24, 48, and 72 hours after knockdown (**Figure 25d**) and found no differences between control CIP4-knockdown cells. These data indicate that CIP4 is required for cellular migration.



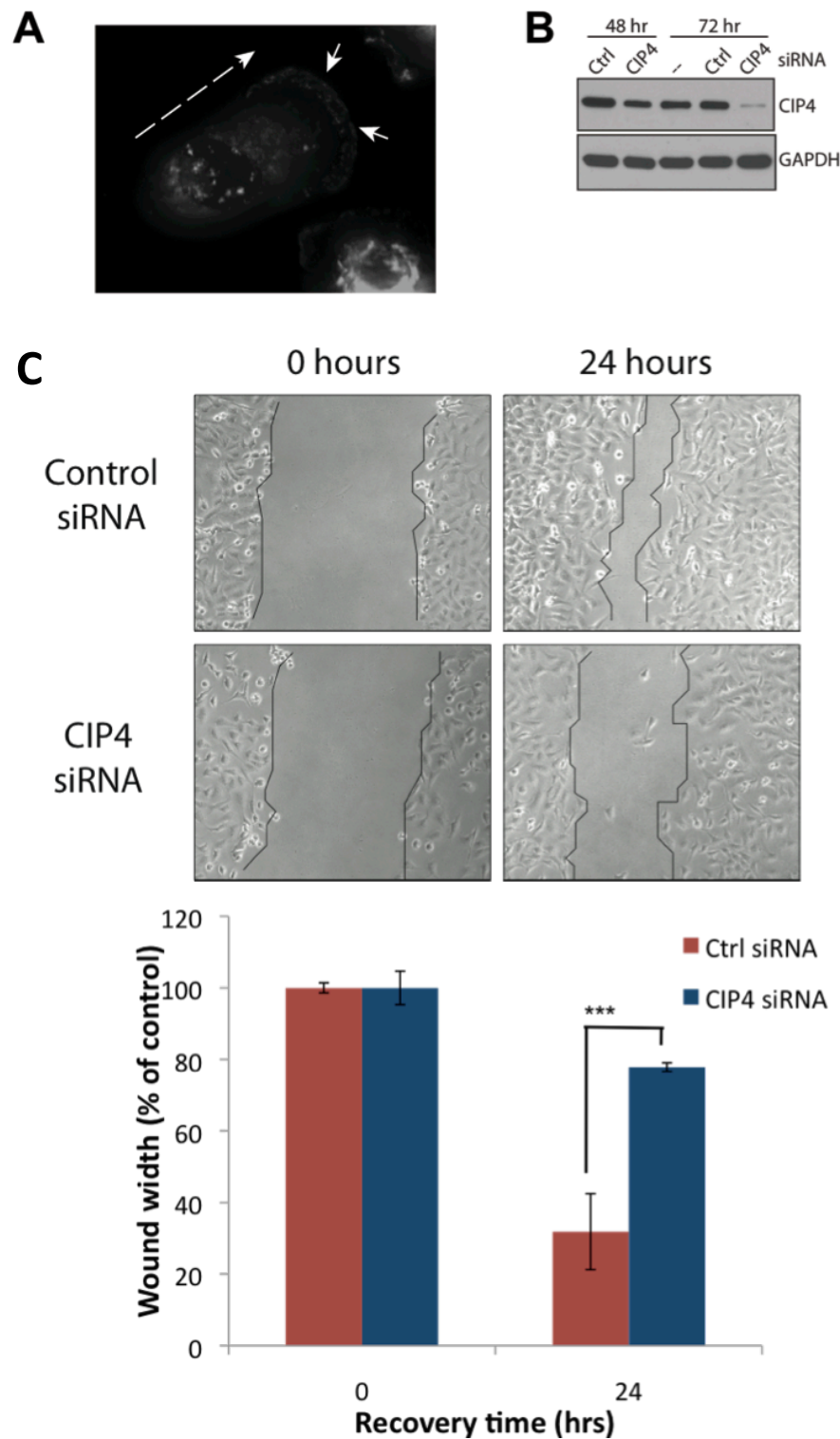
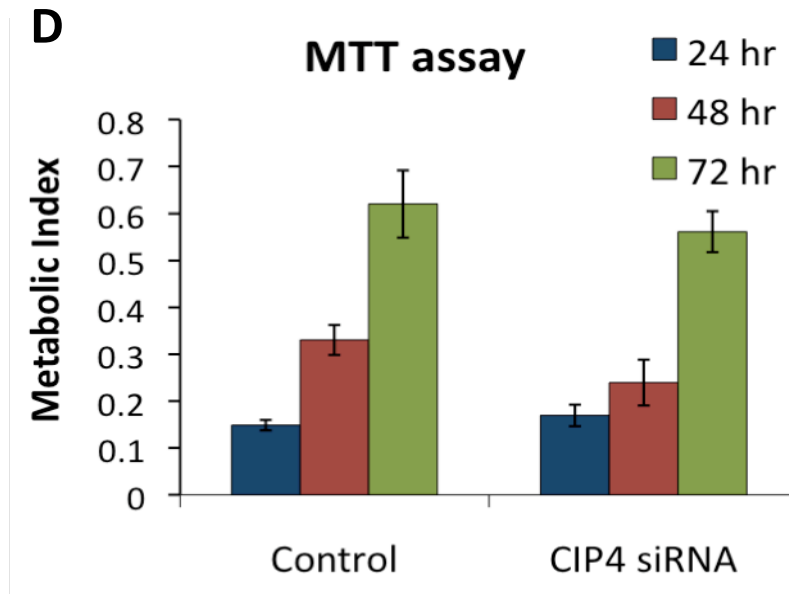


**Figure 25: Depletion of CIP4 impairs migration, not proliferation.** A) Endogenous CIP4 in actively migrating MDAMB-231 cell (solid arrows). Dashed arrow indicates direction of movement. B) Knockdown of CIP4 protein 48 and 72 hours after siRNA transfection. C) Wound-healing assay at 0 and 24 hour after wound in CIP4-depleted cells. Quantification based on average width of wound before and after recovery. D) MTT assay after siRNA transfection.



### 3.3.3 CIP4 controls N-WASp activation in response to EGF

EGF stimulation activates N-WASp via Cdc42 (91, 167). Given that CIP4 interacts with Cdc42 (101) and localizes with EGFR-containing vesicles (168), I speculated that CIP4 might interact with N-WASp in an EGF-dependent manner. Initially, co-immunoprecipitation experiments indicated that EGF transiently increased CIP4-N-WASp interaction at around 1 minute after treatment (data not shown). To confirm this effect and investigate the kinetics more precisely, we used acceptor photobleaching FRET microscopy to quantify the energy transfer between YFP-CIP4 and CFP-N-WASp in MDA-MB-231 cells. Indeed, EGF treatment produced a spike in interaction at around 10 seconds (**Figure 26a**).

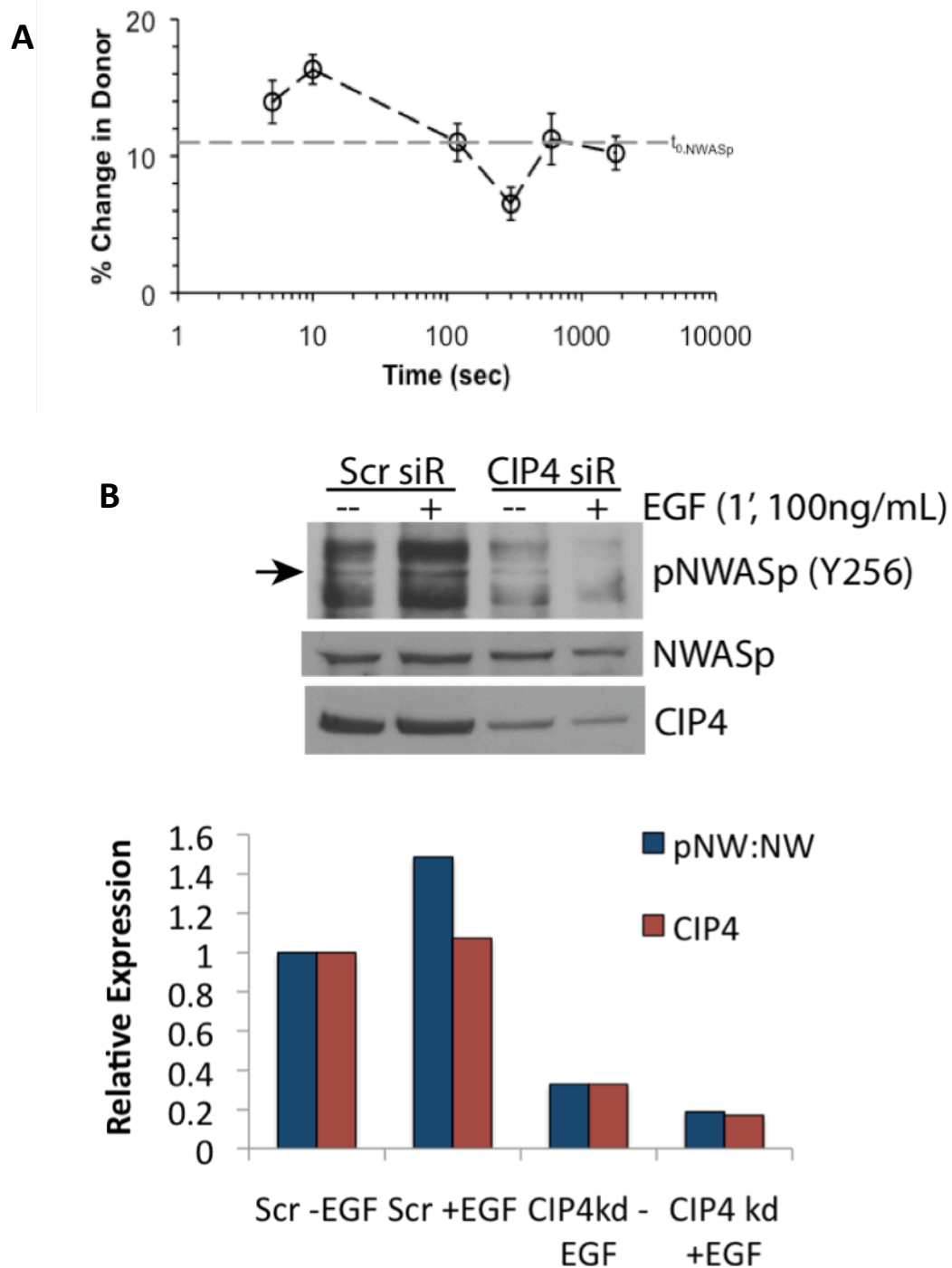


**Figure 26: CIP4 interacts and increases activation of N-WASp downstream of EGFR.** A) Quantification of apFRET experiments demonstrating increase in interaction between YFP-CIP4 and CFP-N-WASp in MDA-MB-231 cells after EGF treatment. B) Western blot for phospho-N-WASp (Y256) (arrow) in cells after siRNA transfection. Quantification based on densitometric analysis.

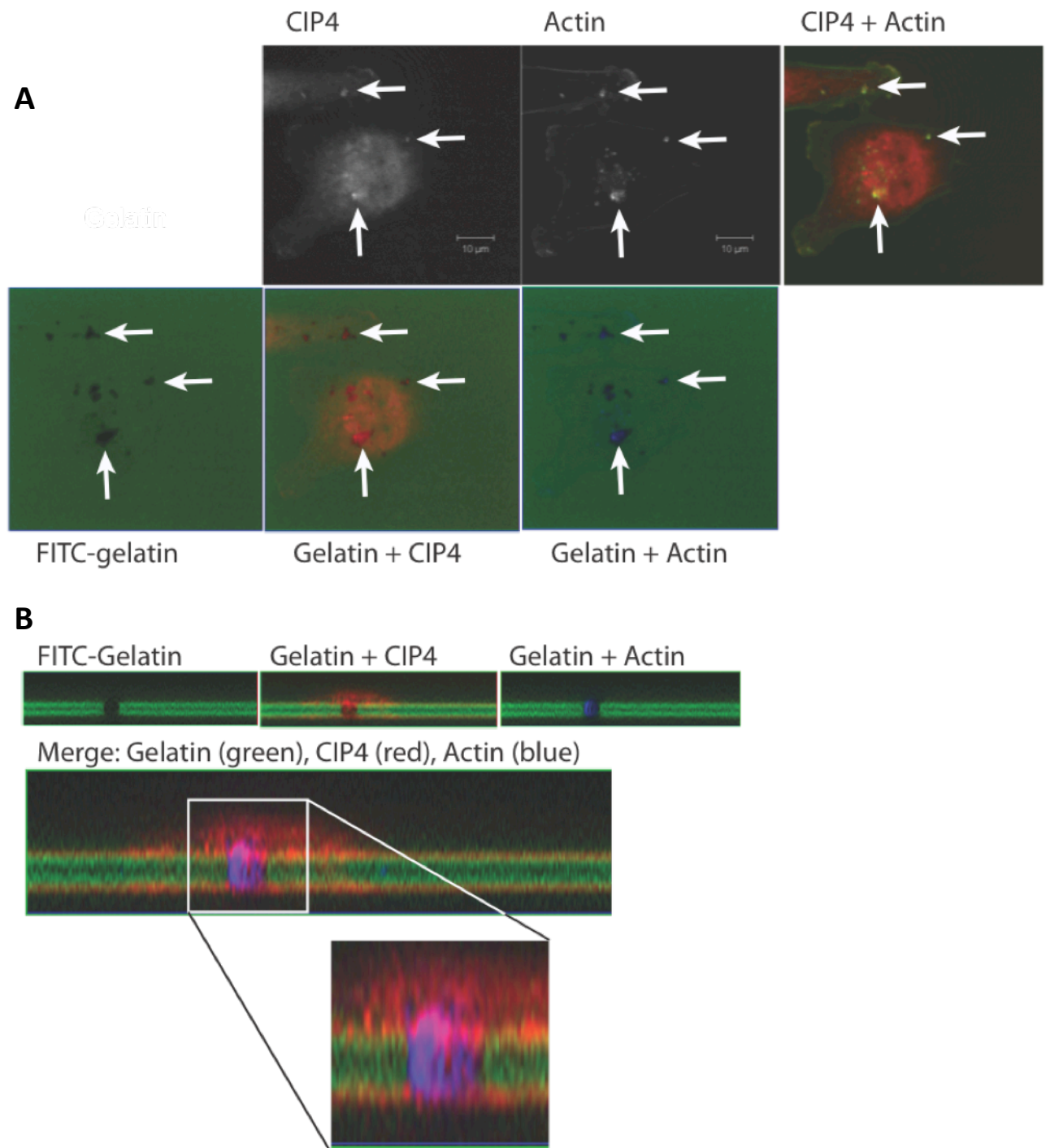


**Figure 27: CIP4 enriched at invadopodia of MDA-MB-231 cells on gelatin.** A) Staining of CIP4 and actin in cells grown on FITC-labeled gelatin reveals active invadopodia (arrows). B) Z-stack projections demonstrate CIP4 at base of invadopodia.

The Src-targeted Tyr256 of N-WASp is only accessible in the open conformation and is associated with increased activity (97, 160-162). Therefore, I used the phosphorylation status of Tyr256 as a surrogate marker for N-WASp activity downstream of EGFR activation. In control cells, stimulation of EGFR increased N-WASp phosphorylation (**Figure 26b**). To determine whether the expression level of CIP4 affected N-WASp activation, I immunoblotted for phospho-N-WASp in control and CIP4-depleted cells treated with EGF. This demonstrated that CIP4 is required N-WASp phosphorylation in resting and EGF-stimulated cells, suggesting that CIP4 promotes the activation of N-WASp.

### ***3.3.4 CIP4 is required for optimal invadopodia formation***

Previous studies have demonstrated that N-WASp and Cdc42 are required for invadopodia formation (68, 71, 74). Because CIP4 regulates the activation of N-WASp and interacts with active Cdc42, it may also participate in invadopodia formation. To visualize invadopodia in cultured cells, MDA-MB-231 cells were grown over a thin layer of FITC-gelatin overnight. Active invadopodia were evident as dots of strong actin staining that co-localized with areas of degraded gelatin substrate (**Figure 27a**, arrows) (58, 71, 155). I found that endogenous CIP4 was also enriched at the invadopodia structures. Z-stack projections of the invadopodia demonstrated that CIP4 was specifically located at the base of the invadopodia, whereas actin was present throughout the length of the structure (**Figure 27b**).

To determine whether CIP4 is also required for invadopodia formation, I used the FITC-gelatin assay to quantify invadopodia in MDA-MB-231 cells after CIP4 depletion. In comparing the percentage of cells that were positive for invadopodia, there was no significant difference (**Figure 29a**). However, there was a significant difference in the number of invadopodia formed by each cell (**Figure 28c**,  $p < 0.05$ ) that was comparable to the defect seen with N-WASp depletion (**Figure 28b**). Furthermore, the average area of

gelatin degradation per cell was significantly decreased by CIP4 knockdown (**Figure 28d**,  $p < 0.001$ ). Again, this effect was comparable to that seen with N-WASp knockdown.

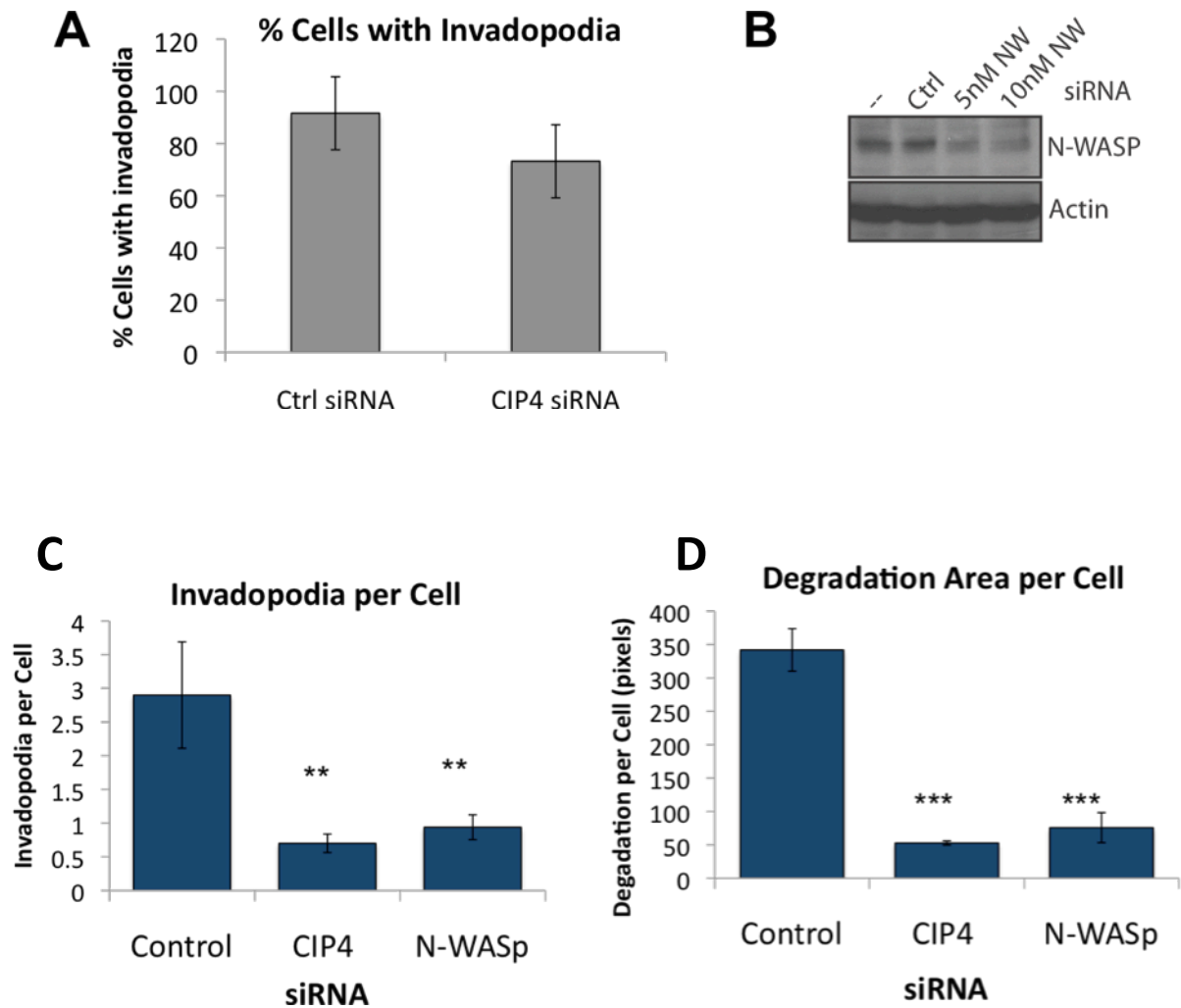


**Figure 28: CIP4 required for formation and function of invadopodia.** A) Quantification of invadopodia by scoring cells as with or without invadopodia. B) Western blot of N-WASp knockdown by siRNA. C) Quantification of invadopodia formation after siRNA knockdown by average number of invadopodia formed per cell. D) Average area of gelatin degradation, normalized to cell number, after siRNA transfection.

### **3.3.5 CIP4 promotes invasion of MDA-MB-231 cells in vitro**

Because invadopodia formation correlates with cellular invasion, I continued the study of CIP4 knockdown in MDA-MB-231 cells to Boyden chamber assays. After 72 hours of CIP4-siRNA treatment, cells were transferred to Matrigel-coated chambers and allowed to invade for an additional 24 hours. CIP4-depletion by two-independent siRNA sequences demonstrated that CIP4 loss significantly inhibited invasion (**Figure 30a**,  $p<0.01$ ) as compared with control cells. This represents a decrease in invasion of approximately 76%, which is similar to the degree of inhibition with N-WASp-siRNA or Src-inhibition (**Figure 20b**).

Although MDA-MB-231 cells invade through Matrigel spontaneously, the presence of EGF in the lower chamber can increase their rate of invasion (**Figure 30b**). This responsiveness to EGF was completely abrogated by CIP4-depletion.

**A**

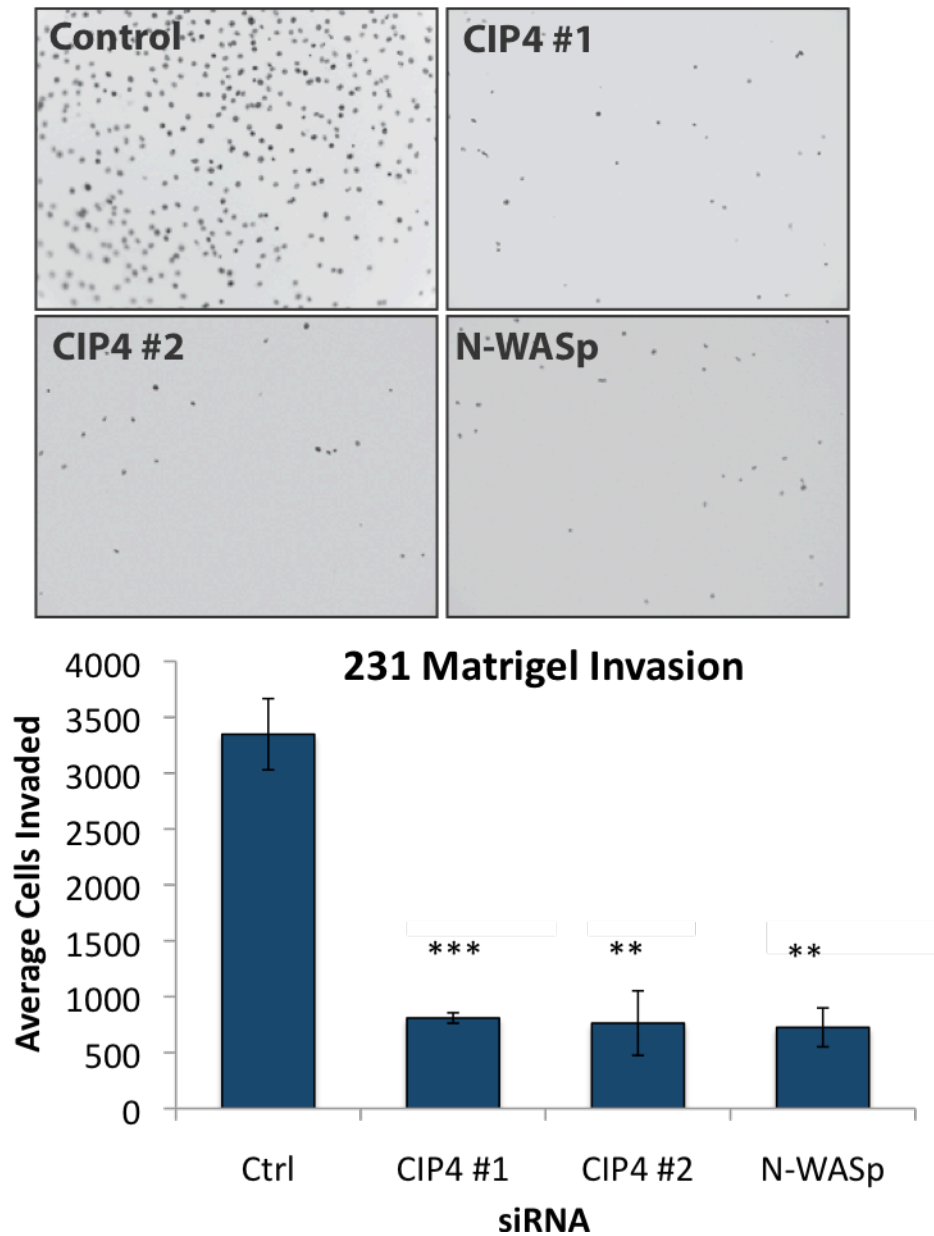
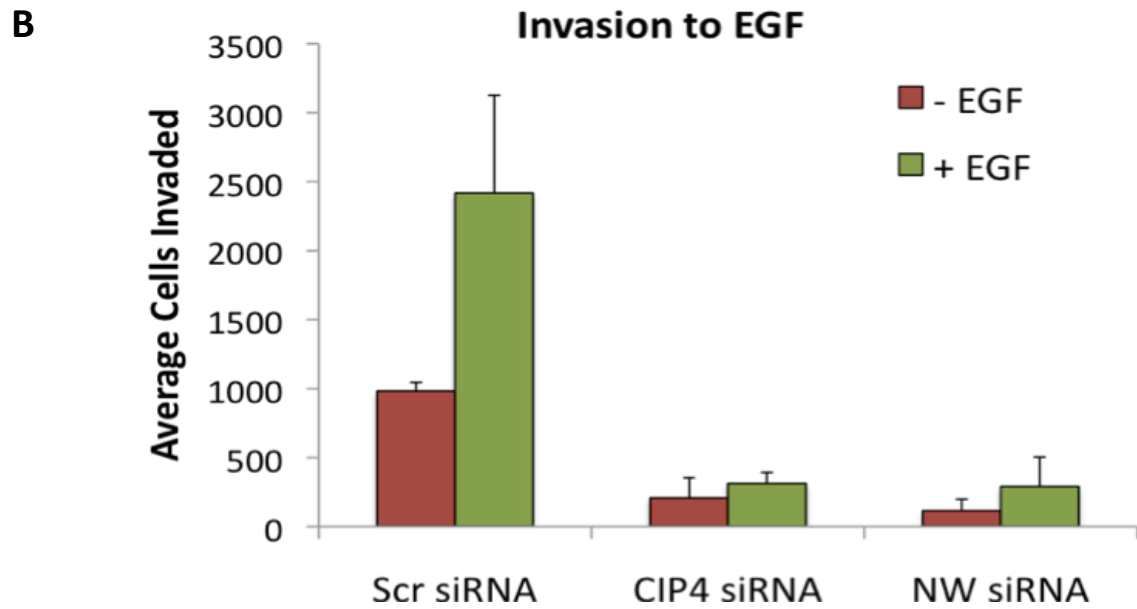


**Figure 29: CIP4 required for basal and EGF-dependent invasion.** A) Matrigel-coated Boyden chamber assay with MDA-MB-231 cells after siRNA transfection. Representative images of each sample after invasion. B) Invasion assay with EGF-spiked media in lower chamber.





### 3.4 DISCUSSION

Several CIP4-associated proteins such as Cdc42, N-WASp, and Src are well established as regulators of cellular invasion and invadopodia formation in cancer cells. However, a role for CIP4 and the F-BAR family of proteins in cancer cell motility has not been previously investigated. In this set of experiments, I demonstrated that CIP4 expression is upregulated at both the protein and mRNA levels in invasive breast cancer cells, suggesting that CIP4 could be a predictive marker for invasion. CIP4 expression also correlated with the clinically significant “triple-negative” cell line. Therefore, CIP4 could be included as a protein in the “invasive signature” as a prognostic marker.

In resting cells, I demonstrated that endogenous CIP4 was concentrated at the plasma membrane of cells with high CIP4 expression, indicating that subcellular localization of CIP4 may have a significant role in its function. Using the highly invasive,

triple-negative breast cancer cell line MDA-MB-231 as a model, I found that siRNA-mediated depletion of CIP4 impaired the 2D migration of cells in wound-healing assays. This reinforces the notion that CIP4 regulates the actin cytoskeleton. While Cdc42 and N-WASp are not typically implicated in lamellipodia formation, they are both required for the formation of the direction-sensing filopodia at the leading edge of the cell. Loss of CIP4 may impair mechanisms of filopodia formation, therefore disrupting directional cell migration.

N-WASp serves as a major effector for the Rho GTPase Cdc42, mediating Cdc42-dependent Arp2/3 activation and actin polymerization (47, 94, 98, 159, 169). Previously, Ho *et al* demonstrated that TOCA-1, a related F-BAR protein, strengthens the Cdc42-mediated activation of N-WASp, resulting in increased actin polymerization in fluorescence-based, cell-free assays (105). Using liposomes, Takano *et al* demonstrated that FBP17 and Toca-1 increased N-WASp-mediated actin polymerization through a membrane-curvature dependent mechanism. I hypothesized that CIP4 may function through a similar mechanism, stabilizing the activation of N-WASp. Because N-WASp activation at the plasma membrane is increased downstream of EGF (71), I investigated whether the interaction between CIP4 and N-WASp might also be responsive to EGF stimulation.

Through co-immunoprecipitation and apFRET microscopy, I demonstrated that the interaction between CIP4 and N-WASp is rapidly and transiently increased after EGFR activation. The peak in interaction was seen at approximately 10 seconds after stimulation and lingers for approximately one minute. This time-frame corresponds with the activation of a FRET-based N-WASp biosensor, as demonstrated by Lorenz *et al* (71). Activation of N-WASp is regulated through auto-inhibitory folding, which precludes phosphorylation of Tyr256 by Src/FAK (97, 162, 170). In the absence of CIP4, basal phosphorylation of Tyr256 was decreased and EGF-induced phosphorylation was abrogated. While not a direct measure of N-WASp activation, phospho-Tyr256 has been correlated with activation and actin polymerization (97, 162, 170). This suggests that CIP4 expression is required for N-WASp activation.

The EGFR-Cdc42-N-WASp signaling pathway has been implicated in the formation of invadopodia, actin-based protrusions that are specialized in matrix degradation (68, 74, 91). Since CIP4 may participate in this cascade, I examined the invadopodia formed by MDA-MB-231 cells in culture through immunofluorescence microscopy. Along with actin, CIP4 was enriched at active invadopodia. CIP4-depletion decreased both the number of invadopodia formed and the area of gelatin-degradation per cell, indicating that CIP4 is critical to the formation and function of invadopodia. No F-BAR family members have been previously associated with invadopodia of cancer cells. Through ELISA assays, I was able to detect a small decrease in the secretion of MMP-9, a gelatin-specific metalloprotease that is relevant in invadopodia. However, the 20% inhibition in MMP-9 is unlikely to account for the approximately 75% decrease in invadopodia formation. The loss of invadopodia and gelatin degradation associated with CIP4 knockdown was comparable to that seen with depletion of N-WASp, which is well established as a critical component of invadopodia formation.

Invadopodia are important to cellular invasion, so I examined whether the loss of CIP4 would affect the invasiveness of MDA-MB-231 cells *in vitro*. I found that loss of CIP4 dramatically inhibited invasion through a Matrigel layer and abrogated the chemoinvasive behavior towards EGF. This supports the hypothesis that CIP4 promotes invasion through the Cdc42-N-WASp signaling pathways.

CIP4's structure suggests that it functions as a scaffolding protein to promote actin polymerization at areas membrane curvature by integrating N-WASp regulation with F-BAR mediated membrane curvature. Through upregulation of this mechanism, CIP4 overexpression may contribute to the invasive phenotype of triple-negative, EGFR-positive breast cancers. These results support the further investigation of CIP4 as a potential biomarker for invasive breast cancers.

## CHAPTER 4: GENERAL SUMMARY

Invasion is a phenotypic hallmark of cancer that can lead to metastasis, which is associated with a poor prognosis (9, 157). Five-year survival rates decrease sharply with diagnosis of advanced breast cancer (23.3%) compared with localized disease (98.3%) (2). One subtype of breast cancer that is associated with aggressive disease and increased metastasis is the “triple-negative” tumors, frequently of the basal subtype. These cancers are refractory to current anti-HER2 targeted therapy (166, 171) and frequently overexpress the EGF receptor (EGFR), which also correlates with invasiveness and poor prognosis (172). Therefore, anti-invasion therapies could have a significant impact on the treatment of advanced breast cancers. Several proteins have been associated with the invasive phenotype, many of which are linked to the cytoskeletal system, including Src, Cdc42, N-WASp (31, 63, 173).

My experiments address the role of the tyrosine kinase Src and the F-BAR protein CIP4 in promoting the migration and invasion of breast cancer cells *in vitro*. Increased expression and activity of Src is common in human breast cancers and is frequently co-expressed with elevated EGFR. I demonstrated that inhibition of Src through dasatinib, a small molecule inhibitor of Src and Abl, impairs not only the proliferation of human breast cancer cells, but also their migration and invasion in *in vitro* assays (173). Although dasatinib has been approved for the treatment of imatinib-resistant leukemias, clinical testing of dasatinib in solid tumors is still ongoing. Combination therapies that include dasatinib have not previously been studied in breast cancer. My data presents a novel finding that dasatinib and the anthracycline doxorubicin synergistically inhibit cell proliferation, representing a significant decrease (greater than 40-fold) in the dose of doxorubicin required for 50% inhibition of cell proliferation. Because Src is involved in a wide variety of signaling pathways, the exact mechanism of this synergy is still unknown. In my research, I was unable to identify cooperative inhibition of any single pathway as a result of combination treatments. This may suggest that the synergistic inhibition of proliferation is the result of blockages in independent pathways. Src inhibition also significantly impairs cell migration and invasion of the clinically significant “triple-negative” breast cancer cells, which are associated with a higher rate of metastasis. My

data suggests that this inhibition occurs through downstream inhibition of the cytoskeletal regulators N-WASp and FAK.

Another Src-associated protein is the F-BAR protein CIP4, which also interacts with N-WASp. My preliminary work demonstrated that CIP4 is upregulated in invasive breast cancer cells, leading me to investigate its contribution to cytoskeletal reorganization. Analysis of CIP4 mRNA expression in a larger set breast cancer cell lines confirmed that CIP4 was elevated in “triple-negative” cell lines, which are typically more invasive. To correlate CIP4 expression with invasiveness in patient samples, I attempted to stain tissue samples with anti-CIP4 antibodies. However, immunohistochemical staining for CIP4 (with multiple commercially available and homemade antibodies) was never successful, possibly due to poor retrieval of CIP4 antigen or degradation of CIP4 before the fixation process. Because of this lack of reliable IHC staining, the development of CIP4 as a biomarker of invasion is limited.

CIP4 is considered a scaffolding protein that recruits N-WASp and dynamin to areas of membrane curvature. My results demonstrate that CIP4 also regulates the activation of N-WASp downstream of EGFR activation. I have also shown that CIP4 depletion significantly impairs the migration and invasion of breast cancer cells *in vitro*. Takano *et al* described a model in which the static repulsion between acidic residues near the SH3 domain of FBP17/Toca-1 and the hydrophobic plasma membrane forces the SH3 domain away from the membrane where it binds N-WASp and stabilizes its binding to the membrane (127). Building on this model, I propose that a similar arrangement is present in CIP4 dimers bound to the plasma membrane. As static repulsion pushes the SH3 domain away from the plasma membrane and the hydrophobic outer face of the F-BAR domains, CIP4 acts as a stabilizer for the open conformation of N-WASp (**Figure 10**). N-WASp binds the plasma membrane directly through its basic region, tethering one end of the protein to PI(4,5)P<sub>2</sub>-enriched membranes. The interaction with CIP4 serves two functions: Firstly, binding to CIP4 localizes N-WASp to areas of membrane curvature such as budding vesicles or invadopodia. Secondly, the spring-like action of CIP4 holds N-WASp in an open conformation, potentiating its activation by increasing access to the Src/FAK-

targeted phosphorylation site (Tyr256) and the Cdc42 (GTPase)-binding domain. GTP-Cdc42 and Src phosphorylation are both associated with increased actin polymerization via N-WASp(96, 97, 159). Our lab initially identified CIP4 as a novel binding partner of SFKs and has demonstrated Src-dependent phosphorylation (unpublished results) adjacent to the acidic region described by Takano *et al.* Therefore, I propose that phosphorylation of CIP4 by Src increases the hydrophobic nature of this region and increases the electrostatic repulsion holding CIP4's SH3 domain away from the membrane. Essentially, this stiffens the spring action of CIP4 at the plasma membrane and further strengthens the stabilization of open N-WASp.

F-BAR proteins have not previously been identified at invadopodia. My data demonstrate the novel finding that CIP4 is localized to invadopodia of breast cancer cells *in vitro*. I also show that depletion of CIP4 significantly impairs the formation and function (gelatin-degradation) of invadopodia. Furthermore, this loss of invadopodia translates to a loss in invasiveness through Matrigel-coated Boyden chambers. Together, these data suggest that CIP4 is a critical component of the invasive phenotype. Therefore, the overexpression of CIP4, as seen in triple-negative human breast cancer cell lines, may serve as a predictive marker for invasive disease and potential therapeutic target.



## CHAPTER 5: FUTURE DIRECTIONS

My experiments with dasatinib inhibition of Src demonstrated a high degree of synergy with doxorubicin in impairing cell proliferation. However, the mechanism underlying this phenomenon is still unclear. Future research into combination therapies including both dasatinib and doxorubicin should focus on the molecular pathways that account for the Src-dependent resistance to doxorubicin in breast cancer cells.

Although research in our lab identified a Src phosphorylation site within CIP4, the effects of this modification are unknown. I have postulated that this phosphate group increases the electrostatic repulsion that forces the SH3 domain away from the plasma membrane, stiffening the spring-like mechanism by which CIP4 stabilizes the open conformation of N-WASp. A major drawback in the study of CIP4 is the current lack of any measure of CIP4 function. Similar to the FRET-based studies described by Takano *et al*, the structural arrangement of membrane-bound CIP4 and N-WASp could be studied in response to Src phosphorylation and the availability of curved membranes. Disruption of the phosphorylation by Src, which could be accomplished with dasatinib treatment, may weaken the spring-action of CIP4 and impair its ability to stabilize the open N-WASp conformation. Cell-free actin polymerization assays may provide a quantifiable method for measuring CIP4 function. Src inhibition through dasatinib could be used to study the effects on CIP4 through these assays. Furthermore, the Src binding region of CIP4 may also allow it to act as a scaffold to directly promote N-WASp phosphorylation by Src at the plasma membrane. The establishment of CIP4 as a downstream effector of Src would represent a novel pathway in the Src-signaling cascade. These experiments could initially be carried out using cell-free, liposome based assays but would be more relevant when performed in invadopodia model systems. Because F-BAR interaction with the plasma membrane is curvature-dependent, cells grown on standard culture surfaces may not be the optimal models. Rather, cells grown on gelatin, allowing formation of invadopodia may provide more sites for formation of these complexes. Furthermore, efficient activation of integrins by the presence of extracellular matrix may also encourage these complexes.



Mutants of CIP4 that lack functional binding sites for N-WASp or Cdc42 or which carry point mutations in the Src-phosphorylation site would be useful tools in elucidating which interactions are critical the function of CIP4. Biochemical experiments are needed to determine whether CIP4 is required for N-WASp interaction with Cdc42. Because CIP4 overexpression correlates with invasiveness, biochemical studies should be performed to determine the effects of saturating concentrations of CIP4 in comparison to N-WASp and Cdc42. The SH3 domain of CIP4 also interacts with dynamin, an important component of vesicle fission. Dynamin is also found in invadopodia, although its function there is unknown. More research is needed to determine whether CIP4 is required for recruitment of dynamin to invadopodia or in some way contributes to its function.

My results clearly demonstrated increased CIP4 expression, at the mRNA and protein levels, in invasive and “triple-negative” breast cancer cell lines. However, the regulation of CIP4 expression has not previously been examined. Because “triple-negative” cell lines frequently express high levels of EGFR, it is possible that transcription factors activated downstream of EGFR are responsible for CIP4 expression.

The time-line of invadopodia formation is not well understood, therefore the stage at which CIP4 and N-WASp are recruited to invadopodia is unknown. Live-cell time-lapse microscopy, using fluorescently tagged CIP4 and N-WASp would demonstrate whether CIP4 is required for the early formation of invadopodia or the maintenance of a more stable structure. If CIP4 is required for laying the initial base of branched actin, invadopodia formation will be impaired at a very early stage of development. Breast cancer cells that stably express fluorescently labeled actin monomers would be very useful for this assay.

I demonstrated that CIP4-depletion severely impairs the cellular invasion of breast cancer cells *in vitro*, however this should be transferred to animal models to determine whether inhibition of CIP4 leads to an inhibition in metastasis. Because the experiments here represent localized invasion, the most germane experiments would focus on local tissue invasion of orthotopic tumors in nude mice, as evaluated by histological studies. Our work in the Corey lab has produced CIP4-null transgenic mice (174), which have a minimal phenotype of rapid clearance of blood glucose resulting from delayed endocytosis of the GLUT4 glucose transporter. Although the mice do not suffer any

obvious defects in normal cell migration in development, it is possible that loss of CIP4 may play a more specific role in the invasive process of transformed epithelial cells. Therefore, cross-breeding of the CIP4-null mice with mouse models of metastasis, such as the MMTV model, would be useful to determine the contribution of CIP4 to invasion and metastasis of spontaneously generated tumors *in vivo*. Such a system would also be useful in determining the importance of CIP4 in Src-dependent pathways, using dasatinib as an anti-metastatic agent. Because of the minimal phenotype of the CIP4-null mice and the close homology of CIP4 to FBP17 and Toca-1, the generation of triple-knockout mouse could produce a stronger effect on development or other normal migratory processes.

## REFERENCES

1. Neve, R. M., K. Chin, J. Fridlyand, J. Yeh, F. L. Baehner, T. Fevr, L. Clark, N. Bayani, J. P. Coppe, F. Tong, T. Speed, P. T. Spellman, S. DeVries, A. Lapuk, N. J. Wang, W. L. Kuo, J. L. Stilwell, D. Pinkel, D. G. Albertson, F. M. Waldman, F. McCormick, R. B. Dickson, M. D. Johnson, M. Lippman, S. Ethier, A. Gazdar, and J. W. Gray. 2006. A collection of breast cancer cell lines for the study of functionally distinct cancer subtypes. *Cancer Cell* 10:515-527.
2. Horner, M., L. Ries, M. Krapcho, N. Neyman, R. Aminou, N. Howlader, S. Altekruse, E. Feuer, L. Huang, A. Mariotto, B. Miller, D. Lewis, M. Eisner, D. Stinchcomb, and B. Edwards. 2009. SEER Cancer Statistics Review, 1975-2006. National Cancer Institute. Bethesda, MD. .
3. Pharoah, P. D., N. E. Day, S. Duffy, D. F. Easton, and B. A. Ponder. 1997. Family history and the risk of breast cancer: a systematic review and meta-analysis. *Int J Cancer* 71:800-809.
4. Colditz, G. A., W. C. Willett, D. J. Hunter, M. J. Stampfer, J. E. Manson, C. H. Hennekens, and B. A. Rosner. 1993. Family history, age, and risk of breast cancer. Prospective data from the Nurses' Health Study. *Jama* 270:338-343.
5. Johnson, N., T. Lancaster, A. Fuller, and S. V. Hodgson. 1995. The prevalence of a family history of cancer in general practice. *Fam Pract* 12:287-289.
6. 2002. Breast cancer and breastfeeding: collaborative reanalysis of individual data from 47 epidemiological studies in 30 countries, including 50302 women with breast cancer and 96973 women without the disease. *Lancet* 360:187-195.
7. Key, T. J., P. K. Verkasalo, and E. Banks. 2001. Epidemiology of breast cancer. *Lancet Oncol* 2:133-140.
8. Key, T., P. Appleby, I. Barnes, and G. Reeves. 2002. Endogenous sex hormones and breast cancer in postmenopausal women: reanalysis of nine prospective studies. *J Natl Cancer Inst* 94:606-616.
9. Hanahan, D., and R. A. Weinberg. 2000. The hallmarks of cancer. *Cell* 100:57-70.
10. Sims, A. H., A. Howell, S. J. Howell, and R. B. Clarke. 2007. Origins of breast cancer subtypes and therapeutic implications. *Nat Clin Pract Oncol* 4:516-525.

11. Cheang, M. C., D. Voduc, C. Bajdik, S. Leung, S. McKinney, S. K. Chia, C. M. Perou, and T. O. Nielsen. 2008. Basal-like breast cancer defined by five biomarkers has superior prognostic value than triple-negative phenotype. *Clin Cancer Res* 14:1368-1376.
12. Amoroso, V., F. Valcamonico, E. Simoncini, L. Ardighieri, S. Grisanti, L. Vassalli, P. Marpicati, L. Lucini, V. D. Ferrari, G. Rangoni, and G. Marini. 2005. A retrospective series of long-term survivors of metastatic breast cancer in complete remission. *Oncology* 68:48-51.
13. Nicholson, R. I., J. M. Gee, and M. E. Harper. 2001. EGFR and cancer prognosis. *Eur J Cancer* 37 Suppl 4:S9-15.
14. Lo, H. W., S. C. Hsu, and M. C. Hung. 2006. EGFR signaling pathway in breast cancers: from traditional signal transduction to direct nuclear translocation. *Breast Cancer Res Treat* 95:211-218.
15. Karunagaran, D., E. Tzahar, R. R. Beerli, X. Chen, D. Graus-Porta, B. J. Ratzkin, R. Seger, N. E. Hynes, and Y. Yarden. 1996. ErbB-2 is a common auxiliary subunit of NDF and EGF receptors: implications for breast cancer. *Embo J* 15:254-264.
16. Osborne, C., P. Wilson, and D. Tripathy. 2004. Oncogenes and tumor suppressor genes in breast cancer: potential diagnostic and therapeutic applications. *Oncologist* 9:361-377.
17. Slamon, D. J., G. M. Clark, S. G. Wong, W. J. Levin, A. Ullrich, and W. L. McGuire. 1987. Human breast cancer: correlation of relapse and survival with amplification of the HER-2/neu oncogene. *Science* 235:177-182.
18. Irby, R. B., and T. J. Yeatman. 2000. Role of Src expression and activation in human cancer. *Oncogene* 19:5636-5642.
19. Frame, M. C., V. J. Fincham, N. O. Carragher, and J. A. Wyke. 2002. v-Src's hold over actin and cell adhesions. *Nat Rev Mol Cell Biol* 3:233-245.
20. Playford, M. P., and M. D. Schaller. 2004. The interplay between Src and integrins in normal and tumor biology. *Oncogene* 23:7928-7946.
21. Thomas, S. M., and J. S. Brugge. 1997. Cellular functions regulated by Src family kinases. *Annu Rev Cell Dev Biol* 13:513-609.

22. Gallick, G. E. 2004. SRC as a potential therapeutic target in solid tumor oncology. *Clin Adv Hematol Oncol* 2:435-437.
23. Dehm, S. M., and K. Bonham. 2004. SRC gene expression in human cancer: the role of transcriptional activation. *Biochem Cell Biol* 82:263-274.
24. Irby, R. B., W. Mao, D. Coppola, J. Kang, J. M. Loubeau, W. Trudeau, R. Karl, D. J. Fujita, R. Jove, and T. J. Yeatman. 1999. Activating SRC mutation in a subset of advanced human colon cancers. *Nat Genet* 21:187-190.
25. Irby, R., W. Mao, D. Coppola, R. Jove, A. Gamero, D. Cuthbertson, D. J. Fujita, and T. J. Yeatman. 1997. Overexpression of normal c-Src in poorly metastatic human colon cancer cells enhances primary tumor growth but not metastatic potential. *Cell Growth Differ* 8:1287-1295.
26. Hamaguchi, M., N. Matsuyoshi, Y. Ohnishi, B. Gotoh, M. Takeichi, and Y. Nagai. 1993. p60v-src causes tyrosine phosphorylation and inactivation of the N-cadherin-catenin cell adhesion system. *Embo J* 12:307-314.
27. Mao, W., R. Irby, D. Coppola, L. Fu, M. Wloch, J. Turner, H. Yu, R. Garcia, R. Jove, and T. J. Yeatman. 1997. Activation of c-Src by receptor tyrosine kinases in human colon cancer cells with high metastatic potential. *Oncogene* 15:3083-3090.
28. Hennipman, A., B. A. van Oirschot, J. Smits, G. Rijksen, and G. E. Staal. 1989. Tyrosine kinase activity in breast cancer, benign breast disease, and normal breast tissue. *Cancer Res* 49:516-521.
29. Ottenhoff-Kalff, A. E., G. Rijksen, E. A. van Beurden, A. Hennipman, A. A. Michels, and G. E. Staal. 1992. Characterization of protein tyrosine kinases from human breast cancer: involvement of the c-src oncogene product. *Cancer Res* 52:4773-4778.
30. Rosen, N., J. B. Bolen, A. M. Schwartz, P. Cohen, V. DeSeau, and M. A. Israel. 1986. Analysis of pp60c-src protein kinase activity in human tumor cell lines and tissues. *J Biol Chem* 261:13754-13759.
31. Summy, J. M., and G. E. Gallick. 2003. Src family kinases in tumor progression and metastasis. *Cancer Metastasis Rev* 22:337-358.

32. Verbeek, B. S., T. M. Vroom, S. S. Adriaansen-Slot, A. E. Ottenhoff-Kalff, J. G. Geertzema, A. Hennipman, and G. Rijksen. 1996. c-Src protein expression is increased in human breast cancer. An immunohistochemical and biochemical analysis. *J Pathol* 180:383-388.
33. Biscardi, J. S., R. C. Ishizawa, C. M. Silva, and S. J. Parsons. 2000. Tyrosine kinase signalling in breast cancer: epidermal growth factor receptor and c-Src interactions in breast cancer. *Breast Cancer Res* 2:203-210.
34. Muthuswamy, S. K., and W. J. Muller. 1995. Direct and specific interaction of c-Src with Neu is involved in signaling by the epidermal growth factor receptor. *Oncogene* 11:271-279.
35. Dimri, M., M. Naramura, L. Duan, J. Chen, C. Ortega-Cava, G. Chen, R. Goswami, N. Fernandes, Q. Gao, G. P. Dimri, V. Band, and H. Band. 2007. Modeling breast cancer-associated c-Src and EGFR overexpression in human MECs: c-Src and EGFR cooperatively promote aberrant three-dimensional acinar structure and invasive behavior. *Cancer Res* 67:4164-4172.
36. Jallal, H., M. L. Valentino, G. Chen, F. Boschelli, S. Ali, and S. A. Rabbani. 2007. A Src/Abl kinase inhibitor, SKI-606, blocks breast cancer invasion, growth, and metastasis in vitro and in vivo. *Cancer Res* 67:1580-1588.
37. Park, S. I., J. Zhang, K. A. Phillips, J. C. Araujo, A. M. Najjar, A. Y. Volgin, J. G. Gelovani, S. J. Kim, Z. Wang, and G. E. Gallick. 2008. Targeting SRC family kinases inhibits growth and lymph node metastases of prostate cancer in an orthotopic nude mouse model. *Cancer Res* 68:3323-3333.
38. Rucci, N., I. Recchia, A. Angelucci, M. Alamanou, A. Del Fattore, D. Fortunati, M. Susa, D. Fabbro, M. Bologna, and A. Teti. 2006. Inhibition of protein kinase c-Src reduces the incidence of breast cancer metastases and increases survival in mice: implications for therapy. *J Pharmacol Exp Ther* 318:161-172.
39. Trevino, J. G., J. M. Summy, and G. E. Gallick. 2006. SRC inhibitors as potential therapeutic agents for human cancers. *Mini Rev Med Chem* 6:681-687.
40. Gonzalez, L., M. T. Agullo-Ortuno, J. M. Garcia-Martinez, A. Calcabrini, C. Gamallo, J. Palacios, A. Aranda, and J. Martin-Perez. 2006. Role of c-Src in human MCF7 breast cancer cell tumorigenesis. *J Biol Chem* 281:20851-20864.

41. Alberts, B., A. Johnson, J. Lewis, M. Raff, K. Roberts, and P. Walter. 2002. *Molecular Biology of the Cell*. Garland Science, New York, NY.
42. Chhabra, E. S., and H. N. Higgs. 2007. The many faces of actin: matching assembly factors with cellular structures. *Nat Cell Biol* 9:1110-1121.
43. Le Clainche, C., and M. F. Carlier. 2008. Regulation of actin assembly associated with protrusion and adhesion in cell migration. *Physiol Rev* 88:489-513.
44. Pollard, T. D., and W. Earnshaw. 2002. *Cell Biology: An Illustrated Text*. W.B. Saunders Company, Philadelphia, PA.
45. Pollard, T. D., and J. A. Cooper. 2009. Actin, a Central Player in Cell Shape and Movement. *Science* 326:1208-1212.
46. Cai, L., and J. E. Bear. 2008. Peering deeply inside the branch. *J Cell Biol* 180:853-855.
47. Higgs, H. N., and T. D. Pollard. 2001. Regulation of actin filament network formation through ARP2/3 complex: activation by a diverse array of proteins. *Annu Rev Biochem* 70:649-676.
48. Makale, M. 2007. Cellular mechanobiology and cancer metastasis. *Birth Defects Res C Embryo Today* 81:329-343.
49. Vinogradova, T., P. M. Miller, and I. Kaverina. 2009. Microtubule network asymmetry in motile cells: role of Golgi-derived array. *Cell Cycle* 8:2168-2174.
50. Hall, A. 2009. The cytoskeleton and cancer. *Cancer Metastasis Rev* 28:5-14.
51. Wang, Y. L. 1985. Exchange of actin subunits at the leading edge of living fibroblasts: possible role of treadmilling. *J Cell Biol* 101:597-602.
52. Aspenstrom, P., N. Richnau, and A. S. Johansson. 2006. The diaphanous-related formin DAAM1 collaborates with the Rho GTPases RhoA and Cdc42, CIP4 and Src in regulating cell morphogenesis and actin dynamics. *Exp Cell Res* 312:2180-2194.
53. Gimona, M. 2008. The microfilament system in the formation of invasive adhesions. *Semin Cancer Biol* 18:23-34.
54. Linder, S. 2007. The matrix corroded: podosomes and invadopodia in extracellular matrix degradation. *Trends Cell Biol* 17:107-117.

55. Bowden, E. T., P. J. Coopman, and S. C. Mueller. 2001. Invadopodia: unique methods for measurement of extracellular matrix degradation in vitro. *Methods Cell Biol* 63:613-627.
56. Clark, E. S., A. S. Whigham, W. G. Yarbrough, and A. M. Weaver. 2007. Cortactin is an essential regulator of matrix metalloproteinase secretion and extracellular matrix degradation in invadopodia. *Cancer Res* 67:4227-4235.
57. Machesky, L. M. 2008. Lamellipodia and filopodia in metastasis and invasion. *FEBS Lett* 582:2102-2111.
58. Weaver, A. M. 2006. Invadopodia: specialized cell structures for cancer invasion. *Clin Exp Metastasis* 23:97-105.
59. David-Pfeuty, T., and S. J. Singer. 1980. Altered distributions of the cytoskeletal proteins vinculin and alpha-actinin in cultured fibroblasts transformed by Rous sarcoma virus. *Proc Natl Acad Sci U S A* 77:6687-6691.
60. Chen, W. T., J. M. Chen, S. J. Parsons, and J. T. Parsons. 1985. Local degradation of fibronectin at sites of expression of the transforming gene product pp60src. *Nature* 316:156-158.
61. Tarone, G., D. Cirillo, F. G. Giancotti, P. M. Comoglio, and P. C. Marchisio. 1985. Rous sarcoma virus-transformed fibroblasts adhere primarily at discrete protrusions of the ventral membrane called podosomes. *Exp Cell Res* 159:141-157.
62. Vignjevic, D., and G. Montagnac. 2008. Reorganisation of the dendritic actin network during cancer cell migration and invasion. *Semin Cancer Biol* 18:12-22.
63. Yamazaki, D., S. Kurisu, and T. Takenawa. 2005. Regulation of cancer cell motility through actin reorganization. *Cancer Sci* 96:379-386.
64. Bowden, E. T., E. Onikoyi, R. Slack, A. Myoui, T. Yoneda, K. M. Yamada, and S. C. Mueller. 2006. Co-localization of cortactin and phosphotyrosine identifies active invadopodia in human breast cancer cells. *Exp Cell Res* 312:1240-1253.
65. Artym, V. V., Y. Zhang, F. Seillier-Moiseiwitsch, K. M. Yamada, and S. C. Mueller. 2006. Dynamic Interactions of Cortactin and Membrane Type 1 Matrix Metalloproteinase at Invadopodia: Defining the Stages of Invadopodia Formation and Function. *Cancer Res* 66:3034-3043.



66. Bowden, E. T., M. Barth, D. Thomas, R. I. Glazer, and S. C. Mueller. 1999. An invasion-related complex of cortactin, paxillin and PKC $\mu$  associates with invadopodia at sites of extracellular matrix degradation. *Oncogene* 18:4440-4449.
67. Ayala, I., M. Baldassarre, G. Giacchetti, G. Caldieri, S. Tete, A. Luini, and R. Buccione. 2008. Multiple regulatory inputs converge on cortactin to control invadopodia biogenesis and extracellular matrix degradation. *J Cell Sci* 121:369-378.
68. Yamaguchi, H., M. Lorenz, S. Kempiak, C. Sarmiento, S. Coniglio, M. Symons, J. Segall, R. Eddy, H. Miki, T. Takenawa, and J. Condeelis. 2005. Molecular mechanisms of invadopodium formation: the role of the N-WASP-Arp2/3 complex pathway and cofilin. *J Cell Biol* 168:441-452.
69. Weaver, A. M., A. V. Karginov, A. W. Kinley, S. A. Weed, Y. Li, J. T. Parsons, and J. A. Cooper. 2001. Cortactin promotes and stabilizes Arp2/3-induced actin filament network formation. *Curr Biol* 11:370-374.
70. Wang, W., S. Goswami, K. Lapidus, A. L. Wells, J. B. Wyckoff, E. Sahai, R. H. Singer, J. E. Segall, and J. S. Condeelis. 2004. Identification and Testing of a Gene Expression Signature of Invasive Carcinoma Cells within Primary Mammary Tumors. *Cancer Res* 64:8585-8594.
71. Lorenz, M., H. Yamaguchi, Y. Wang, R. H. Singer, and J. Condeelis. 2004. Imaging Sites of N-WASP Activity in Lamellipodia and Invadopodia of Carcinoma Cells. *Current Biology* 14:697.
72. Fujimura, M., T. Hidaka, and S. Saito. 2002. Selective inhibition of the epidermal growth factor receptor by ZD1839 decreases the growth and invasion of ovarian clear cell adenocarcinoma cells. *Clin Cancer Res* 8:2448-2454.
73. Yang, Z., R. Bagheri-Yarmand, R. A. Wang, L. Adam, V. V. Papadimitrakopoulou, G. L. Clayman, A. El-Naggar, R. Lotan, C. J. Barnes, W. K. Hong, and R. Kumar. 2004. The epidermal growth factor receptor tyrosine kinase inhibitor ZD1839 (Iressa) suppresses c-Src and Pak1 pathways and invasiveness of human cancer cells. *Clin Cancer Res* 10:658-667.
74. Desmarais, V., H. Yamaguchi, M. Oser, L. Soon, G. Mouneimne, C. Sarmiento, R. Eddy, and J. Condeelis. 2009. N-WASP and cortactin are involved in invadopodium-

- dependent chemotaxis to EGF in breast tumor cells. *Cell Motil Cytoskeleton* 66:303-316.
75. Clark, E. S., and A. M. Weaver. 2008. A new role for cortactin in invadopodia: Regulation of protease secretion. *Eur J Cell Biol.*
  76. Desai, B., T. Ma, and M. A. Chellaiah. 2008. Invadopodia and matrix degradation, a new property of prostate cancer cells during migration and invasion. *J Biol Chem* 283:13856-13866.
  77. Coopman, P. J., M. T. Do, E. W. Thompson, and S. C. Mueller. 1998. Phagocytosis of cross-linked gelatin matrix by human breast carcinoma cells correlates with their invasive capacity. *Clin Cancer Res* 4:507-515.
  78. Thompson, E. W., S. Paik, N. Brunner, C. L. Sommers, G. Zugmaier, R. Clarke, T. B. Shima, J. Torri, S. Donahue, M. E. Lippman, and et al. 1992. Association of increased basement membrane invasiveness with absence of estrogen receptor and expression of vimentin in human breast cancer cell lines. *J Cell Physiol* 150:534-544.
  79. Martin, G. S. 2001. The hunting of the Src. *Nat Rev Mol Cell Biol* 2:467-475.
  80. Weernink, P. A., and G. Rijksen. 1995. Activation and translocation of c-Src to the cytoskeleton by both platelet-derived growth factor and epidermal growth factor. *J Biol Chem* 270:2264-2267.
  81. Frame, M. C. 2002. Src in cancer: deregulation and consequences for cell behaviour. *Biochim Biophys Acta* 1602:114-130.
  82. Timpson, P., G. E. Jones, M. C. Frame, and V. G. Brunton. 2001. Coordination of cell polarization and migration by the Rho family GTPases requires Src tyrosine kinase activity. *Curr Biol* 11:1836-1846.
  83. Wu, X., S. Suetsugu, L. A. Cooper, T. Takenawa, and J. L. Guan. 2004. Focal adhesion kinase regulation of N-WASP subcellular localization and function. *J Biol Chem* 279:9565-9576.
  84. Huang, C., Y. Ni, T. Wang, Y. Gao, C. C. Haudenschild, and X. Zhan. 1997. Down-regulation of the filamentous actin cross-linking activity of cortactin by Src-mediated tyrosine phosphorylation. *J Biol Chem* 272:13911-13915.

85. Jaffe, A. B., and A. Hall. 2005. Rho GTPases: biochemistry and biology. *Annu Rev Cell Dev Biol* 21:247-269.
86. Ridley, A. J. 2001. Rho GTPases and cell migration. *J Cell Sci* 114:2713-2722.
87. Bosse, T., J. Ehinger, A. Czuchra, S. Benesch, A. Steffen, X. Wu, K. Schloen, H. H. Niemann, G. Scita, T. E. Stradal, C. Brakebusch, and K. Rottner. 2007. Cdc42 and phosphoinositide 3-kinase drive Rac-mediated actin polymerization downstream of c-Met in distinct and common pathways. *Mol Cell Biol* 27:6615-6628.
88. Kaibuchi, K., S. Kuroda, and M. Amano. 1999. Regulation of the cytoskeleton and cell adhesion by the Rho family GTPases in mammalian cells. *Annu Rev Biochem* 68:459-486.
89. Etienne-Manneville, S. 2004. Cdc42--the centre of polarity. *J Cell Sci* 117:1291-1300.
90. Kim, S. H., Z. Li, and D. B. Sacks. 2000. E-cadherin-mediated cell-cell attachment activates Cdc42. *J Biol Chem* 275:36999-37005.
91. El-Sibai, M., P. Nalbant, H. Pang, R. J. Flinn, C. Sarmiento, F. Macaluso, M. Cammer, J. S. Condeelis, K. M. Hahn, and J. M. Backer. 2007. Cdc42 is required for EGF-stimulated protrusion and motility in MTLn3 carcinoma cells. *J Cell Sci* 120:3465-3474.
92. Parsons, M., J. Monypenny, S. M. Ameer-Beg, T. H. Millard, L. M. Machesky, M. Peter, M. D. Keppler, G. Schiavo, R. Watson, J. Chernoff, D. Zicha, B. Vojnovic, and T. Ng. 2005. Spatially distinct binding of Cdc42 to PAK1 and N-WASP in breast carcinoma cells. *Mol Cell Biol* 25:1680-1695.
93. Yang, L., L. Wang, and Y. Zheng. 2006. Gene targeting of Cdc42 and Cdc42GAP affirms the critical involvement of Cdc42 in filopodia induction, directed migration, and proliferation in primary mouse embryonic fibroblasts. *Mol Biol Cell* 17:4675-4685.
94. Fukuoka, M., S. Suetsugu, H. Miki, K. Fukami, T. Endo, and T. Takenawa. 2001. A novel neural Wiskott-Aldrich syndrome protein (N-WASP) binding protein, WISH, induces Arp2/3 complex activation independent of Cdc42. *J Cell Biol* 152:471-482.

95. Thrasher, A. J. 2002. WASp in immune-system organization and function. *Nat Rev Immunol* 2:635-646.
96. Rohatgi, R., L. Ma, H. Miki, M. Lopez, T. Kirchhausen, T. Takenawa, and M. W. Kirschner. 1999. The interaction between N-WASP and the Arp2/3 complex links Cdc42-dependent signals to actin assembly. *Cell* 97:221-231.
97. Torres, E., and M. K. Rosen. 2006. Protein-tyrosine kinase and GTPase signals cooperate to phosphorylate and activate Wiskott-Aldrich syndrome protein (WASP)/neuronal WASP. *J Biol Chem* 281:3513-3520.
98. Millard, T. H., S. J. Sharp, and L. M. Machesky. 2004. Signalling to actin assembly via the WASP (Wiskott-Aldrich syndrome protein)-family proteins and the Arp2/3 complex. *Biochem J* 380:1-17.
99. Kempiak, S. J., H. Yamaguchi, C. Sarmiento, M. Sidani, M. Ghosh, R. J. Eddy, V. DesMarais, M. Way, J. Condeelis, and J. E. Segall. 2005. A Neural Wiskott-Aldrich Syndrome Protein-mediated Pathway for Localized Activation of Actin Polymerization That Is Regulated by Cortactin. *J Biol Chem* 280:5836-5842.
100. Miki, H., K. Miura, and T. Takenawa. 1996. N-WASP, a novel actin-depolymerizing protein, regulates the cortical cytoskeletal rearrangement in a PIP2-dependent manner downstream of tyrosine kinases. *Embo J* 15:5326-5335.
101. Aspenstrom, P. 1997. A Cdc42 target protein with homology to the non-kinase domain of FER has a potential role in regulating the actin cytoskeleton. *Curr Biol* 7:479-487.
102. Dombrosky-Ferlan, P., A. Grishin, R. J. Botelho, M. Sampson, L. Wang, W. A. Rudert, S. Grinstein, and S. J. Corey. 2003. Felic (CIP4b), a novel binding partner with the Src kinase Lyn and Cdc42, localizes to the phagocytic cup. *Blood* 101:2804-2809.
103. Anton, I. M., G. E. Jones, F. Wandosell, R. Geha, and N. Ramesh. 2007. WASP-interacting protein (WIP): working in polymerisation and much more. *Trends Cell Biol* 17:555-562.
104. Ho, H. Y., R. Rohatgi, A. M. Lebensohn, and M. W. Kirschner. 2006. In vitro reconstitution of cdc42-mediated actin assembly using purified components. *Methods Enzymol* 406:174-190.

105. Ho, H. Y., R. Rohatgi, A. M. Lebensohn, M. Le, J. Li, S. P. Gygi, and M. W. Kirschner. 2004. Toca-1 mediates Cdc42-dependent actin nucleation by activating the N-WASP-WIP complex. *Cell* 118:203-216.
106. Tian, L., D. L. Nelson, and D. M. Stewart. 2000. Cdc42-interacting protein 4 mediates binding of the Wiskott-Aldrich syndrome protein to microtubules. *J Biol Chem* 275:7854-7861.
107. Linder, S., K. Hufner, U. Wintergerst, and M. Aepfelbacher. 2000. Microtubule-dependent formation of podosomal adhesion structures in primary human macrophages. *J Cell Sci* 113 Pt 23:4165-4176.
108. Tsuji, E., Y. Tsuji, T. Fujiwara, S. Ogata, K. Tsukamoto, and K. Saku. 2006. Splicing variant of Cdc42 interacting protein-4 disrupts beta-catenin-mediated cell-cell adhesion: expression and function in renal cell carcinoma. *Biochem Biophys Res Commun* 339:1083-1088.
109. Wang, L., W. A. Rudert, A. Grishin, P. Dombrosky-Ferlan, K. Sullivan, X. Deng, D. Whitcomb, and S. Corey. 2002. Identification and genetic analysis of human and mouse activated Cdc42 interacting protein-4 isoforms. *Biochem Biophys Res Commun* 293:1426-1430.
110. Fuchs, U., G. Rehkamp, O. A. Haas, R. Slany, M. Konig, S. Bojesen, R. M. Bohle, C. Damm-Welk, W. D. Ludwig, J. Harbott, and A. Borkhardt. 2001. The human formin-binding protein 17 (FBP17) interacts with sorting nexin, SNX2, and is an MLL-fusion partner in acute myelogeneous leukemia. *Proc Natl Acad Sci U S A* 98:8756-8761.
111. Toguchi, M., N. Richnau, A. Ruusala, and P. Aspenstrom. 2009. Members of the CIP4 family of proteins participate in the regulation of platelet-derived growth factor receptor-beta-dependent actin reorganization and migration. *Biol Cell*.
112. Itoh, T., K. S. Erdmann, A. Roux, B. Habermann, H. Werner, and P. De Camilli. 2005. Dynamin and the actin cytoskeleton cooperatively regulate plasma membrane invagination by BAR and F-BAR proteins. *Dev Cell* 9:791-804.
113. Tsujita, K., S. Suetsugu, N. Sasaki, M. Furutani, T. Oikawa, and T. Takenawa. 2006. Coordination between the actin cytoskeleton and membrane deformation by a

- novel membrane tubulation domain of PCH proteins is involved in endocytosis. *J Cell Biol* 172:269-279.
114. Itoh, T., and P. De Camilli. 2006. BAR, F-BAR (EFC) and ENTH/ANTH domains in the regulation of membrane-cytosol interfaces and membrane curvature. *Biochim Biophys Acta* 1761:897-912.
  115. Shimada, A., H. Niwa, K. Tsujita, S. Suetsugu, K. Nitta, K. Hanawa-Suetsugu, R. Akasaka, Y. Nishino, M. Toyama, L. Chen, Z. J. Liu, B. C. Wang, M. Yamamoto, T. Terada, A. Miyazawa, A. Tanaka, S. Sugano, M. Shirouzu, K. Nagayama, T. Takenawa, and S. Yokoyama. 2007. Curved EFC/F-BAR-domain dimers are joined end to end into a filament for membrane invagination in endocytosis. *Cell* 129:761-772.
  116. Frost, A., V. M. Unger, and P. De Camilli. 2009. The BAR domain superfamily: membrane-molding macromolecules. *Cell* 137:191-196.
  117. Kakimoto, T., H. Katoh, and M. Negishi. 2006. Regulation of neuronal morphology by Toca-1, an F-BAR/EFC protein that induces plasma membrane invagination. *J Biol Chem* 281:29042-29053.
  118. Henne, W. M., H. M. Kent, M. G. Ford, B. G. Hegde, O. Daumke, P. J. Butler, R. Mittal, R. Langen, P. R. Evans, and H. T. McMahon. 2007. Structure and analysis of FCHo2 F-BAR domain: a dimerizing and membrane recruitment module that effects membrane curvature. *Structure* 15:839-852.
  119. Suetsugu, S., K. Toyooka, and Y. Senju. 2009. Subcellular membrane curvature mediated by the BAR domain superfamily proteins. *Semin Cell Dev Biol*.
  120. Ahmed, S., W. I. Goh, and W. Bu. 2009. I-BAR domains, IRSp53 and filopodium formation. *Semin Cell Dev Biol*.
  121. Mattila, P. K., A. Pykalainen, J. Saarikangas, V. O. Paavilainen, H. Vihinen, E. Jokitalo, and P. Lappalainen. 2007. Missing-in-metastasis and IRSp53 deform PI(4,5)P<sub>2</sub>-rich membranes by an inverse BAR domain-like mechanism. *J Cell Biol* 176:953-964.
  122. Aspenstrom, P. 2009. Roles of F-BAR/PCH proteins in the regulation of membrane dynamics and actin reorganization. *Int Rev Cell Mol Biol* 272:1-31.

123. Wachtler, V., Y. Huang, J. Karagiannis, and M. K. Balasubramanian. 2006. Cell cycle-dependent roles for the FCH-domain protein Cdc15p in formation of the actomyosin ring in *Schizosaccharomyces pombe*. *Mol Biol Cell* 17:3254-3266.
124. Wang, Q., M. V. Navarro, G. Peng, E. Molinelli, S. Lin Goh, B. L. Judson, K. R. Rajashankar, and H. Sondermann. 2009. Molecular mechanism of membrane constriction and tubulation mediated by the F-BAR protein Pacsin/Syndapin. *Proc Natl Acad Sci U S A* 106:12700-12705.
125. Peter, B. J., H. M. Kent, I. G. Mills, Y. Vallis, P. J. Butler, P. R. Evans, and H. T. McMahon. 2004. BAR domains as sensors of membrane curvature: the amphiphysin BAR structure. *Science* 303:495-499.
126. Suetsugu, S. 2009. The direction of actin polymerization for vesicle fission suggested from membranes tubulated by the EFC/F-BAR domain protein FBP17. *FEBS Lett*.
127. Takano, K., K. Toyooka, and S. Suetsugu. 2008. EFC/F-BAR proteins and the N-WASP-WIP complex induce membrane curvature-dependent actin polymerization. *Embo J* 27:2817-2828.
128. Tsuboi, S., H. Takada, T. Hara, N. Mochizuki, T. Funyu, H. Saitoh, Y. Terayama, K. Yamaya, C. Ohya, S. Nonoyama, and H. D. Ochs. 2009. FBP17 Mediates a Common Molecular Step in the Formation of Podosomes and Phagocytic Cups in Macrophages. *J Biol Chem* 284:8548-8556.
129. Mitra, S. K., and D. D. Schlaepfer. 2006. Integrin-regulated FAK-Src signaling in normal and cancer cells. *Curr Opin Cell Biol* 18:516-523.
130. Lombardo, L. J., F. Y. Lee, P. Chen, D. Norris, J. C. Barrish, K. Behnia, S. Castaneda, L. A. Cornelius, J. Das, A. M. Doweyko, C. Fairchild, J. T. Hunt, I. Inigo, K. Johnston, A. Kamath, D. Kan, H. Klei, P. Marathe, S. Pang, R. Peterson, S. Pitt, G. L. Schieven, R. J. Schmidt, J. Tokarski, M. L. Wen, J. Wityak, and R. M. Borzilleri. 2004. Discovery of N-(2-chloro-6-methyl-phenyl)-2-(6-(4-(2-hydroxyethyl)-piperazin-1-yl)-2-methylpyrimidin-4-ylamino)thiazole-5-carboxamide (BMS-354825), a dual Src/Abl kinase inhibitor with potent antitumor activity in preclinical assays. *J Med Chem* 47:6658-6661.

131. Song, L., M. Morris, T. Bagui, F. Y. Lee, R. Jove, and E. B. Haura. 2006. Dasatinib (BMS-354825) selectively induces apoptosis in lung cancer cells dependent on epidermal growth factor receptor signaling for survival. *Cancer Res* 66:5542-5548.
132. Nam, S., D. Kim, J. Q. Cheng, S. Zhang, J. H. Lee, R. Buettner, J. Mirosevich, F. Y. Lee, and R. Jove. 2005. Action of the Src family kinase inhibitor, dasatinib (BMS-354825), on human prostate cancer cells. *Cancer Res* 65:9185-9189.
133. Finn, R. S., J. Dering, C. Ginther, C. A. Wilson, P. Glaspy, N. Tchekmedyian, and D. J. Slamon. 2007. Dasatinib, an orally active small molecule inhibitor of both the src and abl kinases, selectively inhibits growth of basal-type/"triple-negative" breast cancer cell lines growing in vitro. *Breast Cancer Res Treat* 105:319-326.
134. Chou, T. C. 1976. Derivation and properties of Michaelis-Menten type and Hill type equations for reference ligands. *J Theor Biol* 59:253-276.
135. Chou, T. C., and P. Talalay. 1981. Generalized equations for the analysis of inhibitions of Michaelis-Menten and higher-order kinetic systems with two or more mutually exclusive and nonexclusive inhibitors. *Eur J Biochem* 115:207-216.
136. Luo, F. R., Y. C. Barrett, Z. Yang, A. Camuso, K. McGlinchey, M. L. Wen, R. Smykla, K. Fager, R. Wild, H. Palme, S. Galbraith, A. Blackwood-Chirchir, and F. Y. Lee. 2008. Identification and validation of phospho-SRC, a novel and potential pharmacodynamic biomarker for dasatinib (SPRYCEL), a multi-targeted kinase inhibitor. *Cancer Chemother Pharmacol* 62:1065-1074.
137. Serrels, A., I. R. Macpherson, T. R. Evans, F. Y. Lee, E. A. Clark, O. J. Sansom, G. H. Ashton, M. C. Frame, and V. G. Brunton. 2006. Identification of potential biomarkers for measuring inhibition of Src kinase activity in colon cancer cells following treatment with dasatinib. *Mol Cancer Ther* 5:3014-3022.
138. Copland, M., A. Hamilton, L. J. Elrick, J. W. Baird, E. K. Allan, N. Jordanides, M. Barow, J. C. Mountford, and T. L. Holyoake. 2006. Dasatinib (BMS-354825) targets an earlier progenitor population than imatinib in primary CML but does not eliminate the quiescent fraction. *Blood* 107:4532-4539.
139. Lieser, S. A., J. Shaffer, and J. A. Adams. 2006. SRC tail phosphorylation is limited by structural changes in the regulatory tyrosine kinase Csk. *J Biol Chem* 281:38004-38012.



140. Roskoski, R., Jr. 2005. Src kinase regulation by phosphorylation and dephosphorylation. *Biochem Biophys Res Commun* 331:1-14.
141. Wang, X. D., K. Reeves, F. R. Luo, L. A. Xu, F. Lee, E. Clark, and F. Huang. 2007. Identification of candidate predictive and surrogate molecular markers for dasatinib in prostate cancer: rationale for patient selection and efficacy monitoring. *Genome Biol* 8:R255.
142. Schittenhelm, M. M., S. Shiraga, A. Schroeder, A. S. Corbin, D. Griffith, F. Y. Lee, C. Bokemeyer, M. W. Deininger, B. J. Druker, and M. C. Heinrich. 2006. Dasatinib (BMS-354825), a dual SRC/ABL kinase inhibitor, inhibits the kinase activity of wild-type, juxtamembrane, and activation loop mutant KIT isoforms associated with human malignancies. *Cancer Res* 66:473-481.
143. Chen, Z., F. Y. Lee, K. N. Bhalla, and J. Wu. 2006. Potent inhibition of platelet-derived growth factor-induced responses in vascular smooth muscle cells by BMS-354825 (dasatinib). *Mol Pharmacol* 69:1527-1533.
144. Hines, S. J., C. Organ, M. J. Kornstein, and G. W. Krystal. 1995. Coexpression of the c-kit and stem cell factor genes in breast carcinomas. *Cell Growth Differ* 6:769-779.
145. Meric, F., W. P. Lee, A. Sahin, H. Zhang, H. J. Kung, and M. C. Hung. 2002. Expression profile of tyrosine kinases in breast cancer. *Clin Cancer Res* 8:361-367.
146. Zelinski, D. P., N. D. Zantek, J. C. Stewart, A. R. Irizarry, and M. S. Kinch. 2001. EphA2 overexpression causes tumorigenesis of mammary epithelial cells. *Cancer Res* 61:2301-2306.
147. Siu, W. Y., T. Arooz, and R. Y. Poon. 1999. Differential responses of proliferating versus quiescent cells to adriamycin. *Exp Cell Res* 250:131-141.
148. Sarrio, D., S. M. Rodriguez-Pinilla, D. Hardisson, A. Cano, G. Moreno-Bueno, and J. Palacios. 2008. Epithelial-mesenchymal transition in breast cancer relates to the basal-like phenotype. *Cancer Res* 68:989-997.
149. Srinivasan, D., J. T. Sims, and R. Plattner. 2007. Aggressive breast cancer cells are dependent on activated Abl kinases for proliferation, anchorage-independent growth and survival. *Oncogene*.

150. Huang, F., K. Reeves, X. Han, C. Fairchild, S. Platero, T. W. Wong, F. Lee, P. Shaw, and E. Clark. 2007. Identification of candidate molecular markers predicting sensitivity in solid tumors to dasatinib: rationale for patient selection. *Cancer Res* 67:2226-2238.
151. Lu, Y., Q. Yu, J. H. Liu, J. Zhang, H. Wang, D. Koul, J. S. McMurray, X. Fang, W. K. Yung, K. A. Siminovitch, and G. B. Mills. 2003. Src family protein-tyrosine kinases alter the function of PTEN to regulate phosphatidylinositol 3-kinase/AKT cascades. *J Biol Chem* 278:40057-40066.
152. Shin, I., F. M. Yakes, F. Rojo, N. Y. Shin, A. V. Bakin, J. Baselga, and C. L. Arteaga. 2002. PKB/Akt mediates cell-cycle progression by phosphorylation of p27(Kip1) at threonine 157 and modulation of its cellular localization. *Nat Med* 8:1145-1152.
153. Maddika, S., S. R. Ande, E. Wiechec, L. L. Hansen, S. Wesselborg, and M. Los. 2008. Akt-mediated phosphorylation of CDK2 regulates its dual role in cell cycle progression and apoptosis. *J Cell Sci* 121:979-988.
154. Grille, S. J., A. Bellacosa, J. Upson, A. J. Klein-Szanto, F. van Roy, W. Lee-Kwon, M. Donowitz, P. N. Tsichlis, and L. Larue. 2003. The protein kinase Akt induces epithelial mesenchymal transition and promotes enhanced motility and invasiveness of squamous cell carcinoma lines. *Cancer Res* 63:2172-2178.
155. Buccione, R., G. Caldieri, and I. Ayala. 2009. Invadopodia: specialized tumor cell structures for the focal degradation of the extracellular matrix. *Cancer Metastasis Rev* 28:137-149.
156. Vigneron, A., I. B. Roninson, E. Gamelin, and O. Coqueret. 2005. Src inhibits adriamycin-induced senescence and G2 checkpoint arrest by blocking the induction of p21waf1. *Cancer Res* 65:8927-8935.
157. Fidler, I. J. 2003. The pathogenesis of cancer metastasis: the 'seed and soil' hypothesis revisited. *Nat Rev Cancer* 3:453-458.
158. Condeelis, J., R. H. Singer, and J. E. Segall. 2005. The great escape: when cancer cells hijack the genes for chemotaxis and motility. *Annu Rev Cell Dev Biol* 21:695-718.
159. Rohatgi, R., H. Y. Ho, and M. W. Kirschner. 2000. Mechanism of N-WASP activation by CDC42 and phosphatidylinositol 4, 5-bisphosphate. *J Cell Biol* 150:1299-1310.

160. Cory, G. O., R. Garg, R. Cramer, and A. J. Ridley. 2002. Phosphorylation of tyrosine 291 enhances the ability of WASp to stimulate actin polymerization and filopodium formation. Wiskott-Aldrich Syndrome protein. *J Biol Chem* 277:45115-45121.
161. Suetsugu, S., M. Hattori, H. Miki, T. Tezuka, T. Yamamoto, K. Mikoshiba, and T. Takenawa. 2002. Sustained activation of N-WASP through phosphorylation is essential for neurite extension. *Dev Cell* 3:645-658.
162. Torres, E., and M. K. Rosen. 2003. Contingent phosphorylation/dephosphorylation provides a mechanism of molecular memory in WASP. *Mol Cell* 11:1215-1227.
163. Kamioka, Y., S. Fukuhara, H. Sawa, K. Nagashima, M. Masuda, M. Matsuda, and N. Mochizuki. 2004. A novel dynamin-associating molecule, formin-binding protein 17, induces tubular membrane invaginations and participates in endocytosis. *J Biol Chem* 279:40091-40099.
164. Karpova, T. S., C. T. Baumann, L. He, X. Wu, A. Grammer, P. Lipsky, G. L. Hager, and J. G. McNally. 2003. Fluorescence resonance energy transfer from cyan to yellow fluorescent protein detected by acceptor photobleaching using confocal microscopy and a single laser. *J Microsc* 209:56-70.
165. Greeson, J. N., L. E. Organ, F. A. Pereira, and R. M. Raphael. 2006. Assessment of prestin self-association using fluorescence resonance energy transfer. *Brain Res* 1091:140-150.
166. Irvin, W. J., Jr., and L. A. Carey. 2008. What is triple-negative breast cancer? *Eur J Cancer* 44:2799-2805.
167. Ward, M. E., J. Y. Wu, and Y. Rao. 2004. Visualization of spatially and temporally regulated N-WASP activity during cytoskeletal reorganization in living cells. *Proc Natl Acad Sci U S A* 101:970-974.
168. Hu, J., F. Troglio, A. Mukhopadhyay, S. Everingham, E. Kwok, G. Scita, and A. W. Craig. 2009. F-BAR-containing adaptor CIP4 localizes to early endosomes and regulates Epidermal Growth Factor Receptor trafficking and downregulation. *Cell Signal* 21:1686-1697.

169. Prehoda, K. E., J. A. Scott, R. D. Mullins, and W. A. Lim. 2000. Integration of multiple signals through cooperative regulation of the N-WASP-Arp2/3 complex. *Science* 290:801-806.
170. Park, H., and D. Cox. 2009. Cdc42 Regulates Fc{gamma} Receptor-mediated Phagocytosis through the Activation and Phosphorylation of WASP and N-WASP. *Mol Biol Cell*.
171. Sorlie, T., C. M. Perou, R. Tibshirani, T. Aas, S. Geisler, H. Johnsen, T. Hastie, M. B. Eisen, M. van de Rijn, S. S. Jeffrey, T. Thorsen, H. Quist, J. C. Matese, P. O. Brown, D. Botstein, P. Eystein Lonning, and A. L. Borresen-Dale. 2001. Gene expression patterns of breast carcinomas distinguish tumor subclasses with clinical implications. *Proc Natl Acad Sci U S A* 98:10869-10874.
172. Magkou, C., L. Nakopoulou, C. Zoubouli, K. Karali, I. Theohari, P. Bakarakos, and I. Giannopoulou. 2008. Expression of the epidermal growth factor receptor (EGFR) and the phosphorylated EGFR in invasive breast carcinomas. *Breast Cancer Res* 10:R49.
173. Pichot, C. S., S. M. Hartig, L. Xia, C. Arvanitis, D. Monisvais, F. Y. Lee, J. A. Frost, and S. J. Corey. 2009. Dasatinib synergizes with doxorubicin to block growth, migration, and invasion of breast cancer cells. *Br J Cancer* 101:38-47.
174. Feng, Y., S. M. Hartig, J. E. Bechill, E. G. Blanchard, E. Caudell, and S. J. Corey. 2009. The Cdc42 interacting protein 4 (CIP4) gene knockout mouse reveals delayed and decreased endocytosis. *J Biol Chem*.

## **VITA**

Christina Nichol Stewart Pichot was born March 24, 1981 in Houston, Texas. She graduated from Clements High School in Sugar Land, Texas in 1999, after which she attended the University of Texas at Austin. In 2003, she graduated with a B.S. in Microbiology and continued her education at the University of Texas Medical Branch in Galveston, Texas for 2 years. After marrying her husband Travis in 2004, she moved to Houston and enrolled in the Graduate School at the University of Texas Health Science at Houston. She completed her doctoral research in the labs of Seth Corey, M.D, at M.D. Anderson Cancer Center and Jeff Frost, Ph.D. at the University of Texas Medical School. She celebrated the birth of her daughter Sierra Elizabeth in October of 2009 and will graduate with a Ph.D. in Cancer Biology in May of 2010.